

AD-A041 633

ARMAMENT DEVELOPMENT AND TEST CENTER EGLIN AFB FLA  
TRANSONIC PRESSURE DISTRIBUTION ON AN AIRCRAFT WING MODEL DURIN--ETC(U)

F/G 20/4

MAR 77 H J RASMUSSEN

ADTC-TR-77-34

NL

UNCLASSIFIED

1 of 1  
ADA041633

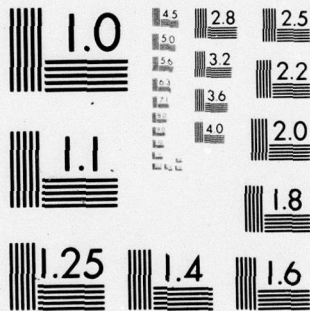


END

DATE

FILMED

8 - 77



MICROCOPY RESOLUTION TEST CHART  
NATIONAL BUREAU OF STANDARDS-1963-A

ADA 041 633





UNCLASSIFIED

SECURITY CLASSIFICATION OF THIS PAGE (When Data Entered)

REPORT DOCUMENTATION PAGE		READ INSTRUCTIONS BEFORE COMPLETING FORM
1. REPORT NUMBER 14 ADTC-TR-77-34	2. GOVT ACCESSION NO.	3. RECIPIENT'S CATALOG NUMBER
4. TITLE (and Subtitle) 6 TRANSONIC PRESSURE DISTRIBUTION ON AN AIRCRAFT WING MODEL DURING ROCKET SLED RUNS,		5. TYPE OF REPORT & PERIOD COVERED 9 Final rept.
7. AUTHOR(s) 18 Hans J. Rasmussen		6. PERFORMING ORG. REPORT NUMBER
9. PERFORMING ORGANIZATION NAME AND ADDRESS 6585th Test Group (AFSC) Test Track Division (TK) Holloman AFB, New Mexico 88330 ADTC		10. PROGRAM ELEMENT, PROJECT, TASK AREA & WORK UNIT NUMBERS JON: 99980000
11. CONTROLLING OFFICE NAME AND ADDRESS 6585th Test Group (AFSC) Holloman AFB, New Mexico 88330		12. REPORT DATE 11 Mar 1977
14. MONITORING AGENCY NAME & ADDRESS (if different from Controlling Office) Same as 11		13. NUMBER OF PAGES 76 (12) 71 p. 15. SECURITY CLASS. (of this report) Unclassified
16. DISTRIBUTION STATEMENT (of this Report) Approved for public release; distribution unlimited.		
17. DISTRIBUTION STATEMENT (of the abstract entered in Block 20, if different from Report) Same as 16		
18. SUPPLEMENTARY NOTES		
19. KEY WORDS (Continue on reverse side if necessary and identify by block number)		
20. ABSTRACT (Continue on reverse side if necessary and identify by block number) Hardware and techniques are described which were used in a series of rocket sled runs aimed at measuring aerodynamic data in the transonic speed regime during rocket sled runs. During these tests surface pressure distribution was measured on an aircraft wing model mounted in vertical position on a rocket sled at Mach numbers between zero and Mach 0.95 and at Reynolds numbers (based on cord length) up to 23 millions. The data were collected while "sweeping" the entire Mach number range both during acceleration and during deceleration. → next page		

DD FORM 1 JAN 73 1473

EDITION OF 1 NOV 65 IS OBSOLETE

UNCLASSIFIED

SECURITY CLASSIFICATION OF THIS PAGE (When Data Entered)

404038

UNCLASSIFIED

SECURITY CLASSIFICATION OF THIS PAGE(When Data Entered)

20.

cont.

Selected data obtained in this test series are presented and compared with wind tunnel and flight test results. The influence of time delay in the pressure tubing is discussed and methods for compensating for this effect are presented.



UNCLASSIFIED


SECURITY CLASSIFICATION OF THIS PAGE(When Data Entered)

## FOREWORD

A series of rocket sled runs was conducted on the Test Track at Holloman Air Force Base, New Mexico, to evaluate and demonstrate the potential of the rocket sled test method for obtaining aerodynamic data in the transonic velocity regime. In this specific test series pressure distribution data were collected on a sledborne aircraft wing model which had been extensively tested in wind tunnels and for which flight test data were also available for comparison. This model was made available by the NASA AMES Research Center.

Prime emphasis in this test series was placed on checkout and demonstration of data acquisition and processing techniques and on assessing flow field quality and interference between the sled and the sledborne test model.

The initiator of this test program was Captain Ronald Gustafson. He was also responsible for sled and instrumentation layout and conducted the initial runs; most of the aerodynamic data processing was performed by Mr. David Cummings. Mr. Thomas R. Bruce was in charge of the sled engineering and trajectory aspects and Mr. Dan J. Krupovage of the sled vibration aspects of this test series. The results are compiled and discussed by Mr. Hans Rasmussen.

ADDITIONAL FOR	White Section	<input checked="checked" type="checkbox"/>
NTIS	Blue Section	<input type="checkbox"/>
DDO		
UNANNOUNCED		
JUSTIFICATION		
BY	DISTRIBUTION/AVAILABILITY CODES	
Dist.	Avail.	and/or SPECIAL
		



## ABSTRACT

This report describes the hardware and techniques used in a series of rocket sled runs aimed at establishing the potential of rocket sled testing for measuring aerodynamic data in the transonic speed regime.

Surface pressure distribution data were collected on an aircraft wing model mounted in vertical position on a "flatbed" rocket sled at Mach numbers between zero and Mach 0.95 and at Reynolds numbers (based on cord length) up to 23 millions.

Data were collected while "sweeping" the entire Mach number range both during acceleration and during deceleration. The velocity-time histories of these sled runs were tailored to provide an extended "sustain period" at very low deceleration levels (approx -1g), after burnout of the prime accelerating propulsion systems. This "sustain" phase after burnout was designated as the prime data acquisition period. Selected data obtained in this test series are presented and compared with wind tunnel and flight test results.

The influence of time delay in the pressure tubing is discussed and methods for compensating for this effect are presented. In addition, methods for flow visualization applied during this sled run series and selected examples of the sled vibration environment experienced during this test series are presented in Appendices 1 and 2 to this report.

## TABLE OF CONTENTS

<u>Section</u>	<u>Page</u>
FOREWORD	i
ABSTRACT	ii
TABLE OF CONTENTS	iii
LIST OF ILLUSTRATIONS	iv
LIST OF TABLES	vi
1. INTRODUCTION	1
2. DISCUSSION	3
a. Test Model	3
b. Sled-Model Interface	4
c. Sled Propulsion and Trajectories	5
d. Data Acquisition and Processing	6
e. Typical Data Presentation	7
f. Time Delay in Pressure Measurements	10
3. SUMMARY	14
REFERENCES	16
APPENDIX I	A1
APPENDIX II	B1

## LIST OF ILLUSTRATIONS

<u>Figure</u>		<u>Page</u>
1	Panel Model (from Reference 4)	21
2	Panel Model End Plate Configurations (from Reference 4)	21
3	Test Sled with Wing Model, Push Column and Pusher Sleds	22
4	Sled Ground Plane without Test Model, with Tufts and Boundary Layer Rake	23
5	Pressure Readings on Centerline of Sled Ground Plane with Boundary Layer Rake	24
6	Typical Velocity-Time History of a Rocket Sled Run (Schematic)	25
7	Typical Velocity-Time History Including Two Constant Speed Periods During Deceleration	25
8	Transducer-Tubing Reference System (Schematic)	26
9	Pressure Data Acquisition (Data Flow, Schematic)	26
10	Pitot Pressure as Function of Time During a Typical Rocket Sled Run	27
11	Time Lag between Mach Number Obtained by Electro-Optical Sled Velocity Measurement and from Pitot Tube Readings	28
12	Typical Change of Shock Location On Top Surface of Wing (Schematic)	29
13	Surface Pressure Versus Time During a Typical Sled Run Location: Wing Top Surface at 5% of Chord; Angle of Attack 3.8 Deg	30
14	Typical Example of Pressure Reading on Upper Surface of Wing as Function of Time During a Rocket Sled Run. (Orifice Location at 59% of Chord; Angle of Attack 3.8 Deg)	31
15	Pressure as Function of Mach Number During Acceleration and Deceleration on the Upper Wing Surface at an Orifice Located at 59% Chord (Angle of Attack 3.8 Deg)	32
16	Pressure Coefficient as Function of Mach Number During Acceleration and Deceleration on the Upper Wing Surface at an Orifice Located at 59% Chord (Angle of Attack 3.8 Deg)	33
17	Pressure as Function of Mach Number During Acceleration and Deceleration on the Upper Wing Surface at an Orifice Located at 59% Chord (Angle of Attack -1.0 Deg; Trajectory with Two Periods of Quasi-Constant Speed)	34



<u>Figure</u>		<u>Page</u>
18	Pressure Coefficient as Function of Mach Number During Acceleration and Deceleration on the Upper Wing Surface at an Orifice Located at 59% Chord (Angle of Attack $-1.0^\circ$ Deg; Trajectory with Two Periods of Quasi-Constant Speed)	35
19	Pressure Distribution over Wing Chord (Upper Surface) at Mach = 0.825 and Angles of Attack of $-1.1^\circ$ , $0^\circ$ , $3.8^\circ$ , $5^\circ$ , as Measured During Rocket Sled Runs	36
20	Chordwise Pressure Distribution on Upper Wing Surface: Sled Data at Mach = 0.825 and Alpha = 0, 3.8 and 5 Deg AEDC 40" Transonic Tunnel Data at Mach = 0.85 and Alpha = 2 Deg (Data: Reference 6)	37
21	Chordwise Pressure Distribution on Upper Wing Surface at Mach = 0.825 and an Angle of Attack of $0^\circ$	38
22	Chordwise Pressure Distribution on Upper Wing Surface at Mach = 0.825 and an Angle of Attack of $3.8^\circ$	39
23	Chordwise Pressure Distribution on Upper Wing Surface at Mach = 0.825 and an Angle of Attack of $5^\circ$	40
24	Chordwise Pressure Distribution on Upper Wing Surface at Mach = 0.825 Sled Data: Angle of Attack = $0^\circ$ Ames 11-ft Transonic Tunnel: Angle of Attack = $0^\circ$ and $1^\circ$ Flight Angle of Attack = $1^\circ$	41

# LIST OF TABLES

<u>Table</u>		<u>Page</u>
1	Orifice Locations Along Centerline of Wing Model	17
2	Repeatability of Pressure Data Under Static Conditions	18
3	Repeatability of Test Data at Mach = 0.825 (Upper Surface Pressure Coefficient for Three Sled Runs) Q = 876 PSF, RN = $5.52 \times 10^6$ Per Foot, Angle of Attack = 5 Deg	19
4	Movement of Shock Across Pressure Orifice	20
5	Examples of Time Lag in Pressure Lines	20



## 1. INTRODUCTION

a. The series of transonic tests reported in this report was conducted to establish and document the potential of rocket sleds to measure transonic aerodynamic data under conditions which are undisturbed by flow blockage and by the effects of perforated walls affecting wind tunnels in this specific speed regime.

b. Rocket sleds are used to simulate selected portions of flight trajectories by moving sledborne payloads and the related instrumentation along a straight-line "flight" path parallel to the ground at accurately programmed, rigorously monitored, and closely repeatable levels and time histories of velocity and acceleration. Unless controlled impact is a mission requirement the test hardware is recovered for post-test inspection and re-use.

c. Rocket sled testing serves a wide variety of mission needs. Its application encompasses, for instance, the checkout and operational qualification of aircraft crew escape systems, the testing of inertial guidance equipment, the dynamic evaluation of seekers and homing devices, material and component evaluation during supersonic flight through rain or dust clouds, evaluation of fuzing functions and damage potential during impact of full-scale warheads, and many other requirements which do not lend themselves to the evaluation by other ground test means.

d. Typical examples of aerodynamic/aeroelastic tests which have been or are routinely conducted on the Holloman AFB Test Track include the study of ejection dynamics and recovery of aircraft crew escape systems, the testing of opening characteristics, stability, and drag of parachutes and other aerodynamic recovery devices, the measurement of boundary layer noise on a scale model of the Saturn V vehicle (Reference 7), the measurement of hinge moments and aeroelastic deflections on a full-scale operational missile in the Mach 2 regime and the evaluation of the response of sledborne test models to the intercept with blast waves.

e. The prime advantages which the sled test method promises for selected aerodynamic investigations of sledborne test models in the transonic regime are:

(1) The absence of flow restrictions on top and to the sides of the model, which effectively eliminates the blockage effects encountered in wind tunnels and the noise generated by perforated tunnel walls.

(2) The ability to determine free stream Mach and Reynolds number as well as ambient pressure, temperature, and air density with a high degree of precision, independent of aerodynamic measurements: The instantaneous sled velocity and acceleration with respect to the ground are obtained by means of a highly accurate ground-fixed

electro-optical reference instrumentation system, and the ambient atmospheric conditions are measured by standard meteorologic techniques.

(3) One operational characteristic of track testing is that during each single run data are continuously collected and transmitted while the sled is accelerating from rest to its burnout speed, and again while it is decelerating from burnout speed to a stop. Therefore, the conventional definition of a data point as used in wind tunnel work is little meaningful if applied to track testing. The sled sweeps its entire operational Mach number range such that for each Mach number two data points are obtained; the first one while accelerating, and the second one while slowing down.

f. Objective of this test series was to minimize and identify interference effects between sled and ground, to determine reliability and repeatability of test data, and to establish, at which acceleration or deceleration levels "sweeping" of the Mach number range will not introduce intolerable errors due to time delay in the pressure lines between orifice and transducer.

g. Two different approaches for carrying the test model are being tested: sledborne pressure distribution models which are installed on top of a sled above a flat ground plane parallel to the direction of sled motion, and sting-mounted models which are carried in free-stream ahead of all sled components to eliminate flow disturbances caused by the sled structure and by interference between sled and ground. The efforts reported in this report deal exclusively with the first of these two approaches.

h. Rocket sleds slide along the rails on steel shoes ("slippers") which are fitted around the rail flange with an all-around clearance of approximately 0.06". This rail gap is required because of small imperfections in rail alignment, irregularities in rail surfaces, etc. The actual longitudinal motion along the rails is characterized by a tendency to perform a superimposed oscillatory ("jumping") motion in pitch and yaw within the constraints of the slipper gap. This motion results in vibration inputs into the rocket sleds and the on-board payload. A typical example of the sled vibrations experienced at selected sled velocities during this test run series is presented in Appendix II to this report.



## 2. DISCUSSION

### a. TEST MODEL

(1) The test item used for this test series is a two-dimensional panel model representing the essential features and the cross-sectional profile of the wing of an operational large transport aircraft at a location 38.9% of the semi-wing span from the aircraft centerline. This model was made available by the NASA AMES Research Center. It was selected for this purpose because comprehensive wind tunnel data on this specific configuration and on other models of the same aircraft wing are available, and full scale flight test results are also in existence for comparison.

(2) The model and its attachment tang weighed 3,200 lbs. Its shape, its dimensions, its relationship to the complete aircraft wing configuration, and the location of the pressure orifices are schematically shown in Figure 1. The model was equipped with root and tip streamline-contoured end plates (Figure 2) which were specially designed to achieve on this model at  $M = 0.825$ , under the conditions encountered in the AMES - 11 ft Transonic Wind Tunnel, a flow pattern close to the one observed at the same Mach number in full scale flight. Details on the development of this model and on the considerations on which its design is based are presented in Reference 4. It should be noted that the model and its system of contoured end plates is optimized toward this specific wind tunnel, and that it was mounted on the test sled without any modifications or changes with respect to its aerodynamic configuration.

(3) Comprehensive work has been performed both in wind tunnels and in flight to determine the influence of free-stream Reynolds number on the transonic aerodynamic characteristics of this specific aircraft wing. Since the purpose of this test series was the checkout and demonstration of the sled test method for transonic aerodynamic testing, and since the specific model tested was optimized for a specific wind tunnel rather than the sled, no attempt is made in this report to discuss Reynolds number influence on the data obtained during these sled tests.

#### b. SLED-MODEL INTERFACE

(1) An existing "flatbed" sled was modified to accommodate the test item. The modification consisted of adding an aerodynamically clean, flat top surface to the basic sled frame, and installing a hub assembly to carry and position the test item as indicated in Figure 3.

(2) The model was positioned at specified angles of attack with respect to the direction of sled motion. The actual angle of attack was checked by conventional surveys (triangulation) prior to and after each run. Analyses were conducted to confirm that the angle of attack would not change during a run due to aerodynamic or inertial forces:

(a) A deflection of the model, resulting in a change of effective angle of attack due to aerodynamic forces. A structural review indicates that under the acting aerodynamic forces no deflection of the model will occur which could account for a change in angle of attack.

(b) A deflection of the model under inertial forces. Calculations, in part, supported by use of NASTRAN-modeling show that inertial forces acting on the 3,200 lb model as a consequence of being accelerated at 4...5 gs will neither deflect the model, nor the supporting structure, nor the sled structure to an extent which would be noticeable in the pressure measurements.

(3) The smooth top surface of the sled was intended to serve as ground plane for the test model, and to minimize the effect of flow disturbances on the model. Emphasis was placed on eliminating to the extent possible all sources of flow irregularities on top of the sled and on preventing interference between sled and ground from affecting the flow field around the model. A series of thirteen tests runs was performed prior to installing the test model. These tests served to experimentally optimize the ground plane design and the sled flow field. The results of these tests were monitored by photographically observing the crossflow on the ground plane through the use of tufts, by boundary layer rakes, and, to the extent possible, by flow visualization.

(4) The tufts showed some crossflow out of the boundary layer along the sides of the ground plane, but gave no indications of noticeable flow disturbances in the area where the model was to be located (Figure 4). The original plan to conduct a flow survey above the sled ground plane in the area where the model was to be located by means of a large pressure rake above the sled was thwarted by the inability to obtain a suitable pressure rake in the available time.

(5) Boundary layer surveys were conducted using a smaller boundary layer rake. Figure 5 shows pressure readings obtained by means of this rake while the rake was positioned on the centerline of the top surface 92" aft of the (drooped) leading edge of the sled ground plane. The individual probes of this rake were spaced 0.5 inches from each



other. As indicated by the pressure readings, the boundary layer thickness is less than 2 inches; the pressure readings 2" above the sled coincide with those of a pitot tube located in free stream 26" ahead of the leading edge.

(6) The investigations led to a change of leading edge configuration. While the ground plane was originally parallel to the ground all the way to the leading edge, a slightly downward sloped leading edge was adopted. The final shape of the "sloped down" leading edge is visible in Figure 4.

(7) Shadowgraph images were taken to observe the occurrence of local shocks, and various means for streamline visualization were also tried out; the latter, however, with only limited success. A brief review of this work is given in Appendix I.

#### c. SLED PROPULSION AND TRAJECTORIES

(1) Solid or prepackaged liquid rocket motors were used throughout this test series to propel the sled train to mission speed and to "sustain" a reduced level of deceleration while sweeping the Mach number regime of prime interest for data acquisition. In the interest of propulsion economy the Track uses "surplus" rocket motors from outdated, abandoned or discontinued missile systems which are available on a low-cost basis. No propulsion was installed aboard the mission sled itself. In order to minimize interference between the wake behind the test model and structural components of subsequent pusher sleds, a nineteen foot long push column was installed between the mission sled and the next following propulsion vehicle (Figure 3).

(2) During the prime mission runs, a total of three propulsion sleds were used. Two of these served to propel the "train" to mission speed; they were cueesssively separated after burnout. The third pusher sled connected to the mission vehicle by the aforementioned push column, served for low-deceleration "sustain" during the prime data acquisition period. A typical assortment of rocket motors used during primary mission runs consisted of:

Pusher Nr 1 (PDS 6325): 1st Stage 3 "Terrier Mark 7" solid rockets  
2nd Stage 3 "Terrier Mark 7" solid rockets  
Pusher Nr 2 (PDS 6606): 3rd Stage 5 "Bullpup" prepackaged rockets  
Pusher Nr 3 (PDS 6307): 4th Stage 8 "14-DS-1000" solid rockets  
5th Stage 8 "14-DS-1000" solid rockets

(3) A typical sled trajectory (i.e., time history of sled velocity from first motion to stop) is schematically shown in Figure 6. The Mach number range of prime data interest, between approximately 0.6 and 1.0 is covered both during acceleration and deceleration. In order to reduce the influence of time delay in the long tube lines on the pressure measurements, the trajectory was tailored to "sweep" this

range slowly (at a deceleration level of approximately  $-1.0g$ ) by using sustain propulsion to counteract part of the aerodynamic drag in this speed regime. Waterbraking was finally applied to slow down the sled prior to final stop.

(4) A different run profile (velocity-time history) was provided on the last mission run (designated 56X-G11A). In order to obtain more detailed data on time delay effects during the pressure distribution measurements the coast period of the sled run was modified to provide two periods of essentially constant velocity instead of the "slow sweep" used on the preceding missions. This trajectory is schematically indicated in Figure 7. As noticeable in Figure 7 and discussed in more detail in Paragraph f(5)(b) the drag was slightly overcompensated in both periods, and instead of introducing two constant-speed periods, the sled was slightly accelerated in both instances.

#### d. DATA ACQUISITION AND PROCESSING

(1) Sled velocity was determined by the electro-optical velocity measurement system (VMS). This system determines sled position as function of time by means of ground-fixed light-beam interrupters. These interrupters consist of bevel-edged metal plates which are positioned at nominal 13 foot intervals along the east side of the east rail of the track. Time measurements are obtained from a sledborne sensing head which provides a light beam between a light source and a photo-transistor. This beam is interrupted each time the sensing head passes an interrupter. The output is a series of interrupters pulses versus time which is transmitted to the ground station by telemetry, and is recorded and quantized with a standard error of  $3 \mu$  sec. The time versus position data obtained this way are processed by computer to yield velocity, acceleration and related information as function of time and of position. In connection with ambient meteorologic inputs Mach number and dynamic pressure are calculated.

(2) Surface pressure data on the test model were obtained as schematically indicated in Figure 8. Only the orifices on the centerline of the top and bottom surfaces of the wing (36" from bottom of model, see Figure 1) were used in this test series. Table 1 gives the locations of the individual orifices as function of chord length. Each orifice on the wing surface had a diameter of 0.050 inch and was connected with a pressure transducer of the appropriate range by means of plastic and steel tubing of 0.0625 inch internal diameter. Average tube length between orifices and transducer was approximately 60" of stainless steel tubing followed by 60 ... 75 inches of plastic tube lines. The reference side of each transducer was connected to one of four manifolds, which in turn, were vented to the atmosphere at all times prior to sled arming; they were closed during the tests. The transducers used were Bell and Howell type 4-312-0002 instruments with pressure ranges of  $\pm 3$ , 5, 7.5 and 12.5 psid. They were individually subjected to a dynamic calibration prior to each run. On board the sled they were embedded in shock-absorbing styrofoam material to isolate them from sled vibrations.



(3) A standard F-100 aircraft pitot-static tube was installed on the sled such that the pitot-static head protruded approximately 26 inches ahead of the leading edge of the sled-ground plane. The pitot tube was connected to a pressure transducer through a tube line of 115" length. Data obtained from this tube were telemetered and processed for total pressure and Mach number. For one of the runs the tube was connected to a transducer located very close to the aft end of the pitot tube, however, the arrangement was unsuccessful; the transducer used became inoperable due to sled vibrations.

(4) All sledborne data were transmitted from the moving sled to the ground by means of telemetry. Pressure data were digitized on board the sled and transmitted by two pulse-code-modulated (PCM) systems. Each of these systems handles 41 data channels; each channel transmits 8 data bits, resulting in a resolution of 256 discrete pressure steps per channel. The sampling rate is 1,150 samples per second. In addition to the PCM systems, one 12 channel FM/FM telemetry system was used to transmit space-time (=velocity) information and accelerometer data.

(5) Ambient wind velocity and direction were measured by track-side anemometers at selected locations along the track and used to correct the Mach number (downtrack component) and the angle of attack (cross-track component). A schematic outline of the data flow and the recording and processing involved is presented in Figure 9.

(6) As a check on accuracy and repeatability of pressure data acquisition under static conditions, five transducers were subjected simultaneously to identical pressure inputs, monitored by means of a mercury manometer. The transducer outputs were then transmitted through the same signal-conditioning, telemetering and recording equipment used during actual sled runs. The results are presented in Table 2.

(7) For a similar check on the repeatability of the sled run data under dynamic conditions from sled run to sled run, Table 3 shows the pressure coefficients on a selected portion of the upper surface at Mach = 0.825 and an angle of attack of 5 degrees as obtained during three different sled runs.

#### e. TYPICAL DATA PRESENTATION

(1) For two of the typical data runs conducted in this program some characteristic data plots are shown and discussed in the following:

(a) During one of these runs (designated 56X-G10A in the track mission count system), the wing was set to an angle of attack of 3.9 degrees with respect to the direction of sled motion which is equivalent to the free-stream flow direction except for some very minor wind corrections. The velocity-time history during this run corresponds to the one illustrated in Figure 6.

(b) On the second run (designated 56X-G11A) the angle of attack was -1 degree and the velocity-time history corresponds to the one shown in Figure 7; it contained the two quasi-constant speed periods discussed in Paragraph c.(4).

(2) The pitot-pressure as function of time from sled first motion as indicated by the sledborne pitot tube in front of the ground plane is shown in Figure 10. The points in time at which specific Mach numbers are reached (based on the electro-optical sled velocity measurements) are indicated in the graph above the horizontal axis. Figure 11 compares Mach number versus time data calculated from pitot-pressure measurements with Mach number versus time information based on instantaneous sled velocity determined by the electro-optical velocity measurement system (VMS). Since the electro-optical measurements deserve a very high degree of confidence (better than one part in 10,000) the pitot data gives an indication of both the accuracy and the time delay incurred in the pressure measurements involved:

(a) Figure 11 indicates that the Mach number determined from pitot-pressure lags approx 600 msec behind the actual free-stream Mach number during acceleration, and that this lag persists during the deceleration phase and the two "constant speed" periods.

(b) No effort was made to correct the pitot-determined Mach number except for one attempt to locate the pressure transducer in the immediate vicinity of the pitot tube as mentioned in Paragraph d.(3). All Mach number correlations used in the following are based on the Mach number values determined by VMS.

(3) Figure 12 illustrates the characteristic pressure change pattern which is observed versus time at a typical orifice location on top of the wing when the sled "sweeps" through the transonic Mach number regime. The specific orifice selected in this example is located at 59% of the wing chord; the data apply to an angle of attack of 3.8 degrees. The physical interpretation of this pressure-time history requires a brief discussion of some of the typical transonic effects which characterize the flow over an airfoil at supercritical subsonic Mach numbers. Under positive angles of attack supercritical flow tends to develop first on the upper surface; at higher Mach numbers it also occurs at the lower surface. The following discussions pertain to the conditions on the upper surface.

(a) As the free-stream Mach number increases, the flow on top of the wing expands. Above the onset of supercritical flow -- in the schematic sketches shown in Figure 12 approximately at Mach 0.7 -- a local area of supersonic flow begins developing. This supersonic region is terminated by a shock. As the sled velocity and with it the free-stream Mach number is increased the extent of the supersonic region increases, and the shock moves backward. This shock is close to normal in the external field. However, some disturbances connected with the resulting boundary layer separation may move upstream within the boundary layer and produce a system of oblique shocks in the near field close to



the surface and can also cause some turbulence in the area immediately preceding the instantaneous shock location. An area of flow separation (not shown in the schematic of Figure 12) may develop downstream of the shock. A detailed discussion of the phenomena involved and especially the influence of Reynolds number on the shock location is presented in References 3, 4 and 5.

(b) In the pressure-time history example in Figure 12 the passage of the shock across the orifice is indicated by a sudden, discontinuous pressure drop as the flow across the orifice changes from the subsonic condition behind the shock to the local supersonic condition ahead of it. When the sled decelerates, this process reverses, and the shock location wanders forward until it moves across the orifice again, marked by a discontinuous pressure rise to the level characteristic for the subsonic conditions behind the shock.

(4) The actual pressure readings versus time at an orifice on the upper surface close to the wing leading edge (at 5% of the chord length) and at an orifice located at 59% of chord are shown in Figures 13 and 14, respectively. The data pertains to run number 56X-G10A. The 5% of chord data show flow expansion as the Mach number increases, however, the flow is obviously subsonic during the entire run. The 59% of chord data show very distinctly the trend discussed in the preceding paragraph.

(a) At  $t=7$  sec the boundary layer disturbances immediately downstream of the shock become noticeable, and at  $t=7.8$  sec the shock itself moves across the orifice. At  $t=15.6$  sec the shock moves across the orifice again in reverse direction.

(b) According to information presented in References 3, 4 and 5 the shock observed at 7.8 sec is very close to normal. This means the resulting pressure drop from -3.0 psig at  $t=7.8$  sec to -5.8 psig at  $t=8.1$  sec will in actuality occur instantaneously within engineering accuracy, and the slope of the pressure curve must be attributed to time delays in the pressure lines and in instrument response.

(c) The slight irregularity noticeable in the pressure versus time readings at 7.3 sec occurs during the acceleration phase only. It affects all orifices at the same time. It is not considered an aerodynamic but an inertial effect and is attributed to a response of the transducers to a severe change in sled acceleration which occurs at this instance in time due to staging of the "Bullpup" rocket motors.

(d) The observation that the pressure increase during deceleration appears to be more gradual than the pressure drop while the sled accelerates is attributed to the fact that the sled decelerates at a much lower level than it accelerates, and that in consequence, the movement of the shock across the wing chord occurs much slower. Assuming constant rates of acceleration and deceleration, Table 4 shows the time the shock takes to move from 59% of chord to 77% of chord. The movement in reverse direction is by a factor of seven slower, therefore, the influence of oblique shocks in the near-field preceding the actual main shock is more noticeable.

(5) For the 59% of chord location the pressure readings which are shown versus time in Figure 14 are plotted versus Mach number in Figure 15 and in form of pressure coefficients versus Mach number in Figure 16. These plots show that:

(a) At identical Mach numbers below the one at which the shock passes the orifice the observed pressures and pressure coefficients are lower (i.e., higher negative) in the decelerating than in the accelerating mode.

(b) The pressure change as consequence of the shock movement across the orifice does not occur instantaneously, but the  $C_p=f(M)$  curve shows a distinct slope, and this slope is different for the acceleration and for the deceleration phase. A physical interpretation of these observations is given in Paragraph 2.f.

(c) The Mach number at which the shock hits the orifice, i.e., at which the steep pressure rise or pressure drop begins is - within the accuracy of these measurements - identical during acceleration and during deceleration. This observation confirms that the instantaneous shock location depends - for a given orifice location and angle of attack, on aerodynamic parameters (Mach number) only and is independent of whether the sled is accelerating or decelerating (Figure 16).

(6) For the same (59% chord) location Figures 17 and 18 show pressure and pressure coefficients versus Mach number measured during run 58X-G11A which provided two periods of "quasi-constant" speed. These figures show the same trend noticeable in Figures 15 and 16 except for two "loops" due to the fact that the sled did not reach constant speed, but that the drag was slightly overcompensated resulting in two brief periods of acceleration.

#### f. TIME DELAY IN PRESSURE MEASUREMENTS

(1) The problem of time delay is not, as a rule, a major obstacle inherent in the track test method. In test setups which are genuinely designed for surface pressure measurements during rocket sled runs the problem of time delay is circumvented and extremely high frequency responses are achieved by locating the transducer in the immediate vicinity of the orifice. This method is successfully used on a routine basis in track tests where surface pressure measurements are performed to study shock on shock interactions, to assess the effects of blast wave intercepts with aircraft models and missile components under simulated flight conditions, and in support of aero-elastic investigations involving full scale hardware components.

(2) It was recognized from the beginning of this test series that the use of this test model, which was built for wind tunnel testing under equilibrium conditions at specific fixed Mach numbers and uses long, small diameter tube lines between the orifices and the transducers would require the development of methods to assess the magnitude and to compensate for the effects of the resulting time delays.



(3) Time delay in tube lines depends upon tube lengths, tube diameter, tube material, the resistance of obstructions, connections, etc in the tubes, and the original pressure differential. Various theoretical methods and computer programs are available to solve this problem - Reference 11 is an example. Various theoretical methods were investigated, but without real success; primarily because the question in track testing is not to calculate the time until equilibrium is reached following, e.g., a step function change, but to compensate the readings, on a continuing basis, as a function of varying sled velocity and sled acceleration.

(4) In order to reduce time delay effects the sled trajectories were arranged as described in Paragraph 2.c. and the period of "sustained" deceleration was designated as the prime data acquisition phase of each run.

(5) The following considerations, which were not developed until the test series was completed, are intended to physically interpret the data presented in Figures 15 - 18 and to show how the time delay problems may be minimized in future track tests of this kind:

(a) Let  $\Delta t$  be the time delay, i.e., the time elapsed from the instant the orifice sees a specified surface pressure  $P_e$ (psig) to the point in time when the transducer actually reads this pressure. Let the subscript 1 refer to the acceleration phase of the run, subscript 2 to the deceleration phase, and let:

$$\begin{aligned}\dot{V} \text{ ft/sec}^2 &= \text{sled acceleration} \\ a \text{ ft/sec} &= \text{speed of sound} \\ M &= \text{Mach number}\end{aligned}$$

(b) Let us assume that the observation reported in Paragraph e.(5)(c) is generally applicable, and that for a given angle of attack and a given set of ambient conditions the surface pressure sensed by a particular orifice is strictly a function of Mach number and independent of whether the sled is accelerating or decelerating. During the acceleration phase the pressure  $P_e$  which the transducer reads at the Mach number  $M_1$  while the sled is accelerating at the rate  $\dot{V}_1$  is actually the pressure which affected the orifice  $\Delta t_1$  sec earlier, while the sled was at a Mach number  $M_e$ . Likewise, during the deceleration phase the transducer reads the same pressure  $P_e$  while the sled travels at the Mach number  $M_2$ , which occurs  $\Delta t_2$  sec later than the pressure  $P_e$  actually acted at the orifice. Then:

$$\begin{aligned}M_e &= M_1 + \Delta M_1 = M_2 + \Delta M_2 \\ \Delta M_1 &= \Delta t_1 \frac{\dot{V}_1}{a} \\ \Delta M_2 &= \Delta t_2 \frac{\dot{V}_2}{a} = \Delta t_1 \frac{\Delta t_2}{\Delta t_1} \frac{\dot{V}_2}{a} \\ \Delta t_1 &= a \frac{M_1 - M_2}{\dot{V}_1 - \dot{V}_2 \frac{\Delta t_2}{\Delta t_1}}\end{aligned}$$

Numerical values for the ratio  $\Delta t_2/\Delta t_1$  as function of the accelerations  $\dot{V}_1$  and  $\dot{V}_2$  need to be established experimentally. Let us, for simplicity, assume that  $\Delta t$  is independent of the acceleration rate. Then  $\Delta t_2 = \Delta t_1 = \Delta t$  and

$$\Delta t = a \frac{M_1 - M_2}{\dot{V}_1 - \dot{V}_2}$$

The assumption that the difference between  $\Delta t_1$  and  $\Delta t_2$  is insignificant is certainly questionable, however, it appears to be experimentally supported for the case at hand by the data reported in the following example 2.

(c) Two examples are illustrated in Table 5 and Figure 17, using data from run number 56X-G11A where the attempt was made to provide two constant speed periods. The first example shows that during deceleration at  $-44.8 \text{ ft/sec}^2 = -1.39g$ 's the time delay is - as expected - rather low, while the values obtained during the acceleration phase ( $176 \text{ ft/sec}^2 = 5.5g$ 's) are very strongly affected. The second example is selected to demonstrate that the assumption of an equal delay time  $\Delta t$  for acceleration and deceleration despite differences in acceleration rates is supportable.  $M_1$  and  $M_2$  are selected to show the same pressure  $P_e$  which is reached during the short period while the sled travels at the constant Mach number  $M_3 = .797$ . As indicated, within the accuracy of pressure and sled performance listings (not included in this report) the calculated Mach number  $P_e = .797$  is equal to the one at which the sled traveled at constant Mach number, providing a short equilibrium period between transducer and orifice.

(d) This procedure of estimating time delay can easily be programmed and incorporated in the data evaluation process to produce corrected curves  $P_e = f(M)$ . At the time when the data reported in this report were processed, this analysis had not yet been performed, and data recorded during the "sustained" deceleration period (not exceeding  $-1g$ ) are used in Figures 19 - 24 for the comparison between sled and wind tunnel measurements.

#### COMPARISON OF SLED DATA WITH WIND TUNNEL AND FLIGHT TEST RESULTS

1. Figure 19 presents the chordwise pressure distribution on the upper surface of the wing section as obtained during sled runs at which the model was aligned to angles of attack of  $-1.10^\circ$ ,  $0^\circ$ ,  $3.80^\circ$  and  $5.00^\circ$  with respect to the nominal free-stream flow direction. The data are expressed in terms of the pressure coefficient.

$$c_p = \frac{P - P_\infty}{q_\infty}$$

for a free-stream Mach number of 0.825, which is typical for the cruise Mach number of the airplane under consideration. All of these data were taken during the "sustained" deceleration phase of the run at a nominal deceleration rate of approximately  $-1g$ .

2. Figure 20 shows the same sled data for angles of attack of 0, 3.8 and 5 degrees compared with data taken at 2 degrees angle of attack and at  $M = 0.85$  in the AEDC 40 inch transonic wind tunnel as presented in Reference 6. The data compare reasonably well except for a mismatch in shock location which is most likely due to the mismatch in Reynolds number.

3. Figures 21 - 23 compare the sled test data with measurements obtained in the NASA-AMES-11 ft transonic wind tunnel for which this specific model and its contoured end plate configuration were originally designed. The wind tunnel data were made available by direct communication between the Test Track and the AMES Research Center. Figure 23 includes the pressure distribution on the lower surface. While the pressures up to approximately 10% of chord and the shock location compare reasonably well, the pressure data obtained on the sled at chord-wise positions between 10% and the shock location are persistently higher than the wind tunnel results.

4. Figure 24 compares sled test results at 0 degree angle of attack with data obtained in the NASA-AMES-11 ft transonic wind tunnel at -0.026 degrees and at 1.1 degree. The NASA-AMES data at 1.1 degree and the flight test data were taken from Reference 4; the wind tunnel data at -0.026 degrees were made available by direct communication between the Test Track and the NASA-AMES Research Center. The data show a surprising similarity between the sled measurements at 0 degree angle of attack and the wind tunnel data at 1 degree. The flight data are considerably higher than both the sled and wind tunnel results, however, the shock location matches the shock location obtained on the sled although the sled Reynolds number is by a factor of two lower than the one experienced in flight.



### 3. SUMMARY

a. A series of rocket sled runs was conducted on the Test Track at Holloman AFB, New Mexico, during which pressure distributions were measured on a sled-borne aircraft wing model at Mach numbers up to 0.95. The wing model used in these tests had been originally built for testing in the NASA-AMES-11 ft transonic wind tunnel and had been made available for these tests by the NASA-AMES Research Center.

b. Test hardware, test instrumentation, data acquisition/processing and operational aspects of this test series are described. Selected examples of data obtained in the course of those tests are presented, discussed and compared with wind tunnel and flight test results.

c. Boundary layer measurements and tuft observation of the flow over the sled top surface (model ground plane) did not indicate any effects of sled-ground interference on the flow over the wing model. The lower contoured end plate of the model effectively isolated the flow over the model from the sled-top surface boundary layer.

d. No problems were encountered in adjusting and holding the preset angles of attack. Model deflections due to inertial forces were shown by analysis to be of no influence on the aerodynamic data obtained.

e. After an initial learning period no problems were encountered with respect to accuracy and repeatability of on-board instrumentation, data transmission by PCM telemetry and data processing.

(1) A response of the pressure sensing transducers (unbonded strain gage type instruments) to high onsets (rates of change of acceleration) was noted during rocket staging. These responses could easily be isolated and identified.

(2) Determination of free-stream Mach number as function of time was performed by means of electro-optical sled velocity measurements at a much higher accuracy than could have been achieved by pitot pressure measurements.

f. The ability to "sweep" the entire Mach number regime of interest offers the advantage of obtaining a large number of data points during each test mission. The absence of steady-state conditions during routine rocket sled runs, however, makes provisions mandatory to eliminate or correct for time lag in pressure lines, unless the model is specifically built to alleviate this problem. The long, narrow cross section pressure lines used on this model, which was built for wind tunnel applications, made this problem especially difficult.

(1) This problem is virtually non-existent if the model is specifically designed and built for track testing and the pressure sensing instruments are located immediately below the surface. This is demonstrated by various highly successful test programs (not related to this test series) in the area of measuring response to blast wave intercept.

(2) The pressure time lag can be compensated by running the sled for time increments of 1 - 5 seconds at constant sled velocity; this is difficult to achieve with rocket propulsion, can, however, be accomplished if jet-engine propulsion is used.

(3) The method used in this series - operating the sled for the prime data acquisition period of the trajectory at reduced deceleration levels (less than  $-1g$ ) improved upon, but did not totally eliminate the time lag problem.

(4) Attempts to correct for time lag on the basis of theoretically derived algorithms were unsuccessful; however, a relatively simple semi-experimental correction method, based on data obtained on a specific orifice under acceleration and deceleration, is proposed for future tests of this kind. It can be easily incorporated in the computer programs for processing these data; however, it was recognized only after data processing for this test series had been completed.

## REFERENCES

1. The Holloman Track, Facilities and Capabilities, ADTC, 6585 Test Group, Holloman AFB, New Mexico, 1974.
2. Rasmussen, Hans J., High Reynolds Number Testing by Means of Rocket Sleds, AGARD Conference Proceedings Nr. 83 on Facilities and Techniques for Aerodynamic Testing at Transonic Speeds and High Reynolds Numbers, Paper Nr. 33, Gottingen, Germany, April 1971.
3. Whitcomb, R. T. and Clark, L. R., An Airfoil Shape for Efficient Flight at Supercritical Mach Numbers. NASA TM-X-1109, July 1965.
4. Cahill, Jones F., Treon, Stuart L. and Hofstetter, William R., Feasibility of Testing a Large-Chord, Swept-Panel Model to Determine Wing Shock Location at Flight Reynolds Number. AGARD Conference Proceedings Nr. 83 on Facilities and Techniques for Aerodynamic Testing at Transonic Speeds and High Reynolds Numbers, Paper Nr. 17, Gottingen, Germany, April 1971.
5. Cahill, Jones F., Simulation of Full-Scale-Flight Aerodynamic Characteristics by Tests in Existing Transonic Wind Tunnels. AGARD Conference Proceedings Nr. 83 on Facilities and Techniques for Aerodynamic Testing at Transonic Speeds and High Reynolds Numbers, Paper Nr. 20, Gottingen, Germany, April 1971.
6. Tirres, Carlos, Transonic Scale Effects and Test Techniques. Paper presented at the 1973 AFSC Science and Engineering Symposium, Kirtland AFB, New Mexico, October 1973.
7. Unger, E. and Bandgren H., Rocket Sled Model Study of Prediction Techniques for Fluctuating Pressures and Panel Responses, Proceedings, 41st Structural Vibration and Shock Symposium, October 1970.
8. Cahill, Jones F. and Cooper, Bill L., Flight Test Investigation of Transonic Shock-Boundary Layer Phenomena. AFFDL-TR-68-84 (2 Volumes), July 1968.
9. Cahill, Jones F. and Stanewski, E., Wind Tunnel Tests of a Large-Chord, Swept Panel Model to Investigate Shock-Induced Separation Phenomena, AFFDL-TR-69-78, October 1969.
10. Blakerby, W. T. and Cahill, J. F., High Reynolds Number Tests of a C141A Aircraft Semi-span Model to Investigate Shock-Induced Separation. NASA-CR-2604, October 1975.
11. McKee, M. L., Digital Computer Oriented Methods for Determining the Response of Pressure Measurement Systems to Step and Ramp Forcing Functions. AEDC-TR-66-225, AD 648457, March 1967.



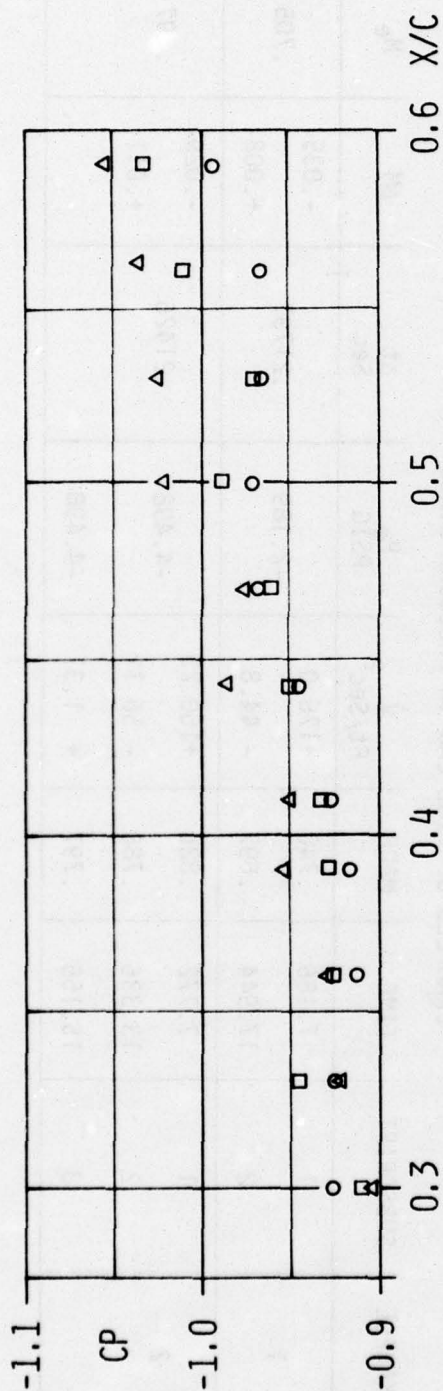
TABLE 1

## LOCATIONS OF ORIFICES ON UPPER AND LOWER WING SURFACE

B L 36.0 (Center Row) Upper Surface			B L 36.0 (Center Row) Lower Surface		
Pressure Orifice (PW No)	Distance X from Chord Station 0.0 (Inches)	X/C	Pressure Orifice (PW No)	Distance X from Chord Station 0.0 (Inches)	X/C
1	.210	.005	38	.210	.005
2	.420	.010	39	.420	.010
3	.840	.020	40	.840	.020
4	1.260	.030	41	1.260	.030
5	1.680	.040	42	1.680	.040
6	2.100	.050	43	2.100	.050
7	3.150	.075	44	3.150	.075
8	4.200	.100	45	4.200	.100
9	5.250	.125	46	5.250	.125
10	6.300	.150	47	6.300	.150
11	7.350	.175	48	7.350	.175
12	8.400	.200	49	8.400	.200
13	9.450	.225	50	9.450	.225
14	10.500	.250	51	10.500	.250
15	11.550	.275	52	11.550	.275
16	12.600	.300	53	13.860	.330
17	13.860	.330	54	16.380	.390
18	15.120	.360	55	18.480	.440
19	16.380	.390	56	21.000	.500
20	17.220	.410	57	23.520	.560
21	18.480	.440	58	26.040	.620
22	19.740	.470	59	28.560	.680
23	21.000	.500	60	31.080	.740
24	22.260	.530	61	33.600	.800
25	23.520	.560	62	36.120	.860
26	24.780	.590	63	38.630	.920
27	26.040	.620	64	41.160	.980
28	27.300	.650			
29	28.560	.680			
30	29.820	.710			
31	31.080	.740			
32	32.340	.770			
33	33.600	.800			
34	36.120	.860			
35	38.640	.920			
36	41.160	.980			
37	42.000	1.000			

TABLE 2

INPUT	OUTPUT												
	Channel 1		Channel 2		Channel 3		Channel 4		Channel 5		MEAN		SIGMA
P <sub>O</sub>	P	P-P <sub>O</sub>	P	P-P <sub>O</sub>	P	P-P <sub>O</sub>	P	P-P <sub>O</sub>	P	P-P <sub>O</sub>	P	P-P <sub>O</sub>	
PSIG	PSIG		PSIG		PSIG		PSIG		PSIG		PSIG		
4.425	4.425	.000	4.406	+.019	4.446	-.021	4.484	-.059	4.472	-.047	4.447	-.022	.032
2.480	2.467	+.130	2.489	-.009	2.468	+.012	2.489	-.009	2.504	-.024	2.483	-.003	.016
0.498	.548	-.050	.544	-.046	.548	-.050	.553	-.055	.517	-.019	.542	-.044	.014
0.000	.000	.000	.000	.000	.000	.000	.000	.000	.0397	-.0397	.008	-.008	.00006304



x/c	Run Nr: PW NO	56X-G6A CP	56X-G7A CP	56X-G8A CP	MEAN	SIGMA	SIGMA 100% MEAN
.300	16	-0.926	-0.905	-0.910	-0.914	.011	1.2
.330	17	-0.925	-0.923	-0.946	-0.931	.013	1.4
.360	18	-0.913	-0.930	-0.924	-0.922	.009	1.0
.390	19	-0.918	-0.955	-0.929	-0.934	.019	2.0
.410	20	-0.927	-0.950	-0.933	-0.937	.012	1.3
.440	21	-0.946	-0.987	-0.951	-0.961	.022	2.3
.470	22	-0.970	-0.977	-0.961	-0.969	.008	0.8
.500	23	-0.971	-1.024	-0.988	-0.994	.027	2.7
.530	24	-0.967	-1.025	-0.969	-0.987	.033	3.3
.560	25	-0.967	-1.035	-1.012	-1.005	.035	3.5
.590	26	-0.994	-1.055	-1.034	-1.028	.031	3.0

TABLE 3 REPEATABILITY OF SLED TEST DATA AT  $M = 0.825$   
 UPPER SURFACE WING PRESS COEF FOR THREE SLED RUNS  
 $Q=876$  PSF  $RN=5.52 \times 10^6$  PER FT  $\alpha=5.0^\circ$  (NOM)



TABLE 4  
MOVEMENT OF SHOCK ACROSS PRESSURE ORIFICE

ORIFICE LOCATION		TIME OF SHOCK PASSING (SEC)		
% Chord	Inch From Leading Edge	Accelerating	Decelerating	
59%	24.78	7.8	14.7	
77%	32.34	8.4	10.6	
Differences:	7.56	0.6	4.10	
Speed of Shock Movement (inch/sec)		12.6	1.84	

TABLE 5  
EXAMPLES OF TIME LAG IN PRESSURE LINES

EXAMPLE	SUBSCRIPT	TIME	MACH	$\dot{V}$ Ft/Sec <sup>2</sup>	$P_e$ PSIG	$\Delta t$ Sec	$\Delta M$	$M_e$
1	1	7.186	.740	+176.0	-2.189	.21797	-.035	.705
	2	17.944	.697	- 44.8			+.008	
2	1	7.772	.826	+150.23	-4.498	.21426	-.029	.797
	2	13.336	.786	- 56.11			+.011	
	3	15.155	.797	+ 1.31	-4.498			

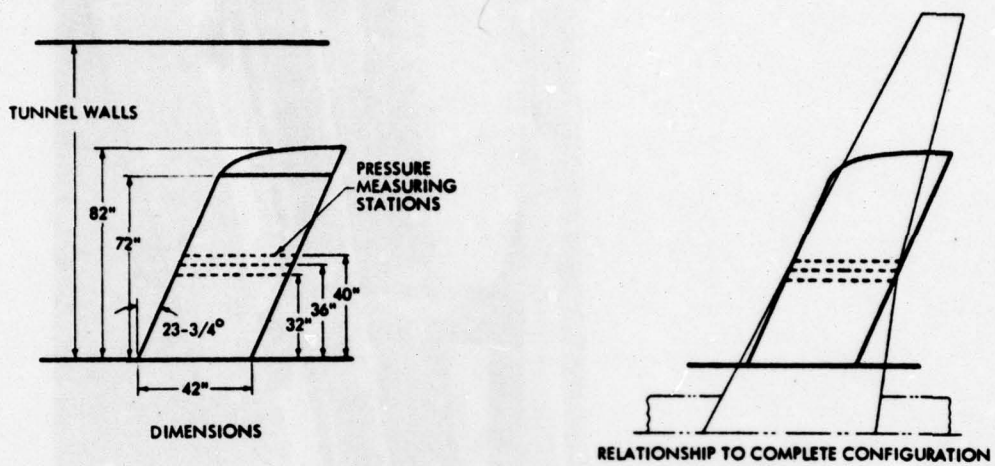


FIGURE 1 PANEL MODEL (FROM REFERENCE 4)

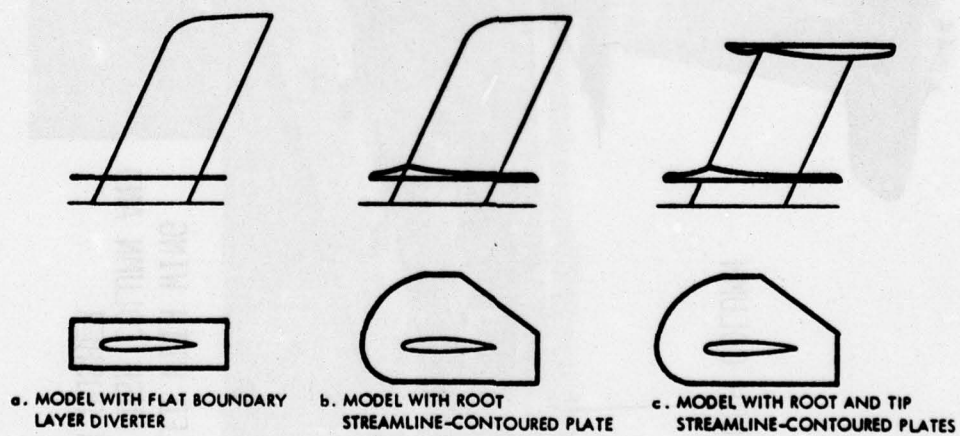
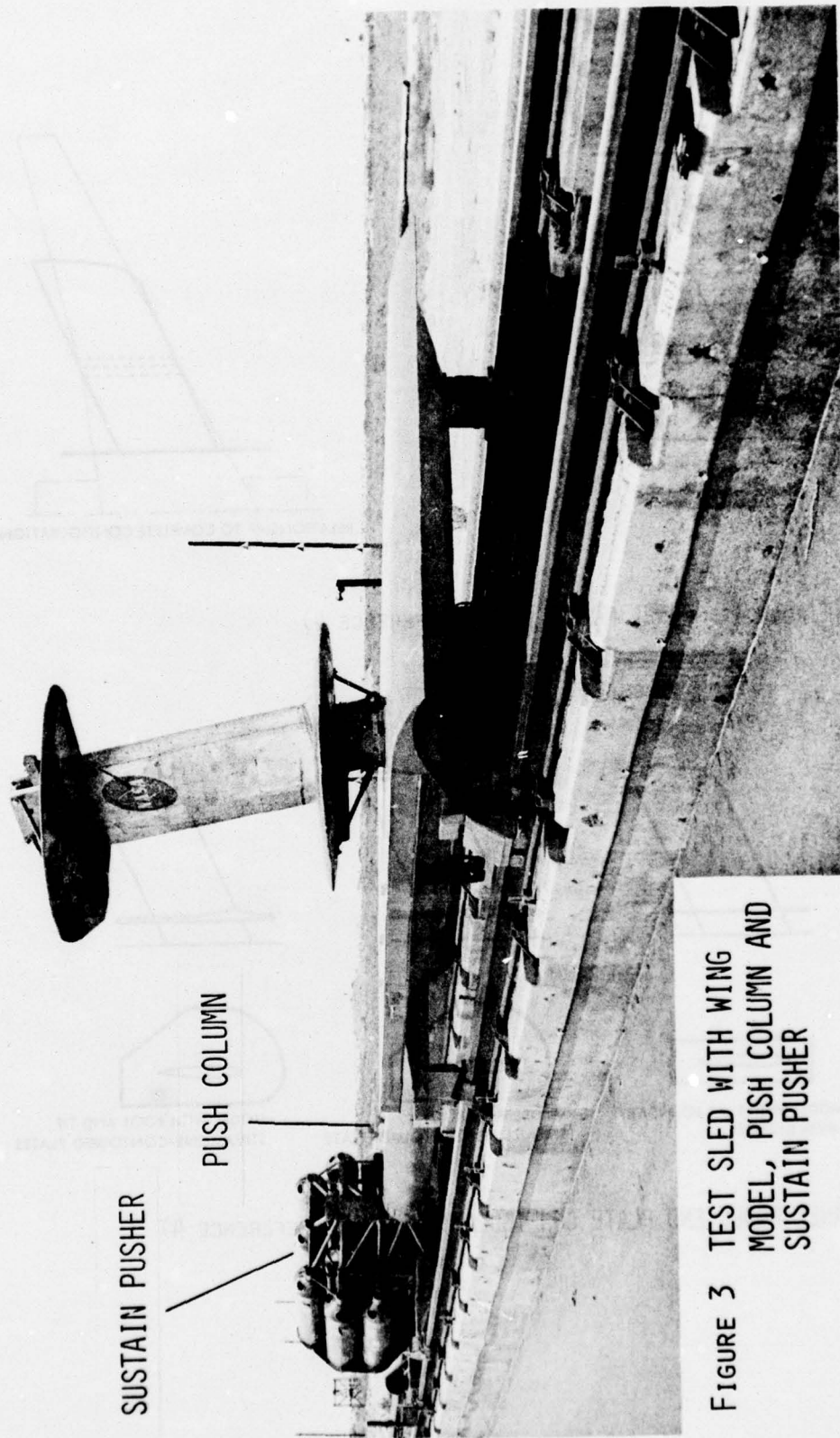


FIGURE 2 PANEL MODEL END PLATE CONFIGURATIONS (FROM REFERENCE 4)



SUSTAIN PUSHER

PUSH COLUMN

FIGURE 3 TEST SLED WITH WING  
MODEL, PUSH COLUMN AND  
SUSTAIN PUSHER



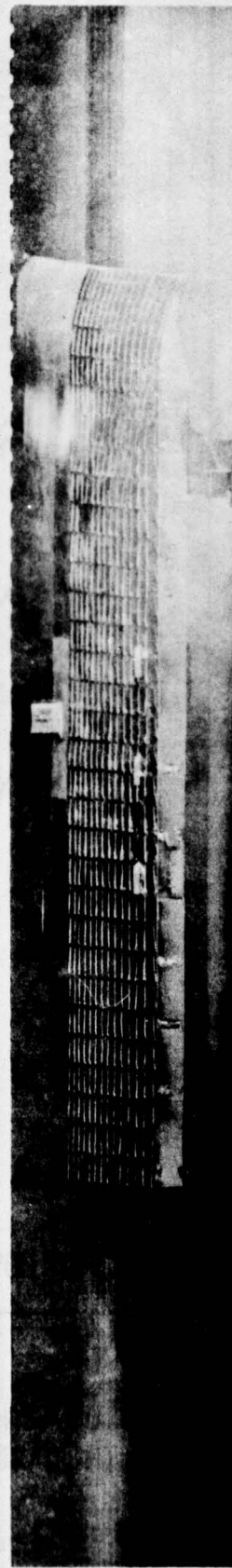
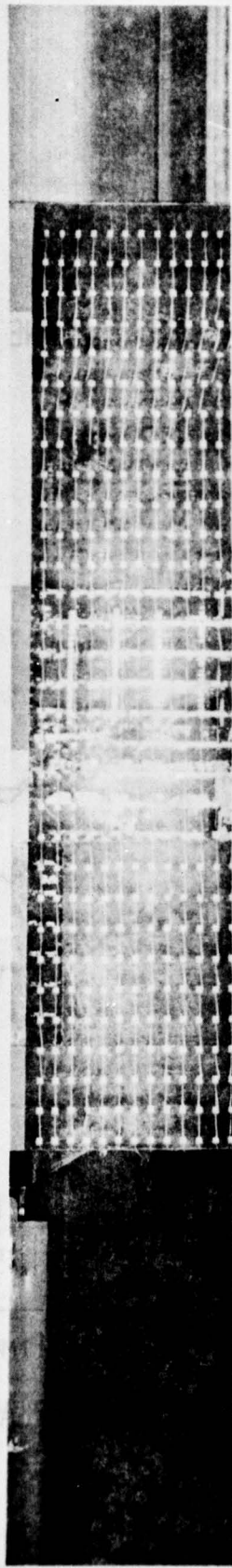


FIGURE 4 SLED GROUND PLANE WITHOUT TEST MODEL, WITH TUFTS  
AND BOUNDARY LAYER RAKE

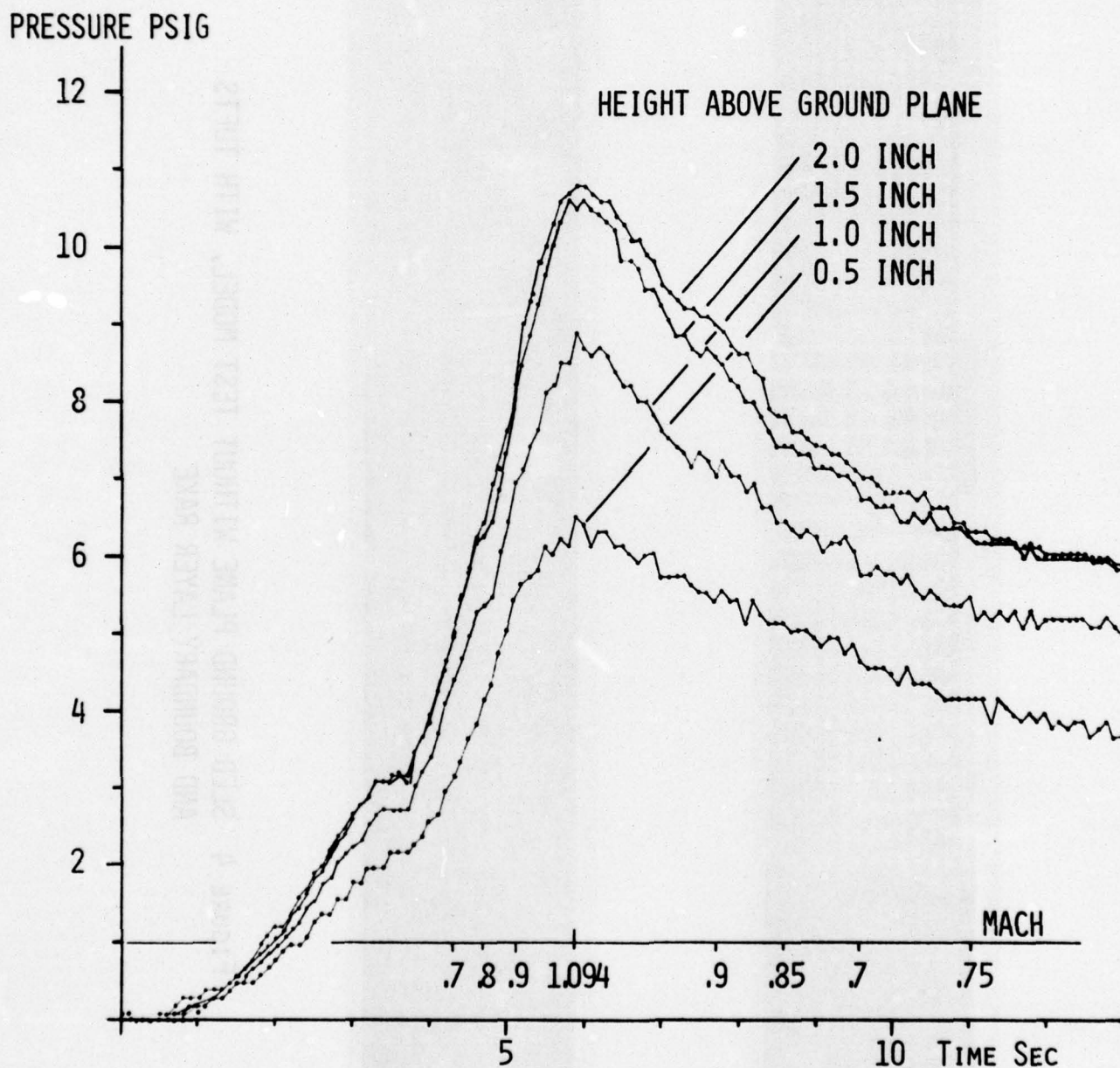


FIGURE 5 PRESSURE READINGS ON CENTERLINE OF SLED GROUND PLANE  
WITH BOUNDARY LAYER RAKE



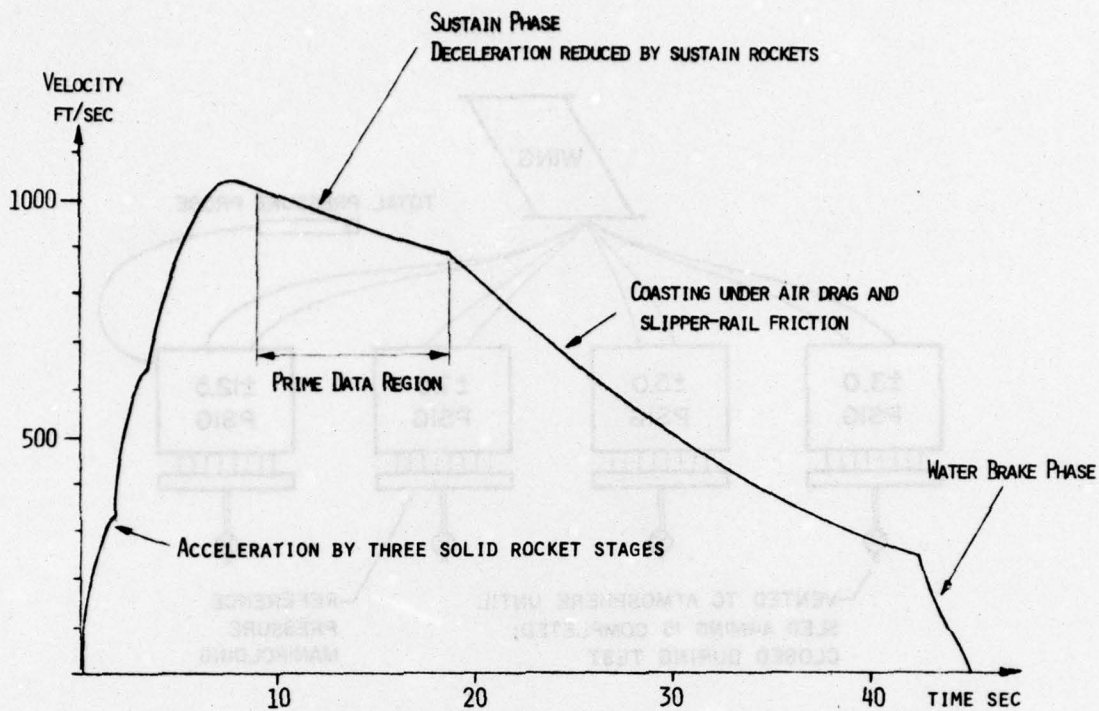


FIGURE 6 TYPICAL VELOCITY - TIME HISTORY OF A ROCKET SLED RUN (SCHEMATIC)

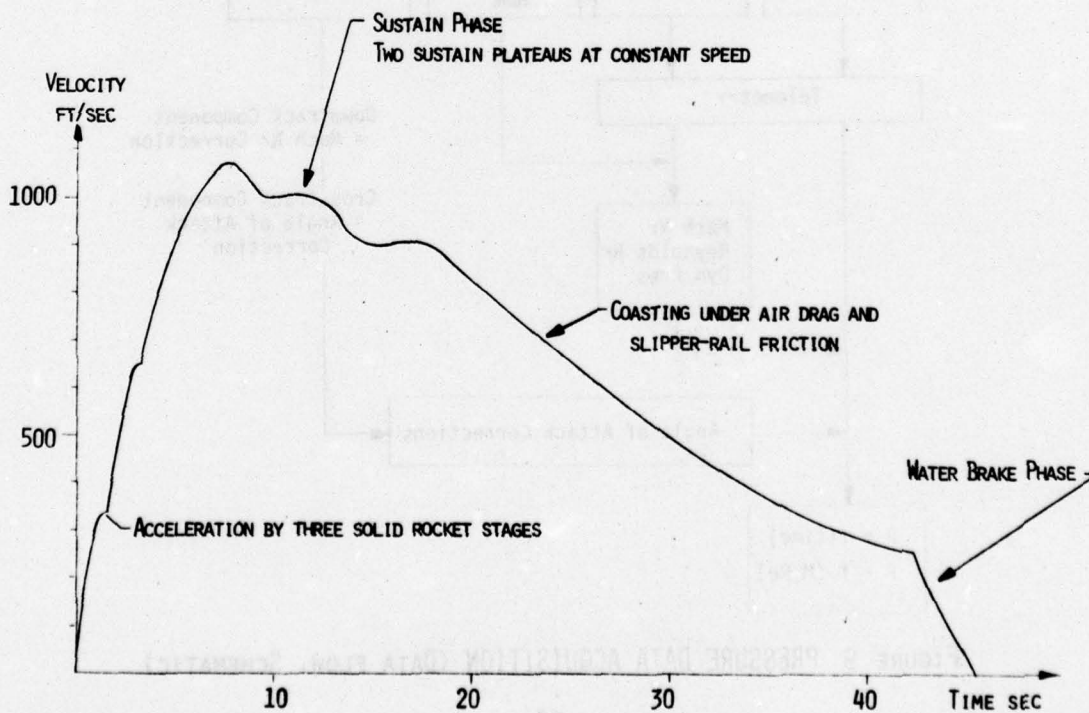


FIGURE 7 TYPICAL VELOCITY - TIME HISTORY OF A ROCKET SLED RUN INCLUDING TWO SUSTAIN PHASES AT CONSTANT SPEED (SCHEMATIC)

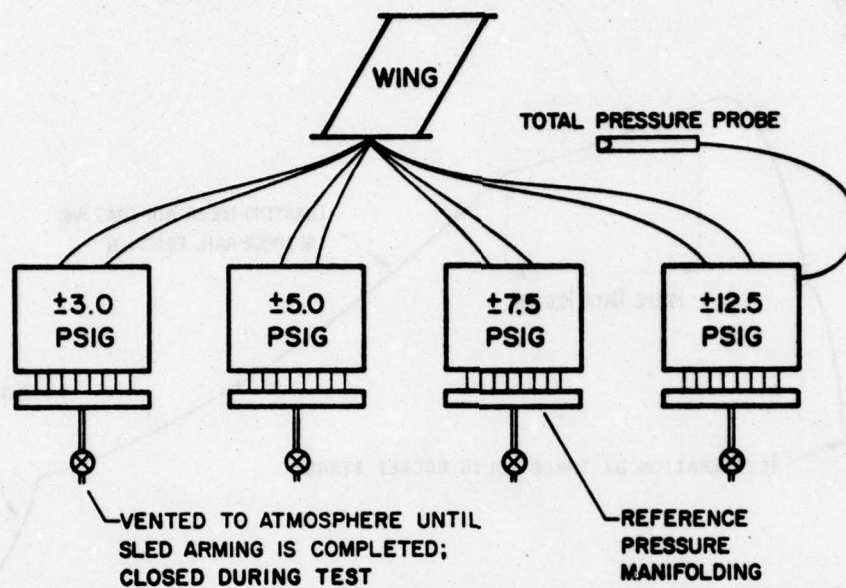


FIGURE 8 TRANSDUCER TUBING AND REFERENCE SYSTEM (SCHEMATIC)

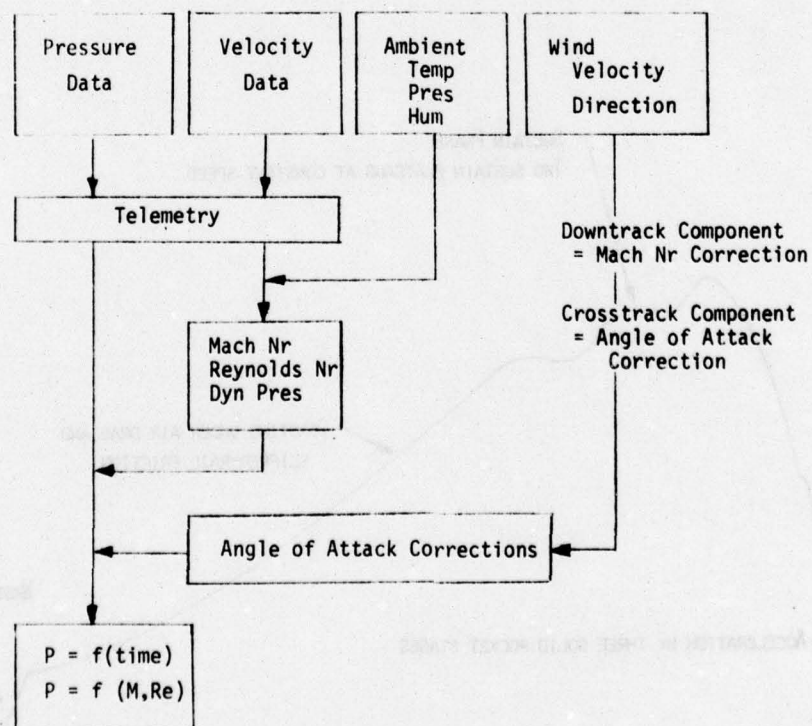


FIGURE 9 PRESSURE DATA ACQUISITION (DATA FLOW, SCHEMATIC)

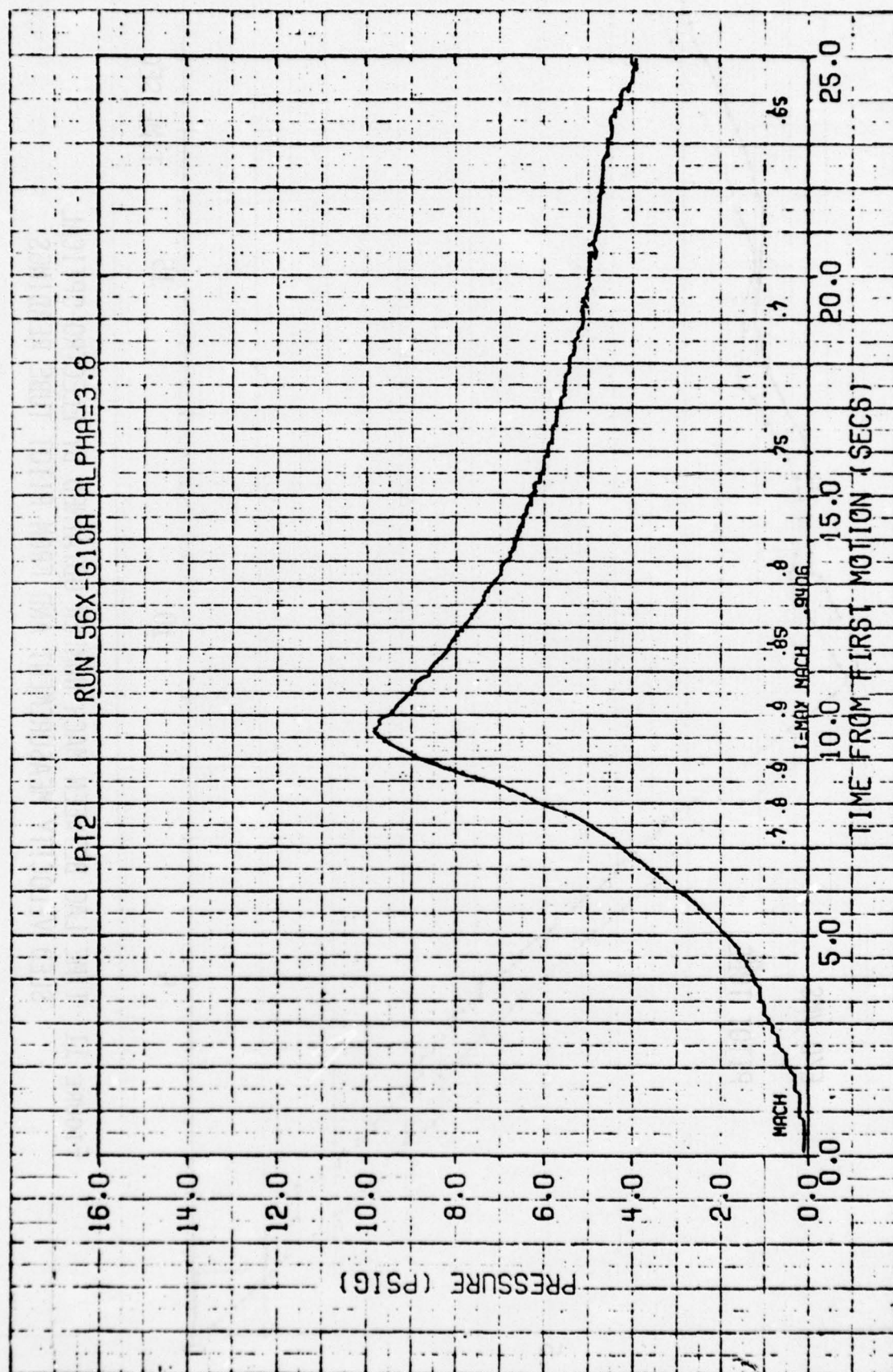


FIGURE 10 PITOT PRESSURE AS FUNCTION OF TIME DURING A TYPICAL ROCKET SLED RUN



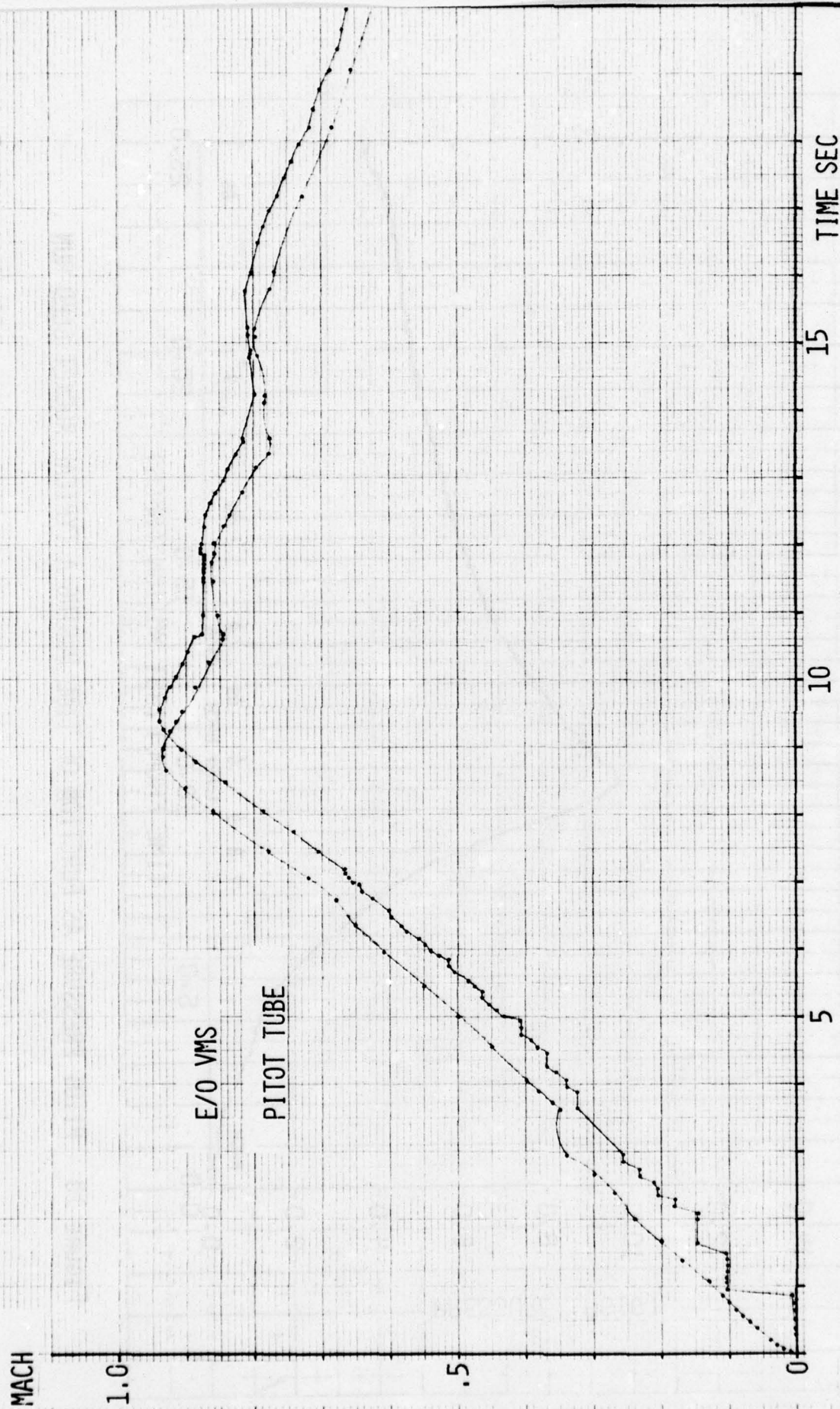


FIGURE 11 TIME LAG BETWEEN MACH NUMBER OBTAINED BY ELECTRO-OPTICAL SLED VELOCITY MEASUREMENT AND FROM PITOT TUBE READINGS

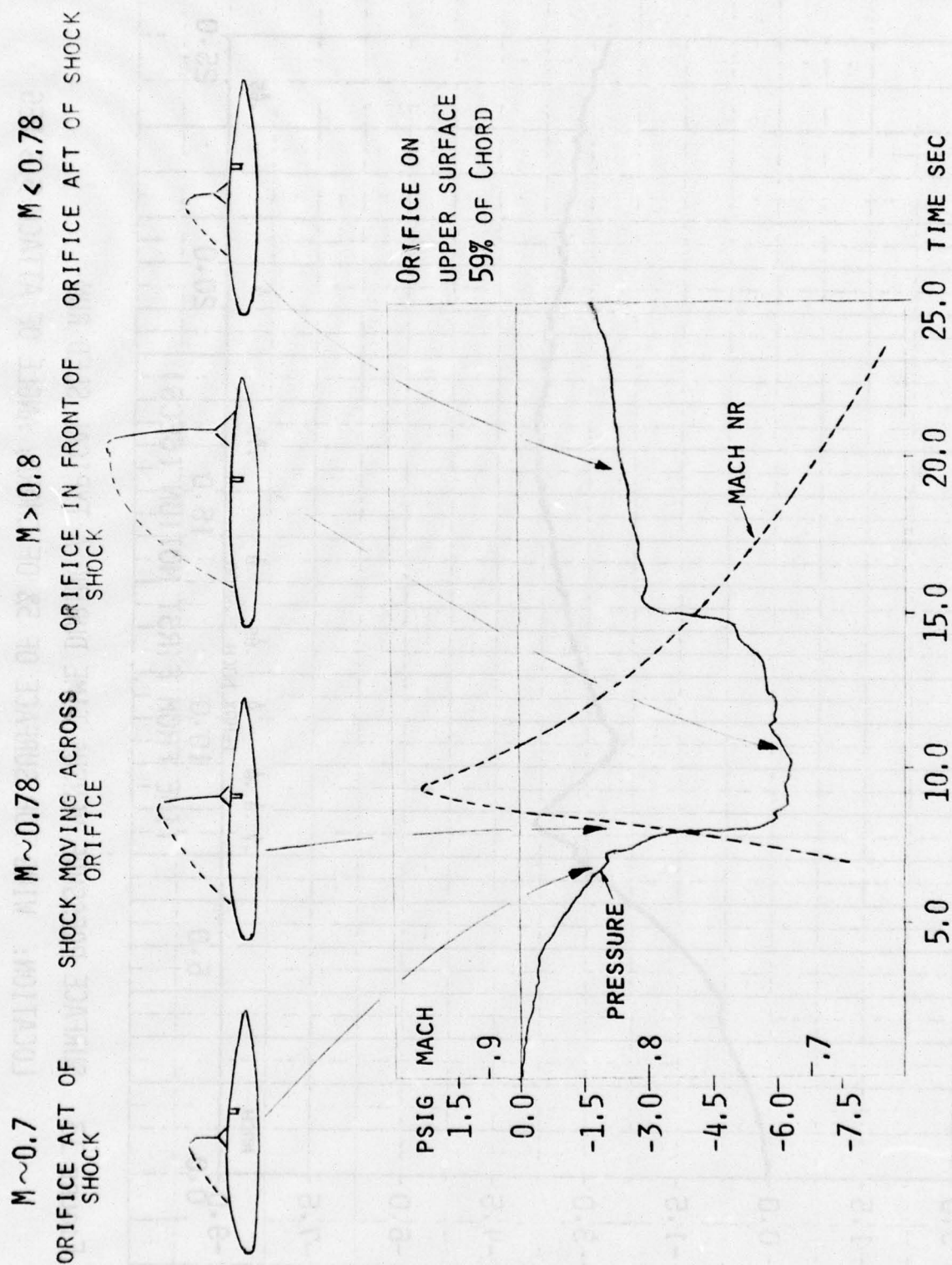


FIGURE 12 TYPICAL CHANGE OF SHOCK LOCATION ON TOP SURFACE OF WING (SCHEMATIC)



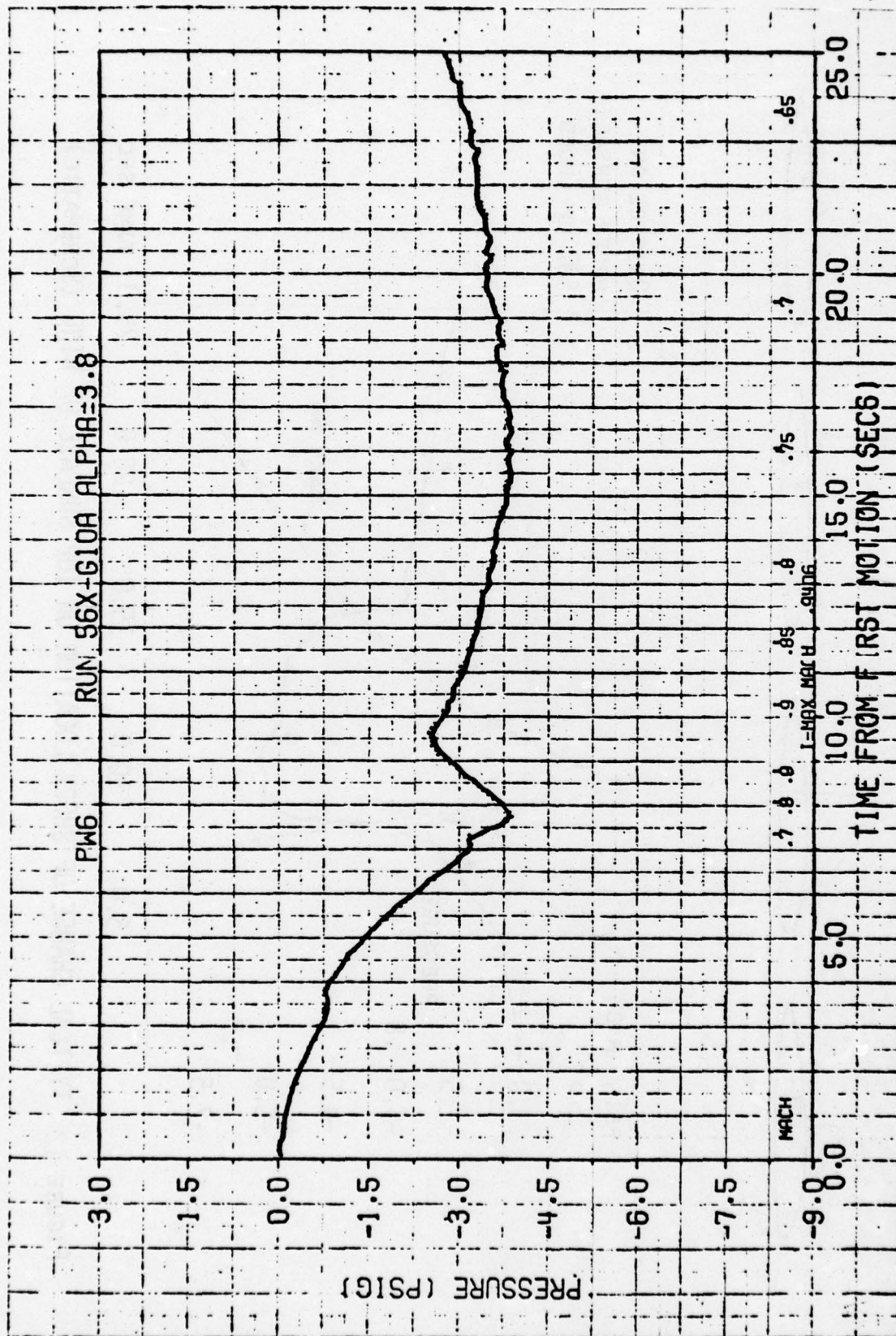


FIGURE 13 SURFACE PRESSURE VERSUS TIME DURING A TYPICAL SLED RUN

LOCATION: WING TOP SURFACE OF 5% OF CHORD; ANGLE OF ATTACK 3.8 DEG



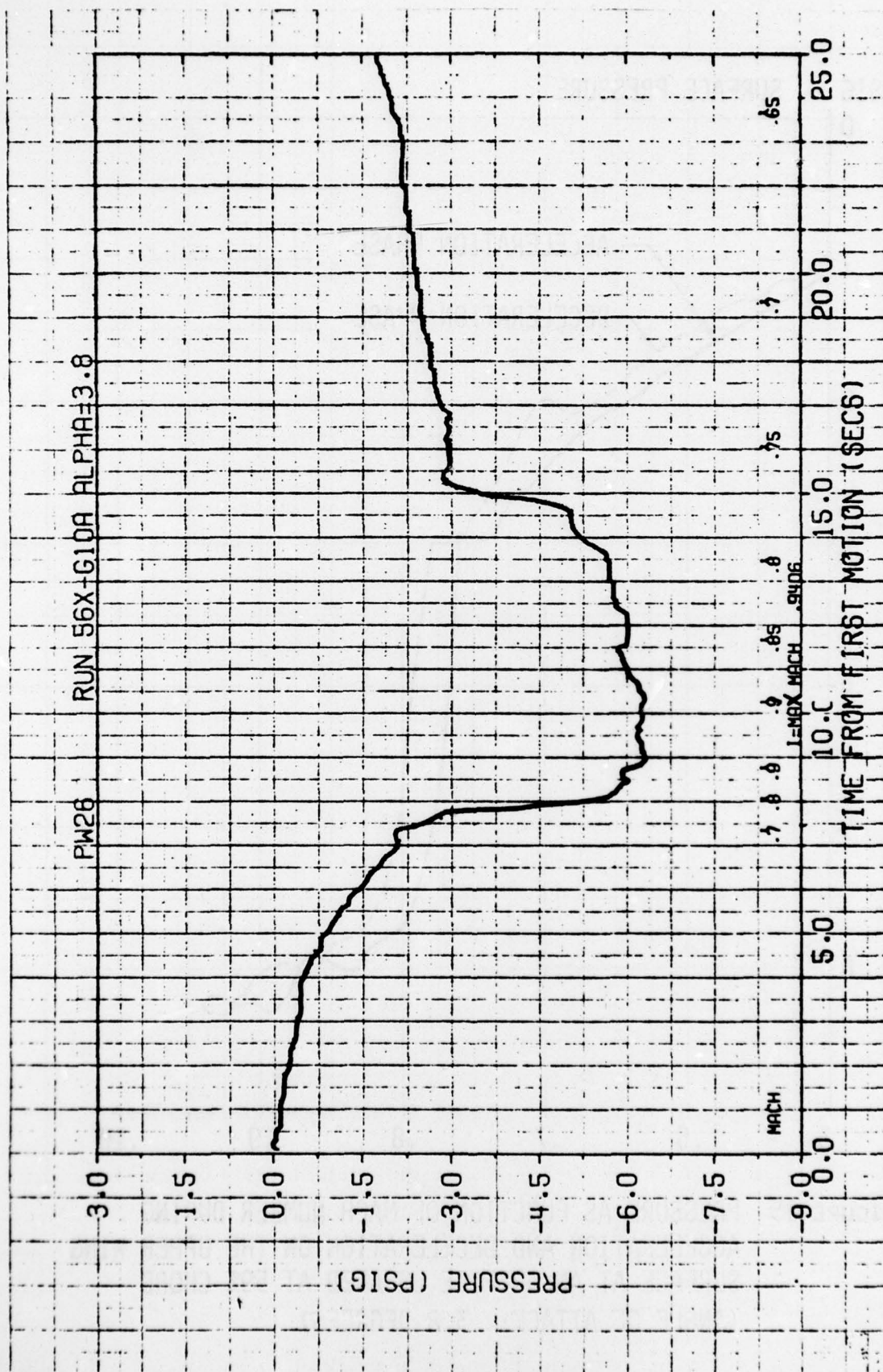


FIGURE 14 TYPICAL EXAMPLE OF PRESSURE READING ON UPPER SURFACE OF WING AS FUNCTION OF TIME DURING A ROCKET SLED RUN. (ORIFICE LOCATION AT 59% OF CHORD; ANGLE OF ATTACK 3.8 DEG)

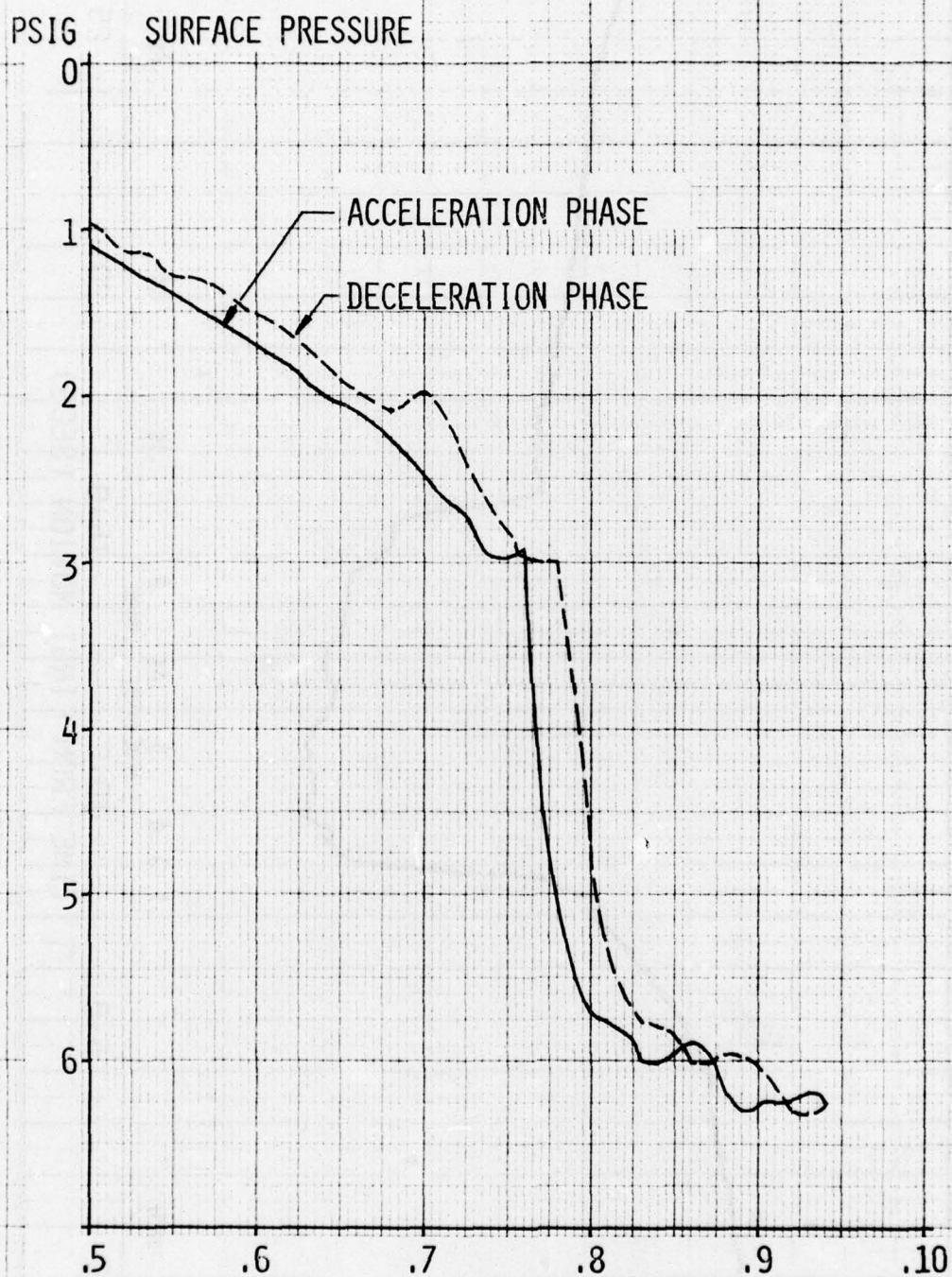


FIGURE 15 PRESSURE AS FUNCTION OF MACH NUMBER DURING ACCELERATION AND DECELERATION ON THE UPPER WING SURFACE AT AN ORIFICE LOCATED AT 59% CHORD (ANGLE OF ATTACK: 3.8 DEGREES)

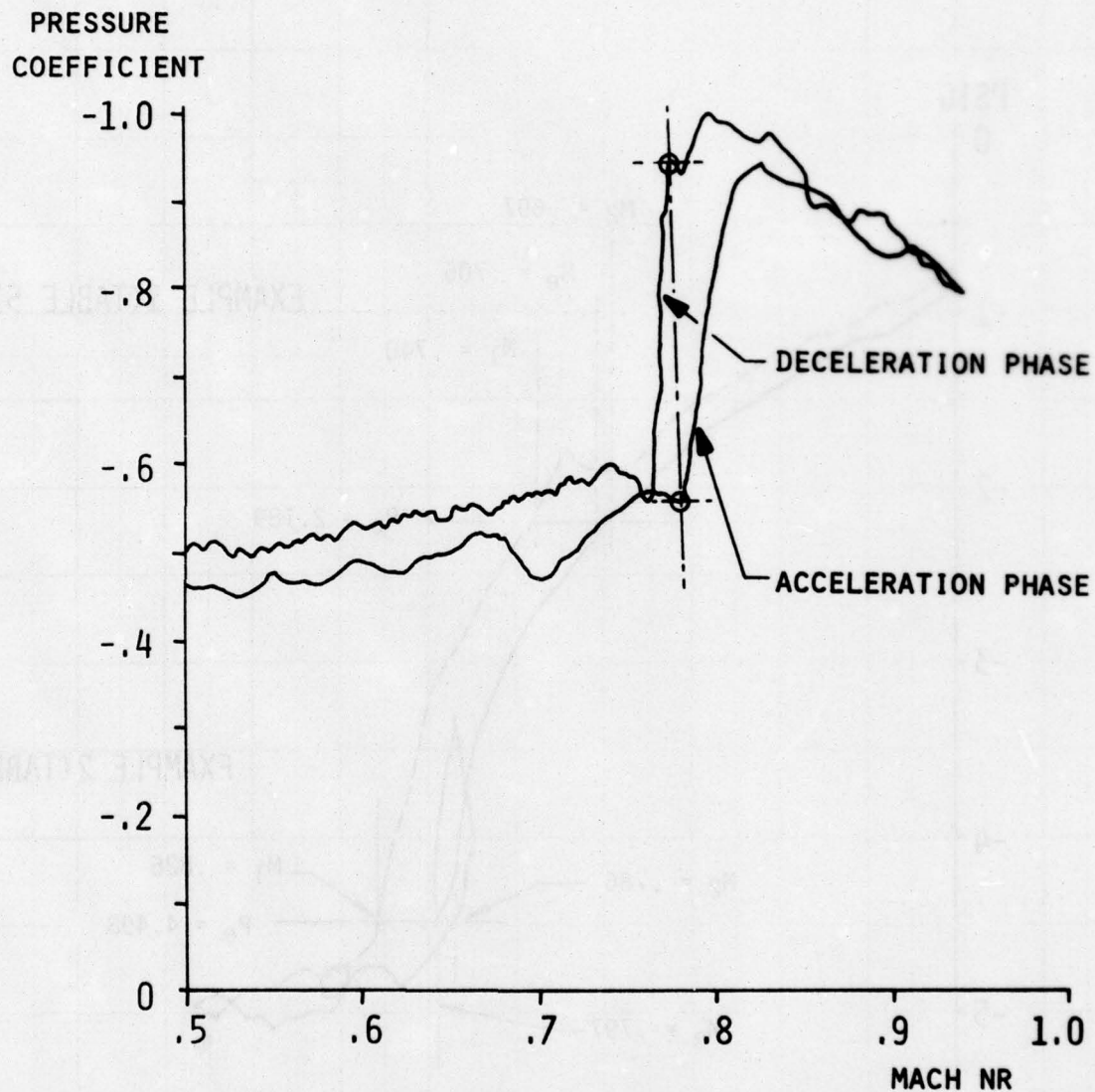


FIGURE 16 PRESSURE COEFFICIENT AS FUNCTION OF MACH NUMBER DURING ACCELERATION AND DECELERATION ON THE UPPER WING SURFACE AT AN ORIFICE LOCATED AT 59% CHORD (ANGLE OF ATTACK: 3.8 DEG)



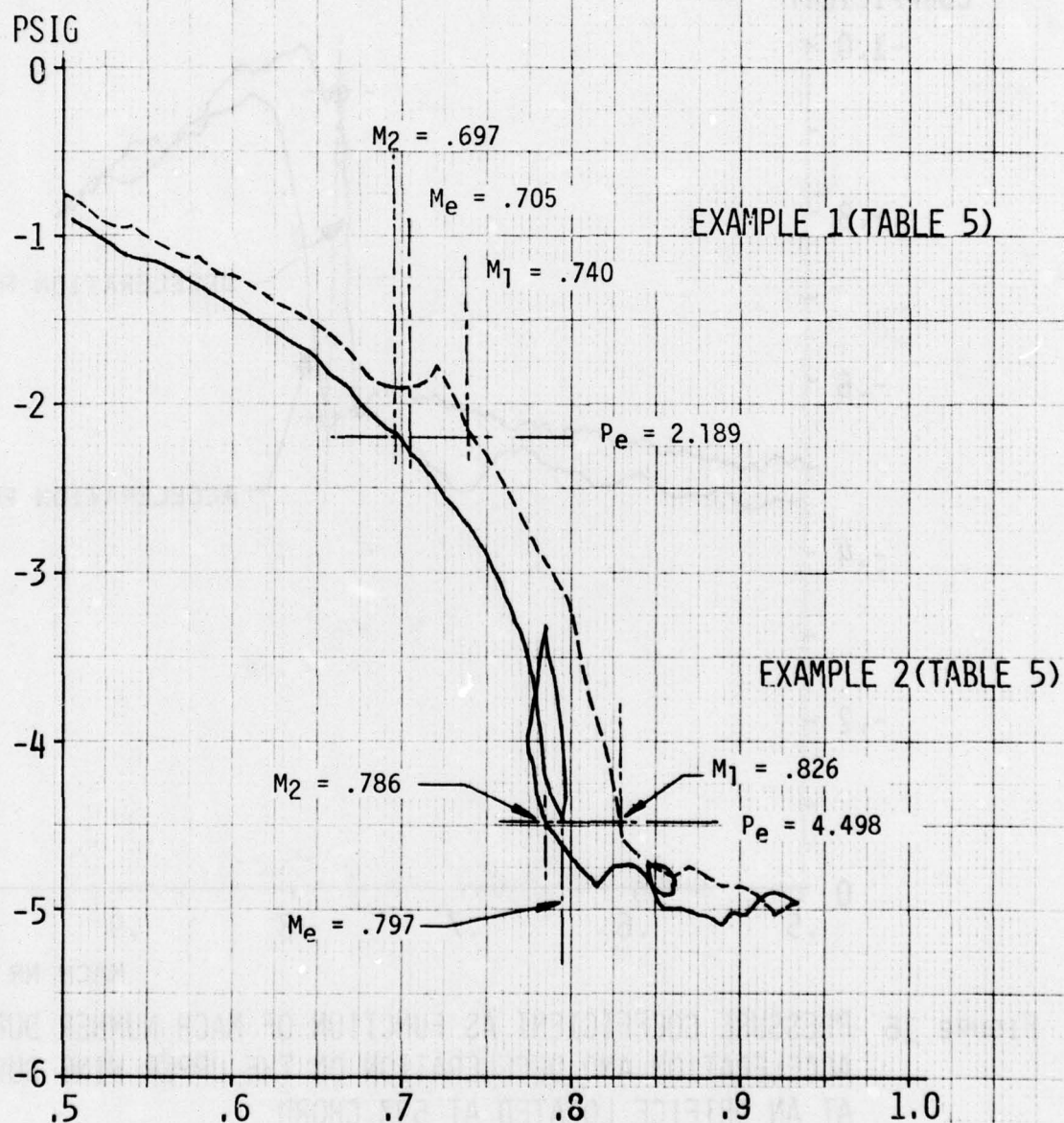


FIGURE 17 PRESSURE AS FUNCTION OF MACH NUMBER DURING ACCELERATION AND DECELERATION ON THE UPPER WING SURFACE AT AN ORIFICE LOCATED AT 59% CHORD (ANGLE OF ATTACK:  $-1.0$  DEGREES; SLED TRAJECTORY WITH TWO SUSTAINED PERIODS OF QUASI-CONSTANT SPEED)

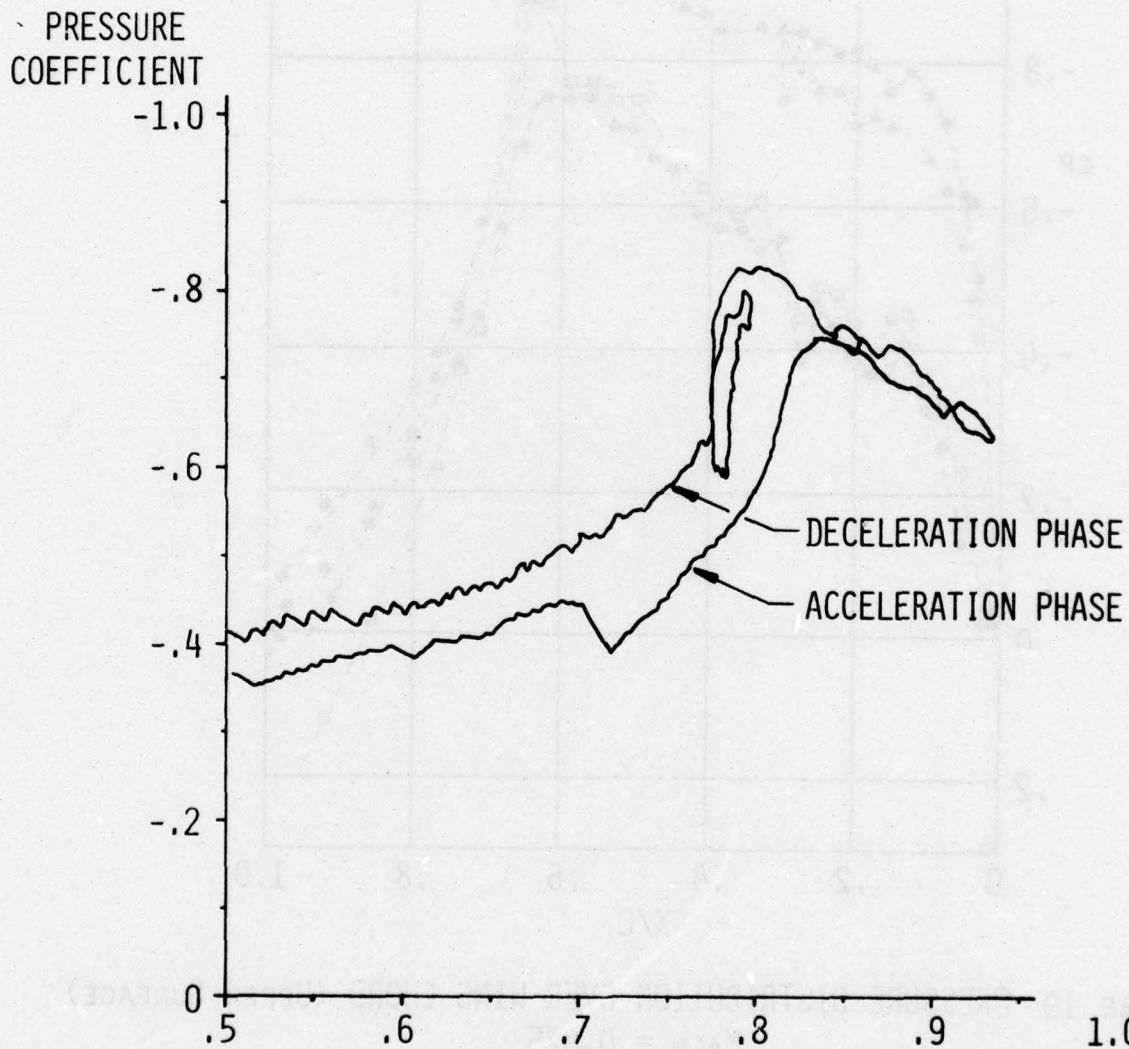


FIGURE 18 PRESSURE COEFFICIENT AS FUNCTION OF MACH NUMBER DURING ACCELERATION AND DECELERATION ON THE UPPER WING SURFACE AT AN ORIFICE LOCATED AT 59% CHORD (ANGLE OF ATTACK:  $-1.0$  DEGREES; SLED TRAJECTORY WITH TWO SUSTAINED PERIODS OF QUASI-CONSTANT SPEED)

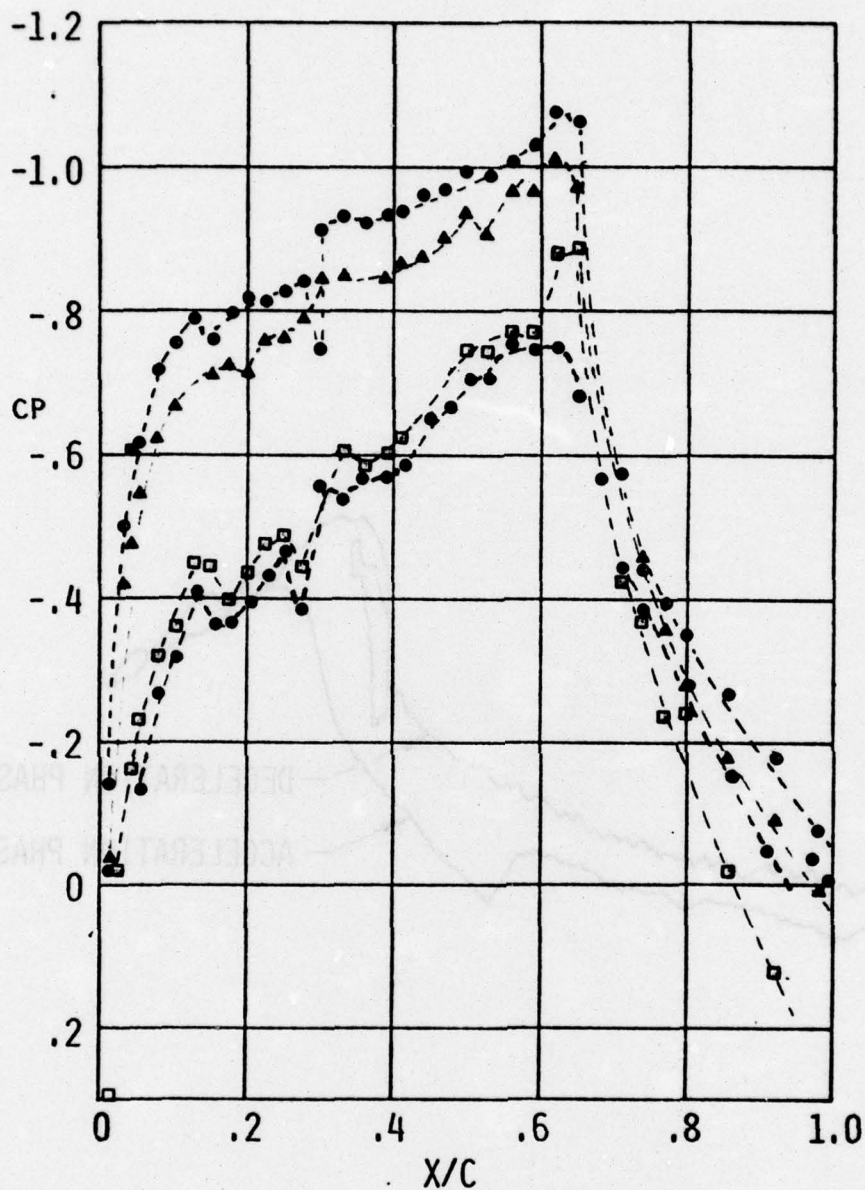


FIGURE 19 PRESSURE DISTRIBUTION OVER WING CHORD (UPPER SURFACE)  
MACH = 0.825

		ALPHA	RE $\times 10^{-6}$
$\bullet$	SLED TESTS	$-1.1^\circ$	5.22/FT = 18.27/CHORD
$\square$	SLED TESTS	$0.0^\circ$	5.09/FT = 17.82/CHORD
$\blacktriangle$	SLED TESTS	$3.8^\circ$	5.52/FT = 19.32/CHORD
$\bullet$	SLED TESTS	$5.0^\circ$	5.52/FT = 19.32/CHORD



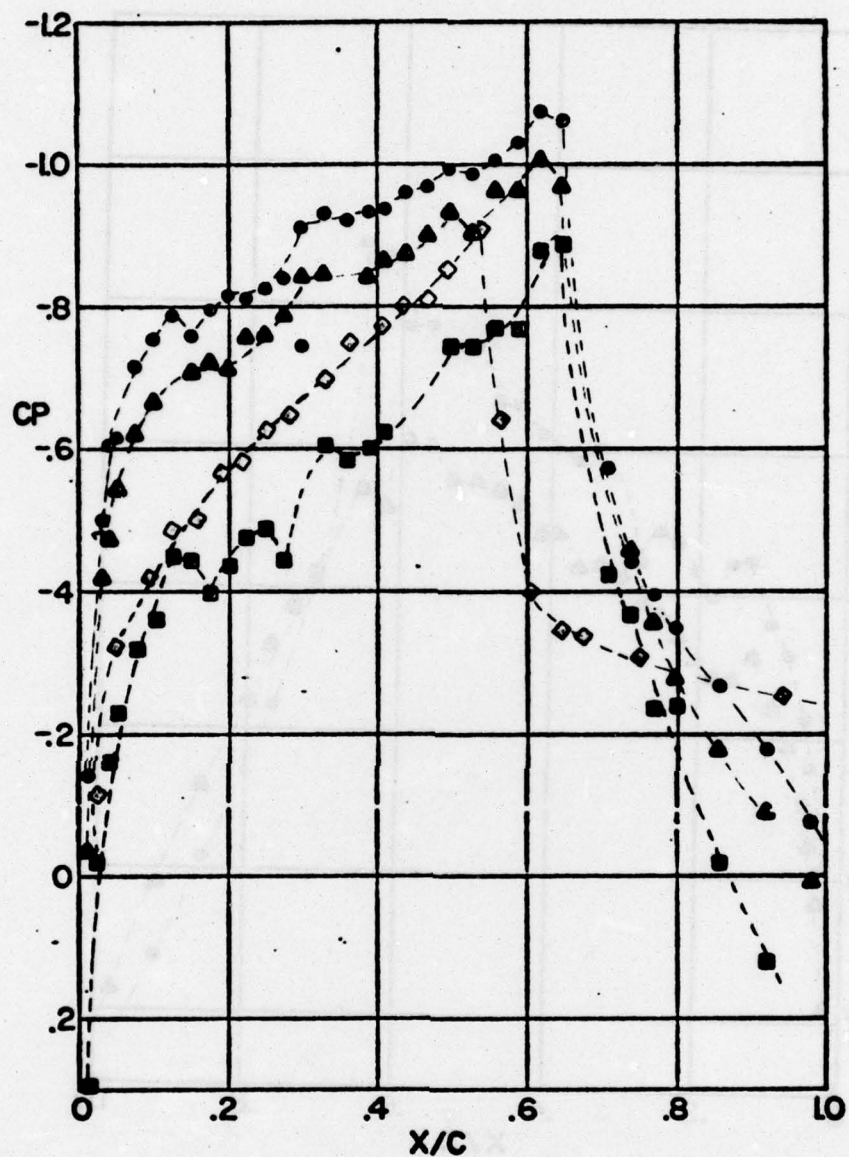


FIGURE 20 PRESSURE DISTRIBUTION OVER WING CHORD (UPPER SURFACE)

		MACH	ALPHA	RE x 10 <sup>-6</sup>
■	SLED TESTS	0.825	0.0°	17.82/CHORD
▲	SLED TESTS	0.825	3.8°	19.32/CHORD
●	SLED TESTS	0.825	5.0°	19.32/CHORD
◇	AEDC 40" TRANS W.T.	0.850	2.0°	5.1/CHORD

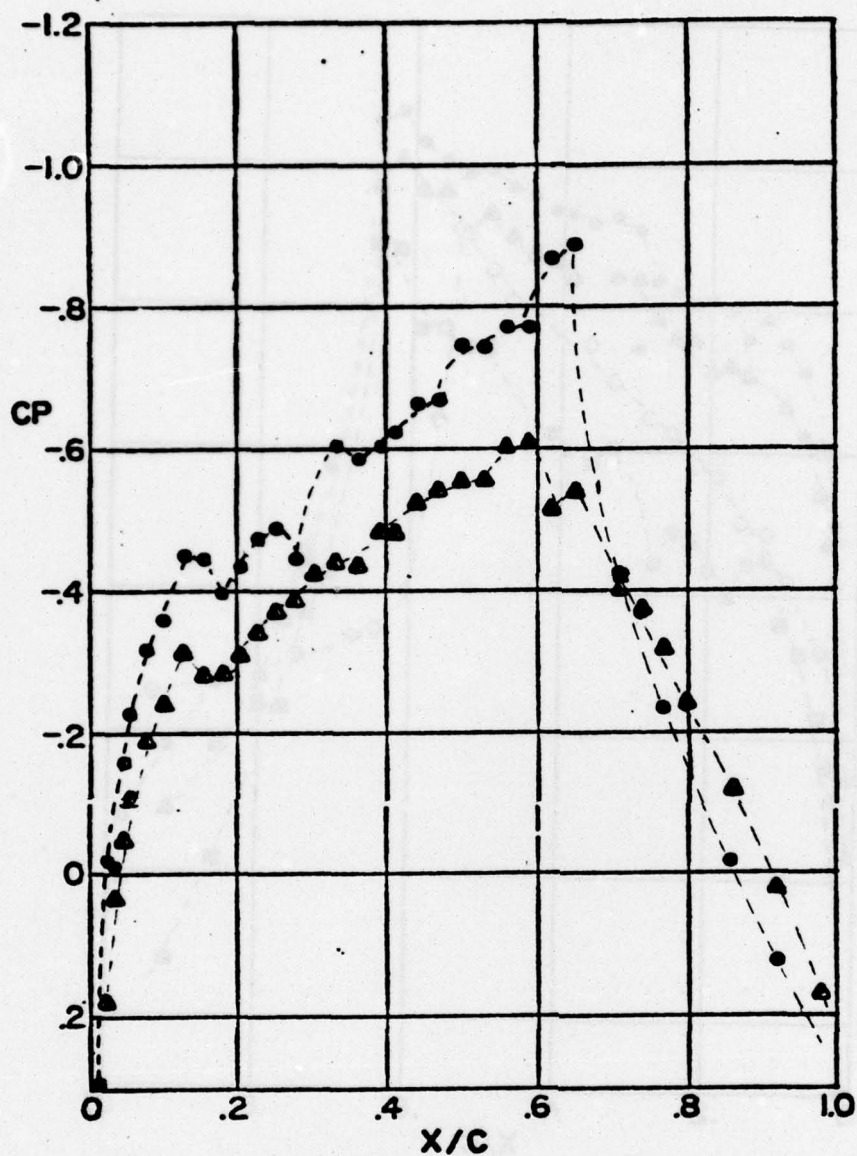


FIGURE 21 PRESSURE DISTRIBUTION OVER WING CHORD (UPPER SURFACE)

MACH = 0.825

	ALPHA	RN X 10 <sup>-6</sup>
● SLED TESTS	0.0 °	5.09/FT = 17.82/CHORD
▲ AMES 11 FT W.T.	-0.026°	6.29/FT = 22.02/CHORD

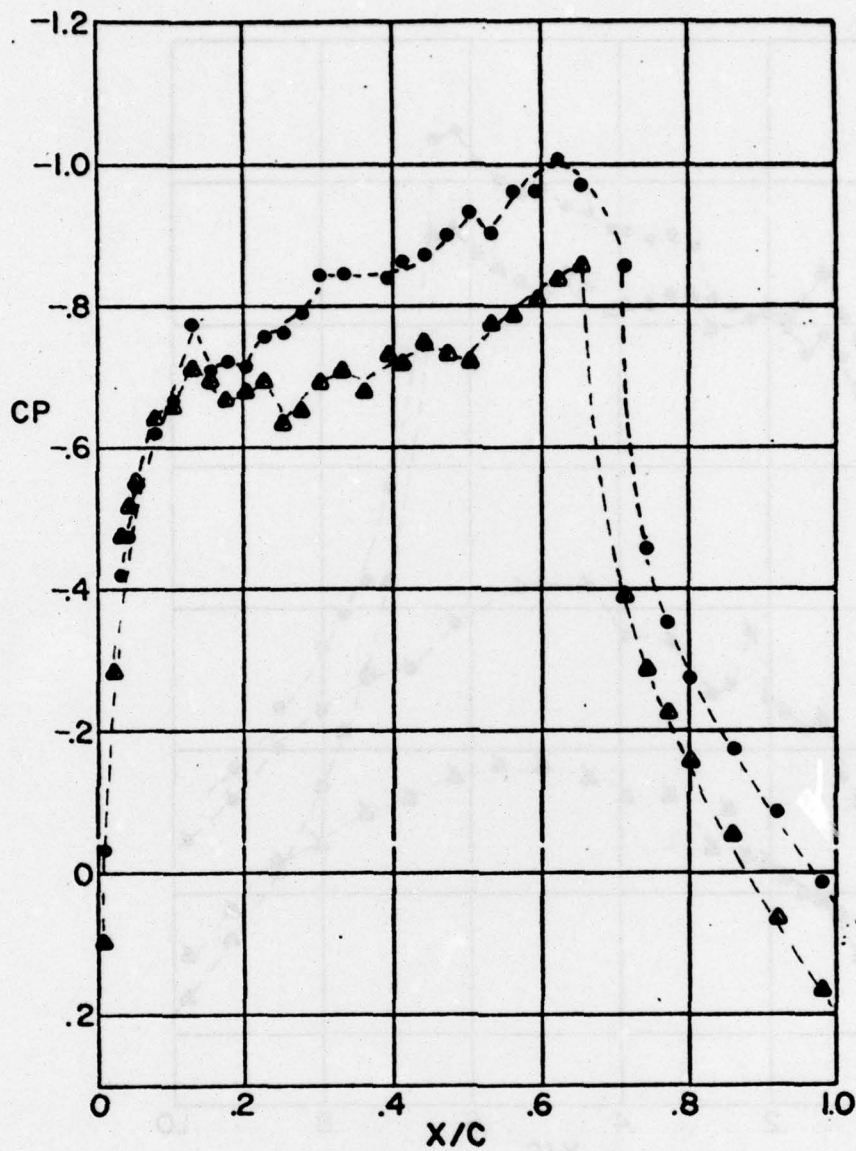


FIGURE 22 PRESSURE DISTRIBUTION OVER WING CHORD (UPPER SURFACE)

MACH = 0.825

		ALPHA	RE $\times 10^{-6}$
●	SLED TESTS	3.8°	5.52/FT = 19.32/CHORD
▲	AMES 11 FT W.T.	3.8°	6.27/FT = 21.95/CHORD



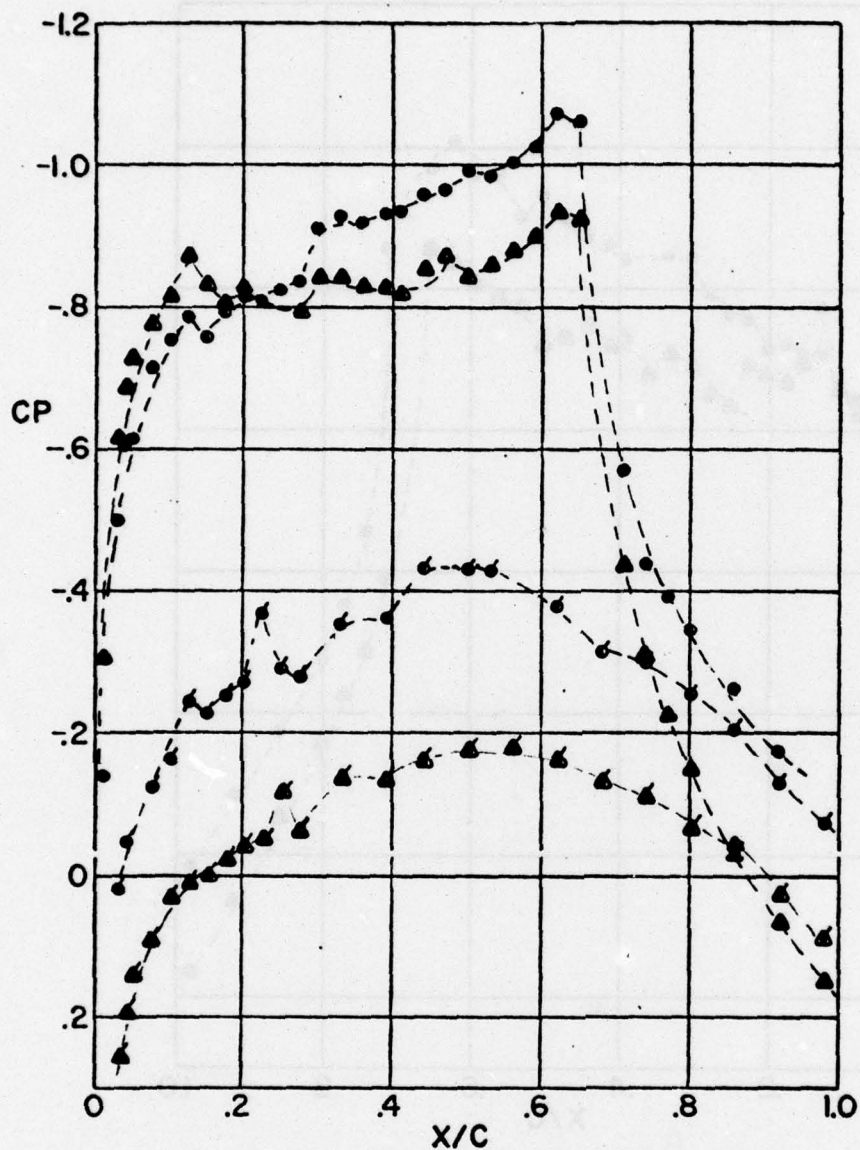


FIGURE 23 PRESSURE DISTRIBUTION OVER WING CHORD

MACH = 0.825

		ALPHA	RE $\times 10^{-6}$
● ●	SLED TEST	5.0 °	5.52/FT = 19.32/CHORD
▲ ▲	AMES 11 FT W.T.	5.27°	6.26/FT = 21.91/CHORD

FLAGGED SYMBOLS DENOTE LOWER SURFACE DATA

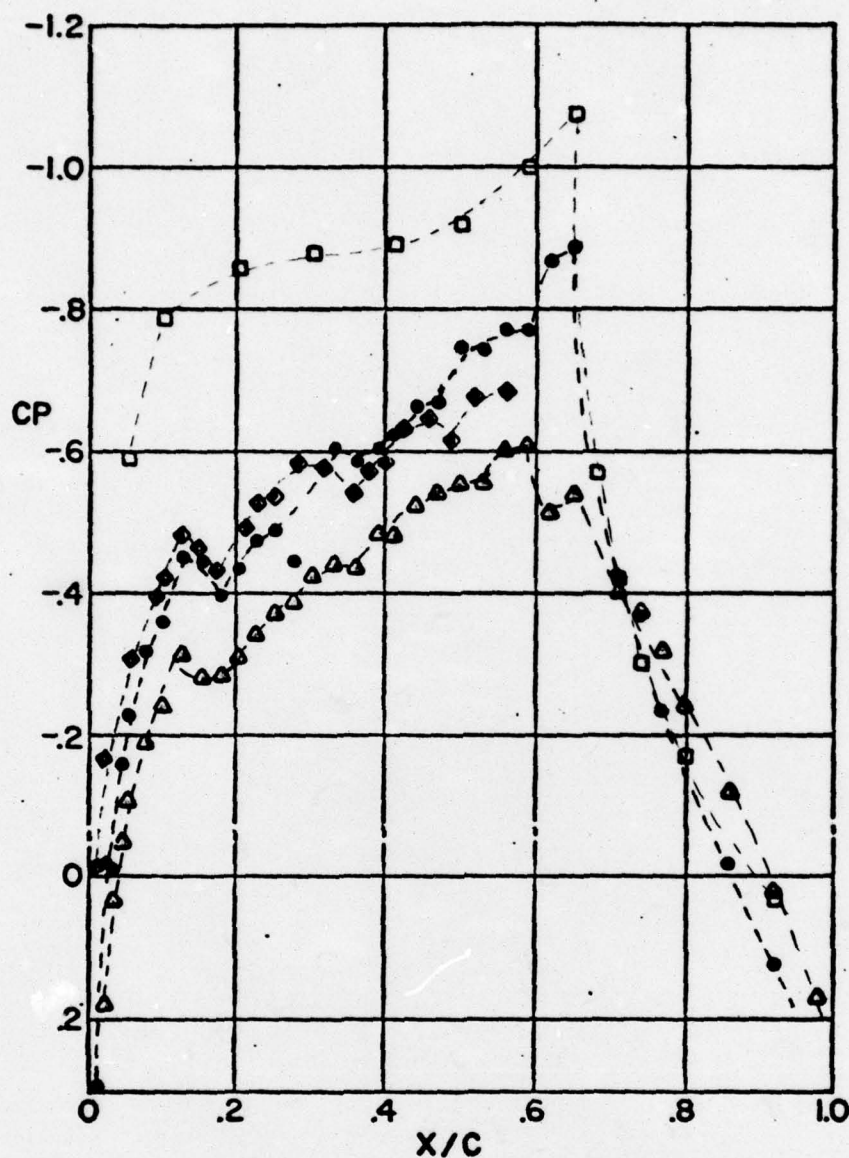


FIGURE 24 PRESSURE DISTRIBUTION OVER WING CHORD (UPPER SURFACE)

MACH = 0.825

	ALPHA	RN X 10 <sup>-6</sup>
• SLED TEST	0.0 °	5.09/FT = 17.82/CHORD
△ AMES 11 FT W.T.	-0.026 °	6.29/FT = 22.02/CHORD
◆ AMES 11 FT W.T.	1.0 °	8.8/CHORD
□ FLT 549-2C	1.1 °	36.0/CHORD

## APPENDIX I

### DISCUSSION OF FLOW VISUALIZATION

1. In connection with, but not as a part of the test run series to measure pressure distribution data on the aircraft wing model, several attempts were made to arrive at techniques for flow visualization during rocket sled runs.
2. One attempt to visualize the flow expansion area following the leading edge of the ground plane is shown in Figure A1. This picture was taken with the original straight leading edge and represents the conditions at Mach = 0.95. In this specific case, the low and high pressure areas are made visible by moving a smoke screen across the track, using a specially designed smoke generator. The smoke was produced by a smoke grenade and blown across the track in the shape of a thin vertical sheet, approximately 2 inches wide, 48 inches high at the nozzle exit. The blower was programmed to begin operating approximately 5 seconds before the sled reached the test location to prevent the smoke from spreading out and obscuring the field of view of the cameras. Conventional clusters of flash bulbs were used as the primary light source.
3. The flow visualization pictures obtained by means of smoke, the tuft images and the shadowgraphs mentioned in the following paragraph were obtained by means of image motion compensation (IMC) photography. This technique is widely used at the track to provide a detailed "stop motion" view of the test object as it passes a selected track station. An IMC picture is achieved by synchronizing the film motion inside the camera to the same relative speed at which the image of the passing sled moves across the focal plane. This way the sled image and the film appear "at rest" with respect to each other. By proper choice of lighting conditions, the IMC technique results in shadowgraph images providing a clear picture of the shock wave patterns around sleds moving at supersonic speeds. "Stop motion" images and shadowgraphs of moving sleds can also be achieved by pulse-laser illumination; however, this technique was not applied during these tests.
4. The shadowgraph depicted in Figure A2 shows the upper portion of the panel model at Mach = 0.91. The relatively strong shock visible aft of the trailing edge of the panel model develops between the upper and lower contoured end plates. The shock system discussed in connection with Figure 12 in the 0.825 Mach regime occurs at locations perpendicular to the wing plan form which cannot be made visible by this technique because of the vertical position of the wing on the sled.



## ILLUSTRATIONS (APPENDIX I)

### Figure

- A1 Low Pressure (Expansion) Area Marked by Smoke Concentration on Top of the Ground Plane with the "Old" Straight Leading Edge in Place (IMC photo taken at Mach = 0.95)
- A2 Shadowgraph of Flow on Upper Portion of Panel Model at Mach = 0.91; Model of Angle of Attack: 3.9 Degrees

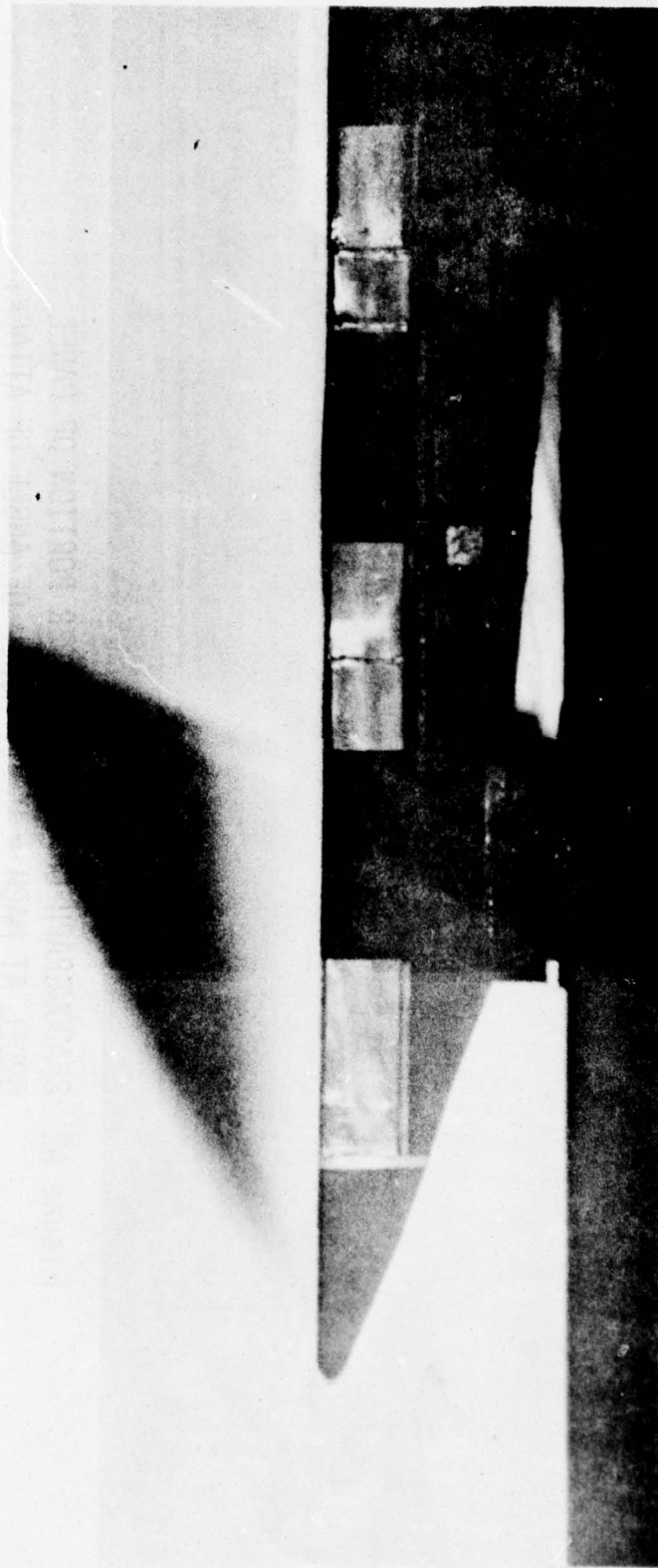


FIGURE A1 LOW PRESSURE (EXPANSION) AREA MARKED BY SMOKE CONCENTRATION  
ON TOP OF THE GROUND PLANE WITH THE "OLD" STRAIGHT LEADING  
EDGE IN PLACE (IMC PHOTO TAKEN AT MACH = 0.95)

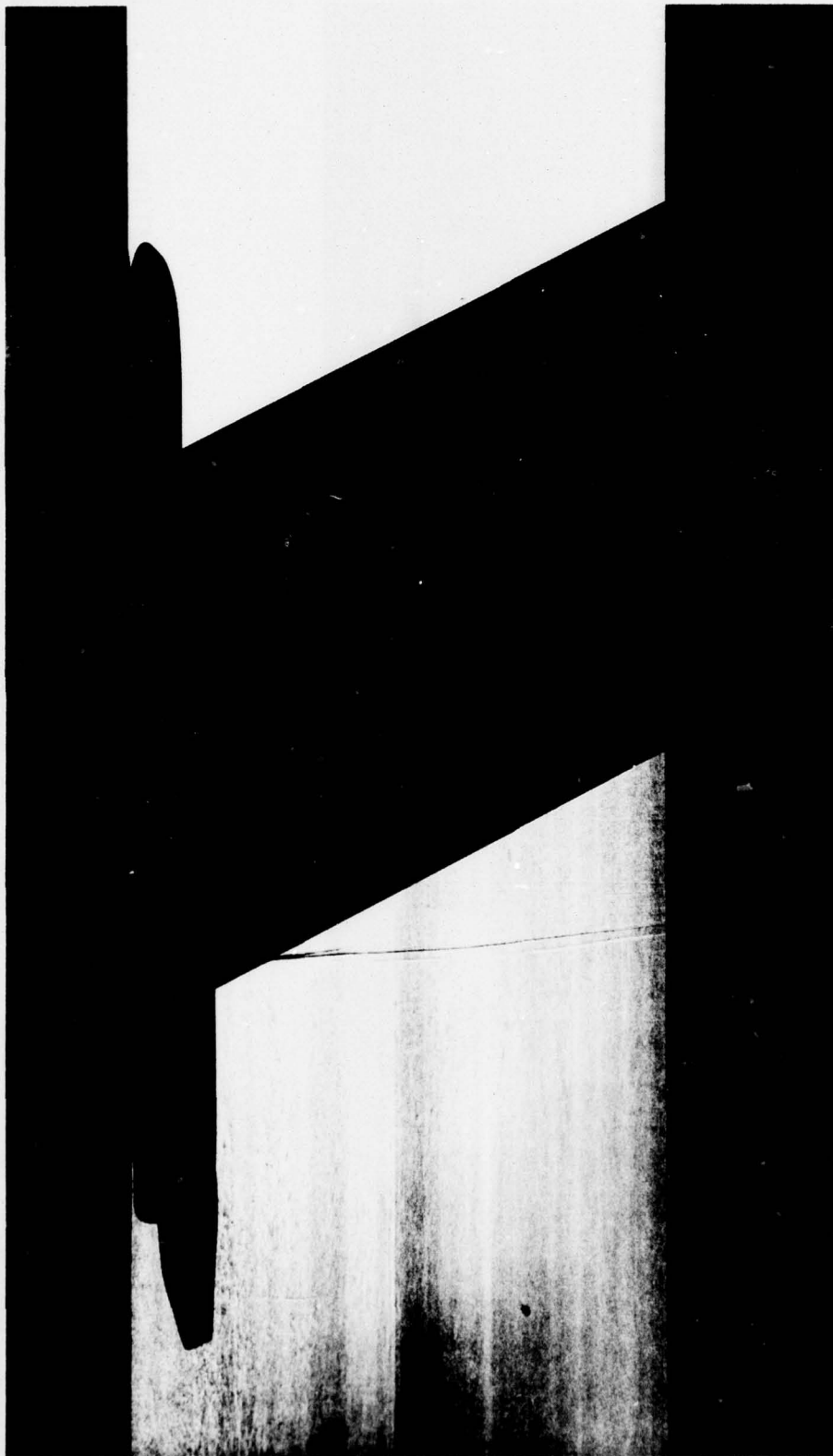


FIGURE A2 SHADOWGRAPH OF FLOW ON UPPER PORTION OF PANEL  
MODEL AT MACH  $\approx 0.91$ ; MODEL OF ANGLE OF ATTACK:  
3.9 DEGREES



## APPENDIX II

### TRANSONIC SLED VIBRATION DATA

1. The data presented in this appendix describe characteristic examples of the vibration environment encountered by the mission sled (designated FDN 6326) while traveling along the Holloman AFB Track. Figure B1 gives the velocity-time history of one typical run with the wing model installed (designated run number 56X-G7A) and of a second run without the wing model (56X-C1). Figure B1 also presents a schematic of the basic structural layout of this sled including the hub assembly which accommodates the wing tang for installation of the wing model. In the following, X-direction means the direction of sled motion, Y designates the lateral (cross-track) direction, and Z the vertical component.
2. The vibration data discussed in the following are based on accelerometer measurements in three axes at the indicated location on the top surface of the hub assembly aft of the wing model. Because of the heavy and rigid sled structural components involved, the data obtained at this location are considered typical for the vibration environment encountered by the base of the wing model itself. Figure B1 also lists the weight breakdown of the mission sled with and without the wing model in place.
3. During this run series the mission sled (FDN 6326) was operated with no rocket propulsion on board. It was at all times connected to a sustain pusher sled. The connecting link between the mission sled and the sustain pusher vehicle consisted of a cylindrical aluminum push column, 19 ft long, 16 inches diameter, with a wall thickness of 0.5 inches. This pusher sled (designated PDS 6307) had a burnout weight of 5,286 pounds. In this configuration, the entire train had a drag reference area of  $A = 32 \text{ ft}^2$  and an effective subsonic drag coefficient of  $C_D = 0.922$  without the wing model installed. With the wing model in place, the respective values were  $A = 36.0 \text{ ft}^2$  and  $C_D = 0.886$ .
4. The end instruments used to obtain the vibration data were Endevco 2260 accelerometers. These accelerometers have a frequency response of 2 kHz. They were calibrated for  $\pm 40$ ,  $\pm 20$  and  $\pm 15$  g's in the vertical, lateral and longitudinal directions, respectively. The accelerometer outputs were multiplexed and transmitted by a constant bandwidth FM/FM telemetry system on a carrier frequency of 797 MHz with each subcarrier having a frequency response of 4 kHz. The transmitted information was placed on magnetic tape and forwarded for processing to the Air Force Weapons Laboratory, Kirtland AFB, New Mexico, where it was digitized and reduced on a CDC 6600 computer. Prior to reading, scaling and digitizing, the data were electronically filtered with a 5 Hz high bypass filter in order to eliminate any effects of base line shifts that might have occurred during the runs. This filtering also eliminated the slow varying quasi-steady-state down track accelerations inherent in accelerating the vehicle to and decelerating it from mission speed. The absence of these slowly changing accelerations and decelerations is apparent in the data presented for the X-direction.

5. Figures B2 through B13 contain plots of acceleration versus time, g's-rms versus time, power spectral density and probability density. The acceleration versus time curve is a graph of the digitized data for selected time intervals with a sampling rate of 10,000 points per second. Calculations performed to arrive at the g's-rms versus time are based on a non-overlapping, moving time interval of 0.01 seconds; the points plotted are the end points of each interval. The power spectral density graph is obtained for the time interval shown using a fast Fourier transformation technique with a 2 Hz bandwidth. The plots of the probability density function contain two curves. One of these represents the actual distribution of the test data. The "expected" curve is an estimate for a Gaussian distribution of the data.

6. The plotted data were taken during a run (56X-G7A) with the wing model in place. Figures B2 through B4 present data for the beginning of the run, including sled first motion. Figures B5 through B7 are selected to represent a time interval during the acceleration period, prior to burnout. During this period, the sled was accelerating from 885 to 1020 ft/sec at an acceleration level of approximately 4.3 g's. The third set of figures illustrates the conditions during the primary data acquisition period while the natural deceleration of the sled due to air drag was slowed by sustain propulsion. The velocity regime was approximately 1040 to 990 ft/sec. The fourth set of data exemplifies the conditions during free-coasting after burnout of the sustain rockets, in the velocity regime 710 to 675 ft/sec.

7. The longitudinal oscillations are attributable to fluctuations of the rocket thrust during the acceleration and sustain periods of a run, superimposed on slipper-rail friction and the response of the sled structure to these inputs. In considering rail friction it is useful to remember that rocket sleds tend to "jump" within the clearance of the slipper gap, both in the vertical and the lateral direction. Frictional forces occur only during the brief periods of slipper-rail contact. For this reason, the forcing functions due to rail friction are characterized by the irregular occurrence of short-time intermittent force inputs in a direction opposite to the direction of sled motion. The very distinct strongly damped 24 Hz oscillation occurring at first motion of the sled is attributed to a step-function-type response of the long push column between mission sled and pusher to the very rapid thrust build-up of the prepackaged liquid rocket motors.

8. The lateral oscillations are a result of the cross-track sled motions within the clearance of the slipper gap. The forcing function due to these inputs is characterized by the irregular occurrence of short-time intermittent lateral impact forces.

9. The vertical force inputs are due to the jumping of the sled within the vertical slipper gap clearance in addition to the roughness of the rail surface during the periods of contact. The structural response to those forces is characterized by the basic structural mode of the



sled structure in pitch (slipper beam bending), recognizable in a distinct peak at approximately 20 Hz in the PSD's for the vertical oscillation.

10. The following Table B1 presents a summary of the maximum rms accelerations measured during the time intervals listed. This information was obtained from the digitized listings for the configurations with wing (sled run 56X-G7A) and without the wing model installed (sled run 56X-C1). The time intervals are selected to compare periods of approximately equal sled velocities.

#### ILLUSTRATIONS (APPENDIX II)

##### Figure

- B1 Velocity-Time History of a Typical Transonic Sled Run With Wing Model Installed (56X-G7A) and Without the Wing Model (56X-C1)
- B2 Vertical Acceleration Data, Run Nr 56X-G7
- B3 Lateral Accelerations, Run Nr 56X-G7
- B4 Longitudinal Accelerations, Run Nr 56X-G7
- B5 Vertical Acceleration Data, Run Nr 56X-G7
- B6 Lateral Accelerations, Run Nr 56X-G7
- B7 Longitudinal Accelerations, Run Nr 56X-G7
- B8 Vertical Acceleration Data, Run Nr 56X-G7
- B9 Lateral Accelerations, Run Nr 56X-G7
- B10 Longitudinal Accelerations, Run Nr 56X-G7
- B11 Vertical Acceleration, Run Nr 56X-G7
- B12 Lateral Accelerations, Run Nr 56X-G7
- B13 Longitudinal Accelerations, Sled Run Nr 56X-G7



TABLE B1

## MAXIMUM RMS - ACCELERATIONS DURING SELECTED

## TIME INTERVALS WITH AND WITHOUT WING MODEL INSTALLED

Sled Run 56X-G7A (With Wing)

$t_{\text{(sec)}}$	Velocity (ft/sec)	$G_{\text{rms}}$	$G_{\text{rms}}$	$G_{\text{rms}}$
		(x)	(y)	(z)
8.0 - 9.0	885 - 1020	1.50	2.65	2.75
9.75 - 10.75	1040 - 990	1.65	2.70	3.5
23.5 - 24.5	710 - 675	1.35	1.95	2.0

Sled Run 56X-C1 (Without Wing)

$t_{\text{(sec)}}$	Velocity (ft/sec)	$G_{\text{rms}}$	$G_{\text{rms}}$	$G_{\text{rms}}$
		(x)	(y)	(z)
4.5 - 5.5	875 - 1105	2.97	5.95	6.52
6.0 - 7.0	1105 - 1055	3.53	6.25	9.40
21.5 - 22.5	677 - 655	1.90	2.90	3.60

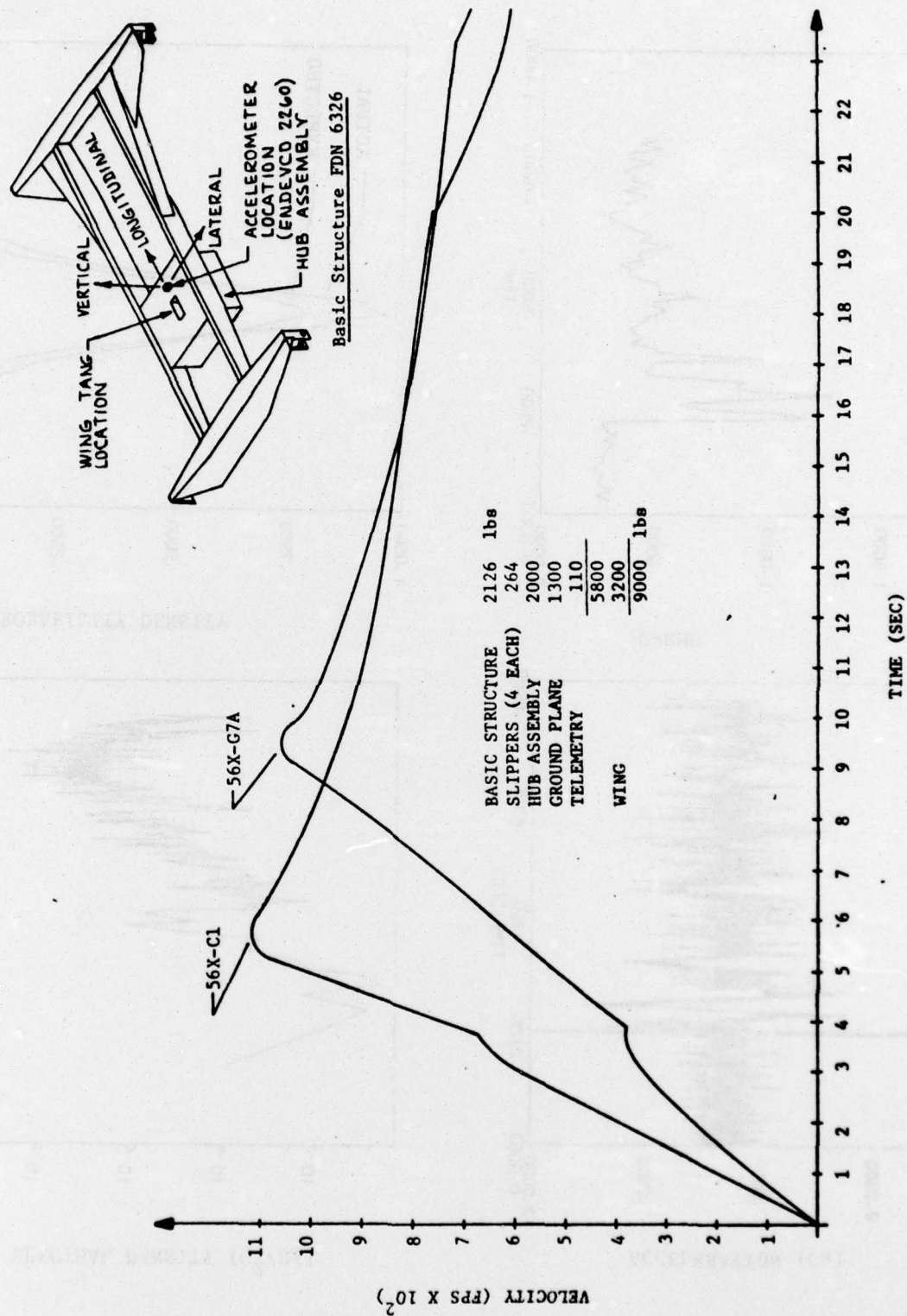
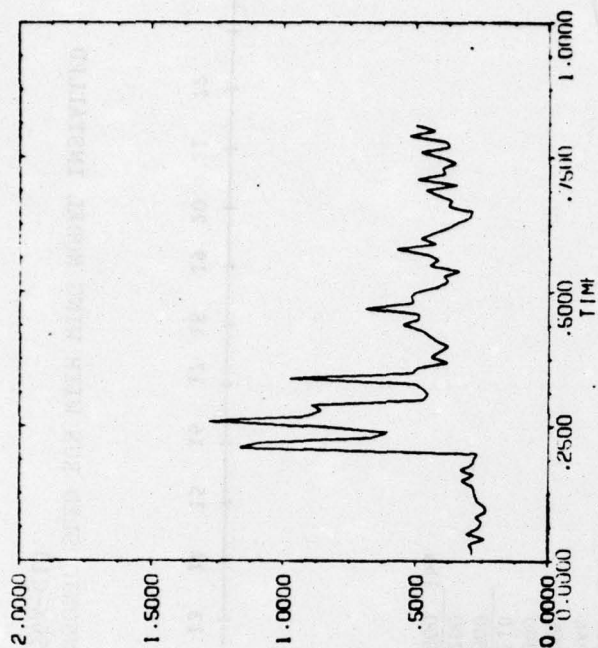
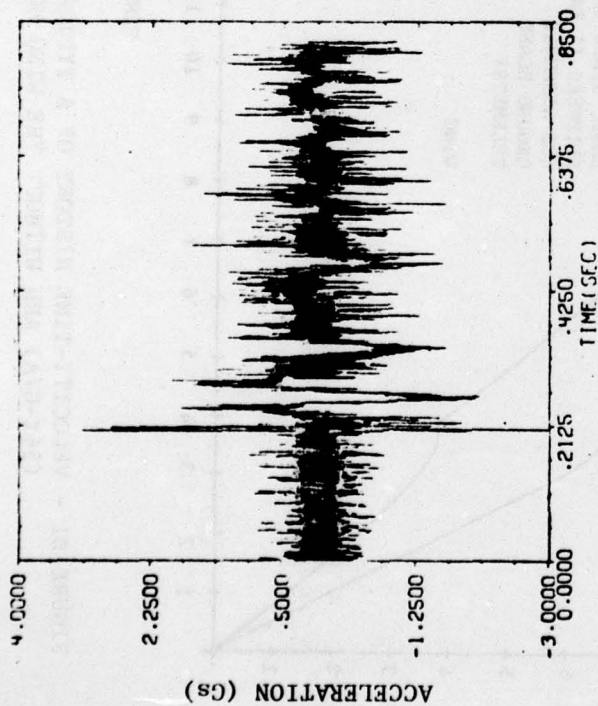


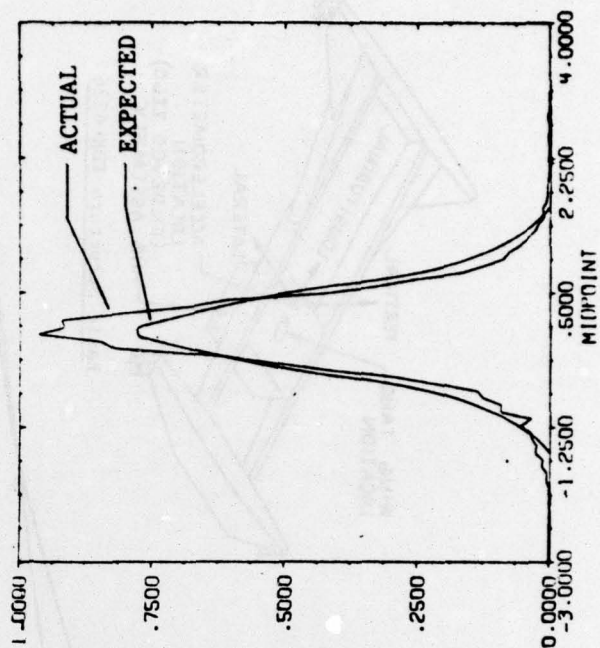
FIGURE B1 - VELOCITY-TIME HISTORY OF A TYPICAL TRANSONIC SLED RUN WITH WING MODEL INSTALLED (56X-G7A) AND WITHOUT THE WING MODEL (56X-C1).



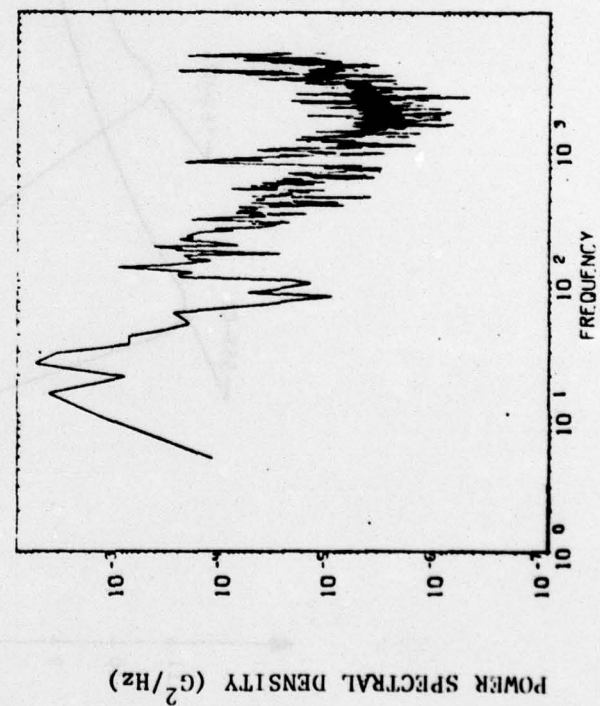
G-RMS



ACCELERATION (Gs)



PROBABILITY DENSITY



POWER SPECTRAL DENSITY (G<sup>2</sup>/Hz)

FIGURE B2 - VERTICAL ACCELERATION DATA, RUN NR 56X-G7  
TIME: 0 ... 0.8 SEC; VELOCITY: 0 ... 100 FT/SEC



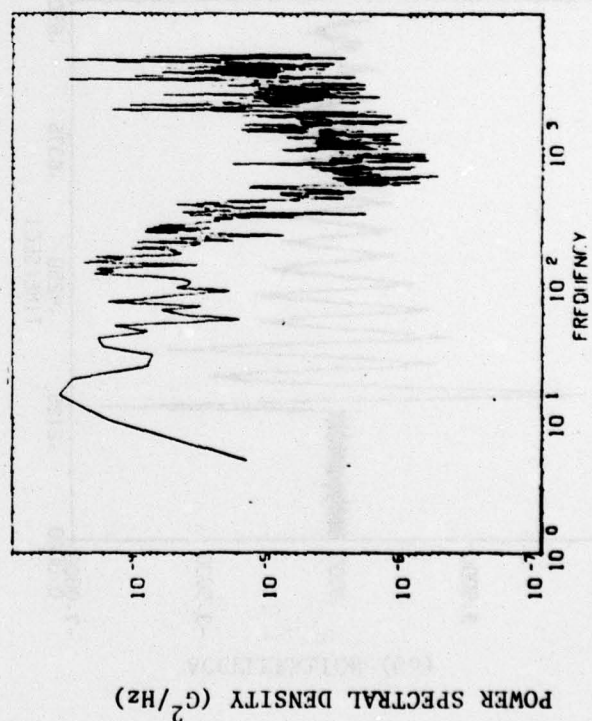
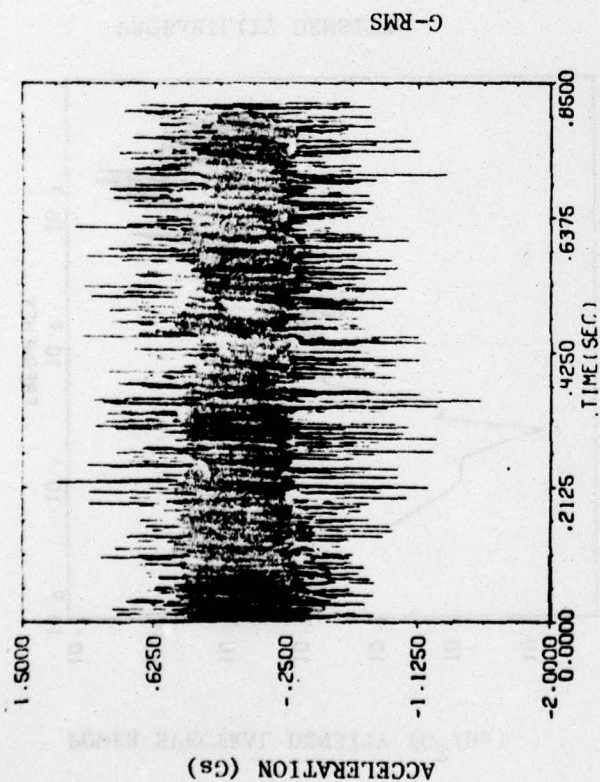
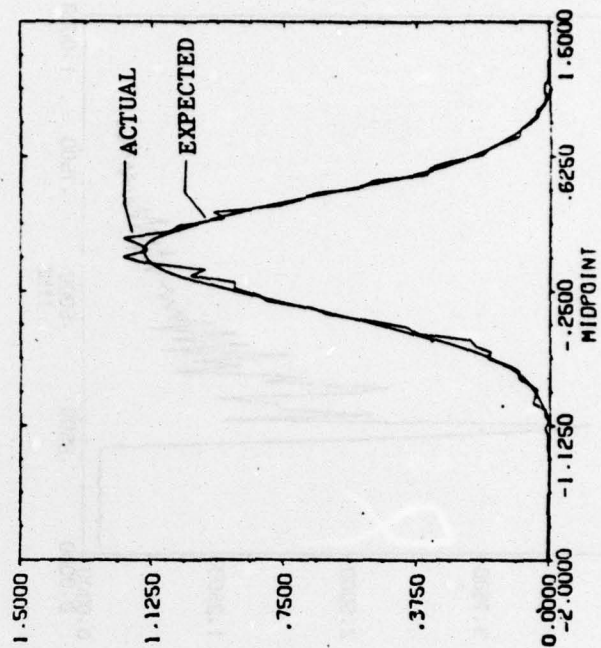
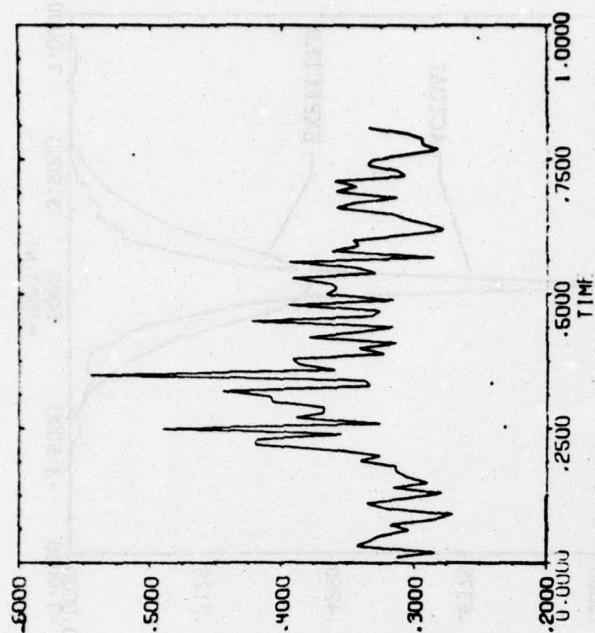


FIGURE B3 - LATERAL ACCELERATIONS, RUN NR 56X-G7  
TIME: 0 ... 0.8 SEC; VELOCITY: 0 ... 100 SEC

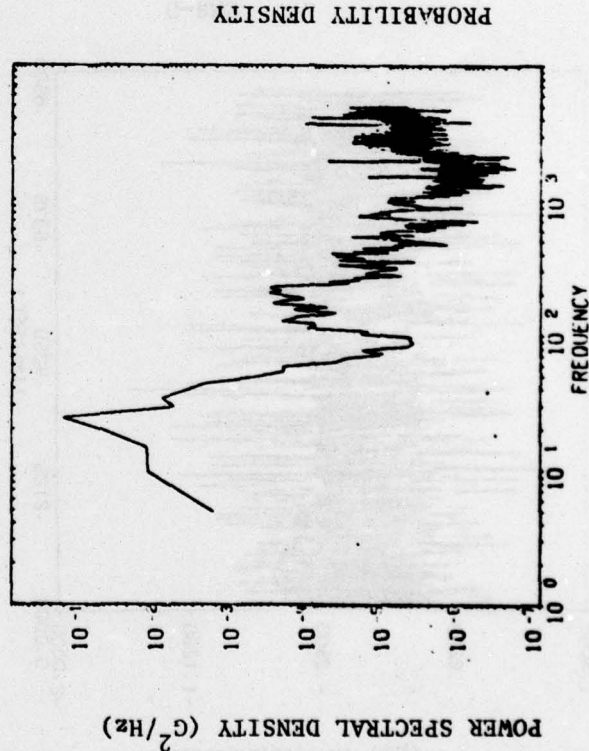
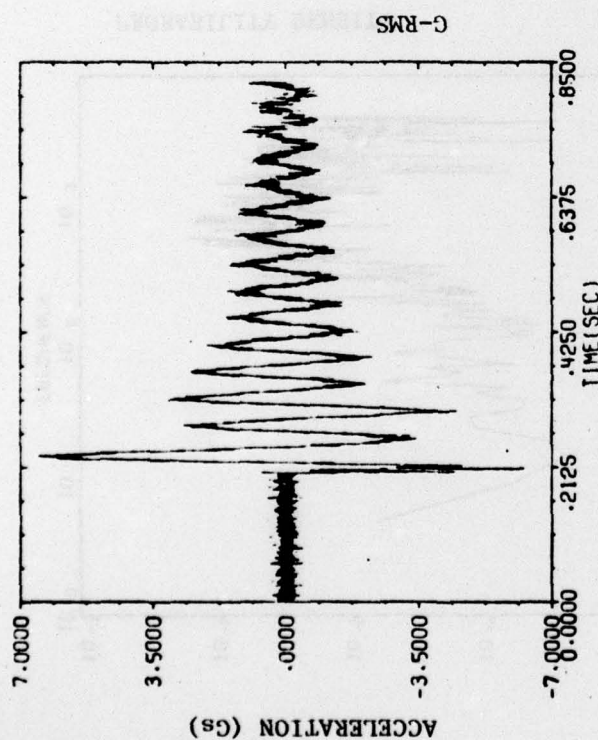
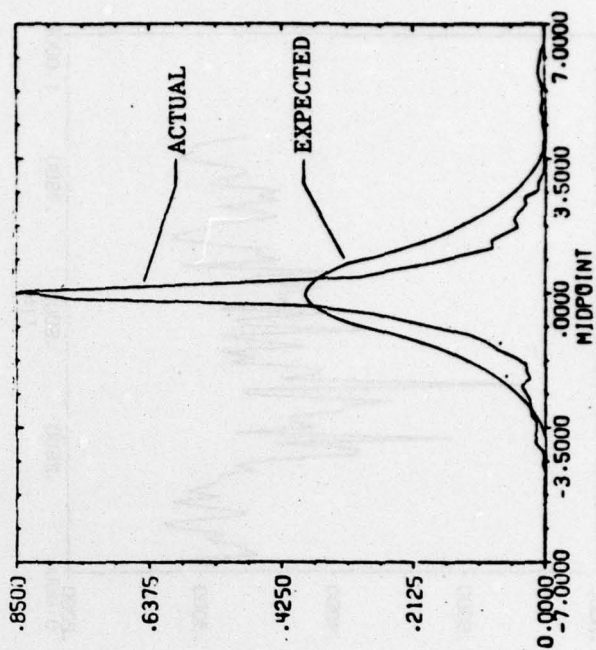
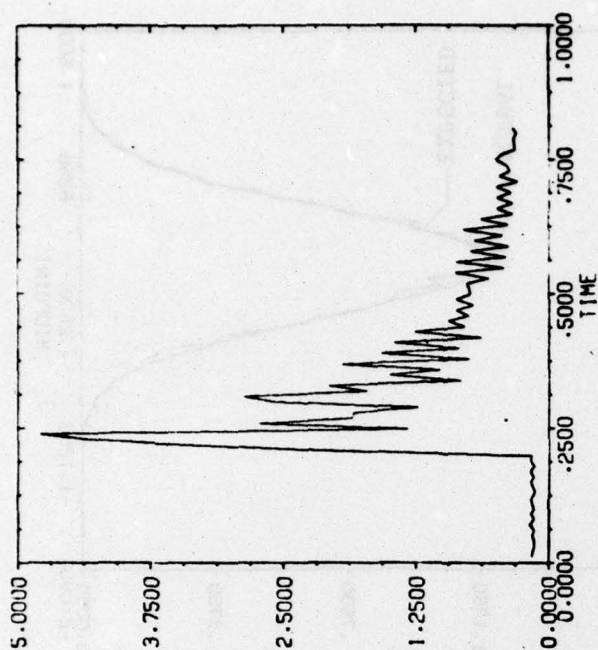


FIGURE B4 - LONGITUDINAL ACCELERATIONS, RUN NR 56X-G7  
TIME: 0 ... 0.8 SEC; VELOCITY 0 ... 100 FT/SEC

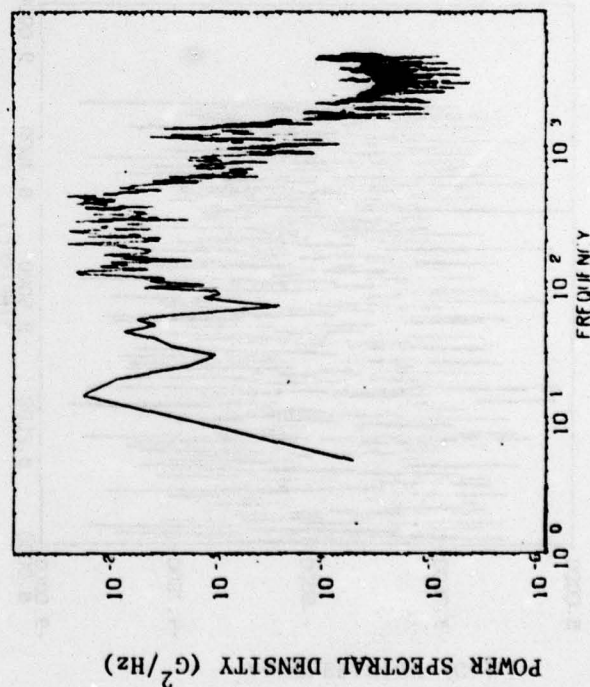
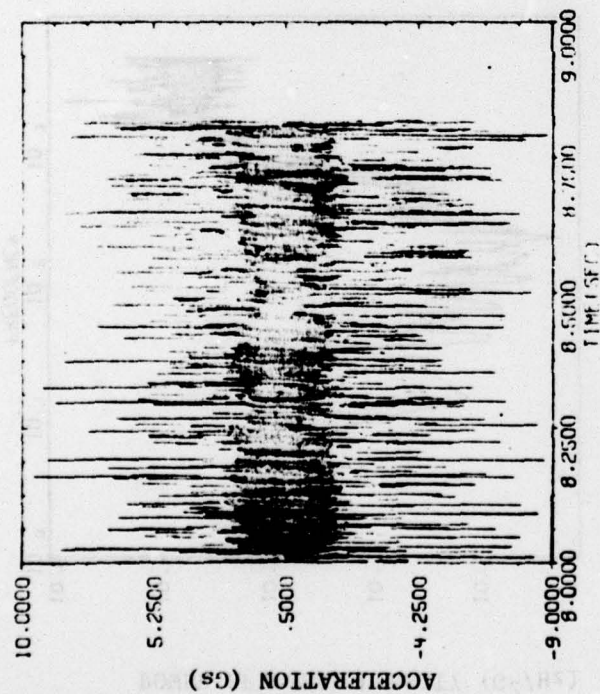
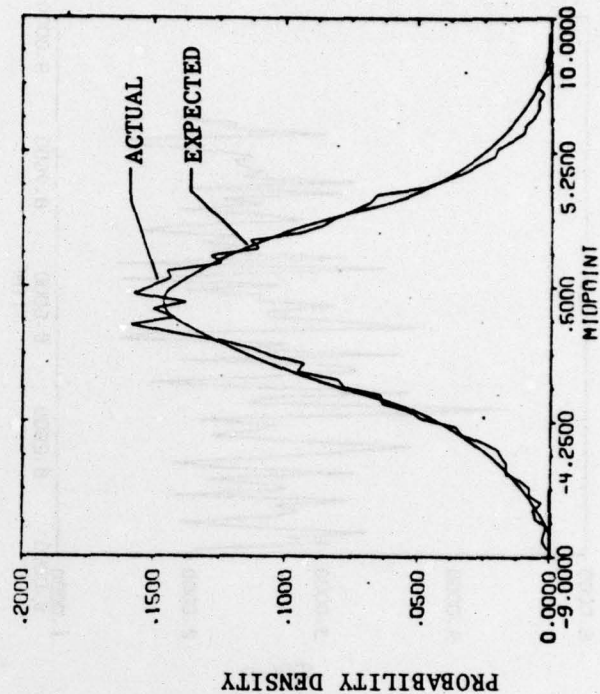
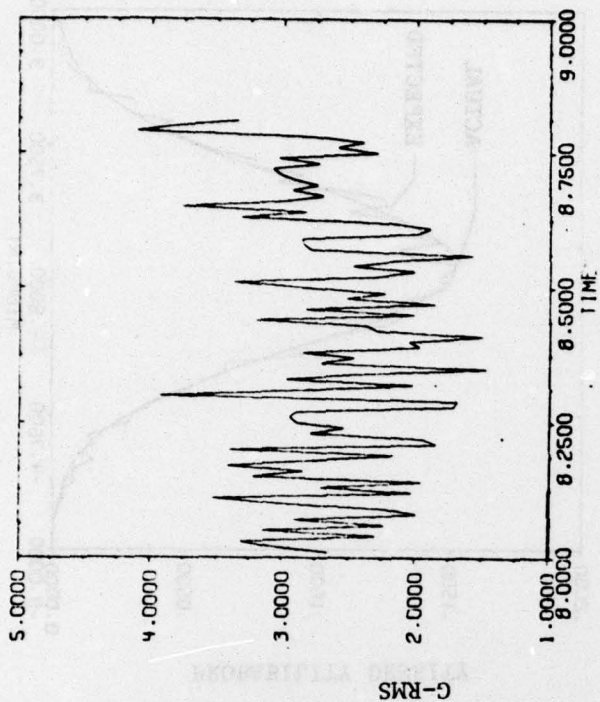


FIGURE B5 - VERTICAL ACCELERATION DATA, RUN NR 56X-G7  
TIME: 8 ... 8.8 SEC; VELOCITY 885 ... 1020 FT/SEC



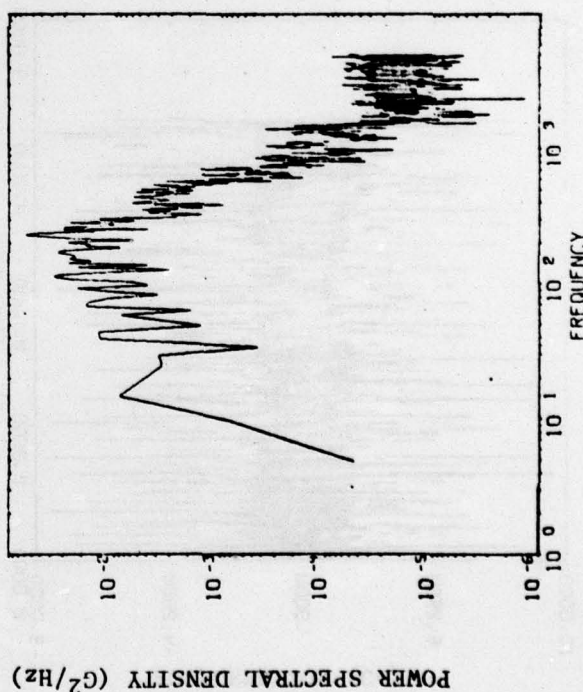
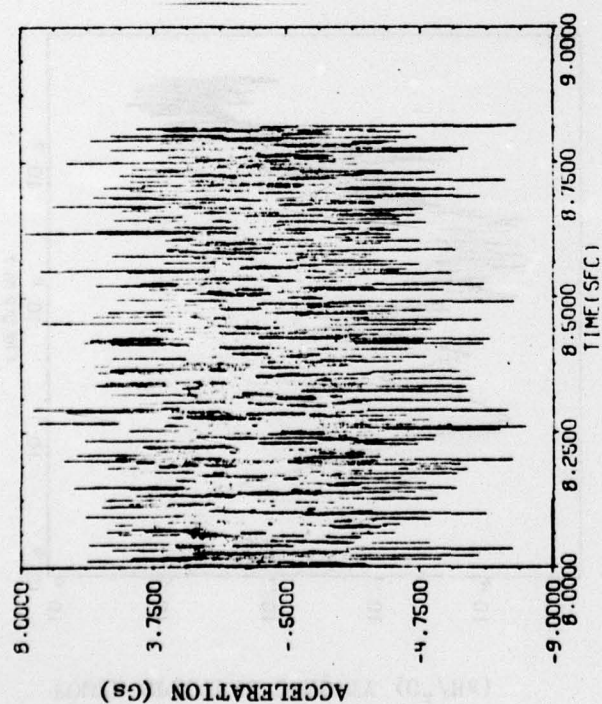
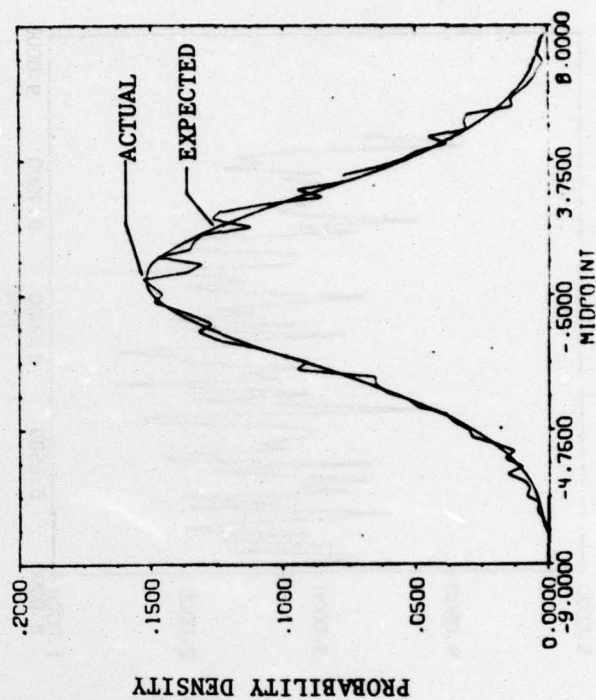
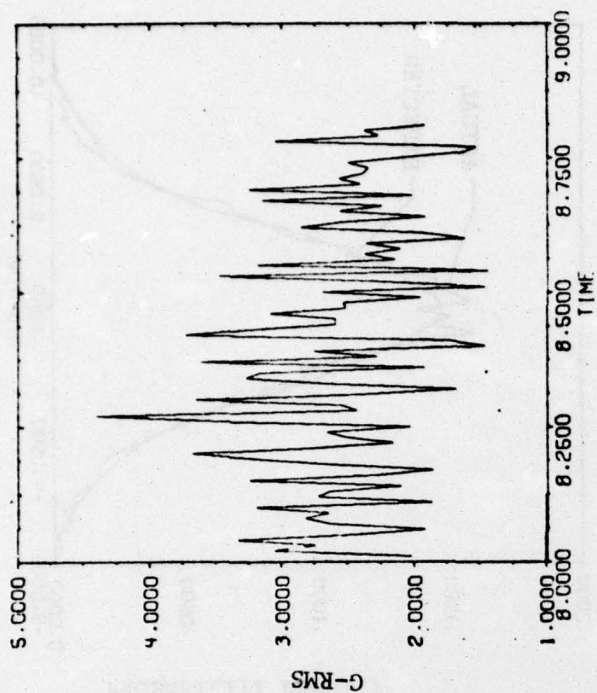


FIGURE B6 - LATERAL ACCELERATIONS, RUN NR 56X-G7  
TIME: 8.0 ... 8.8 SEC; VELOCITY: 885 ... 1020 FT/SEC

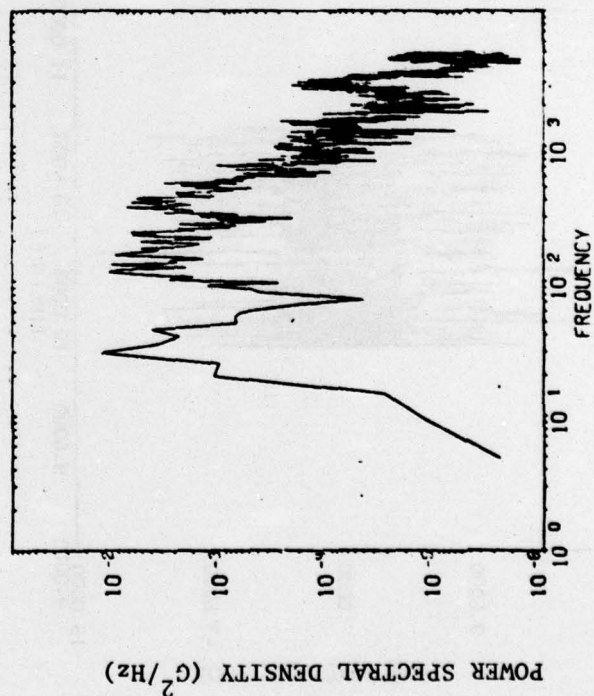
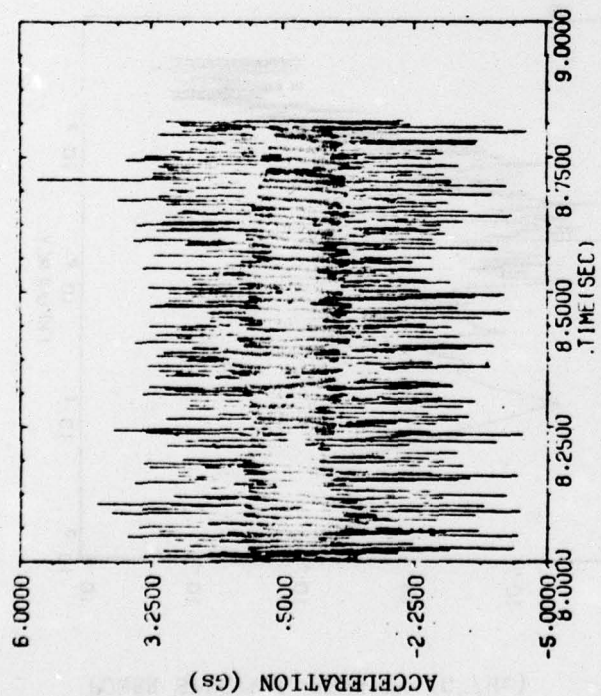
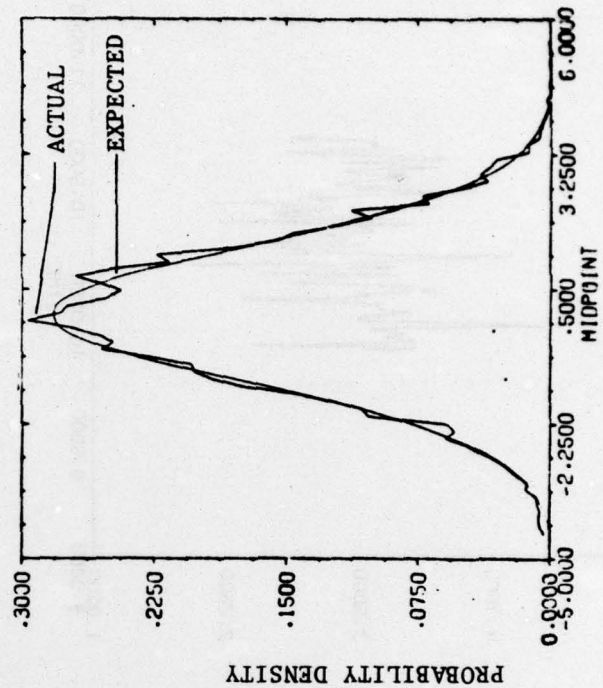
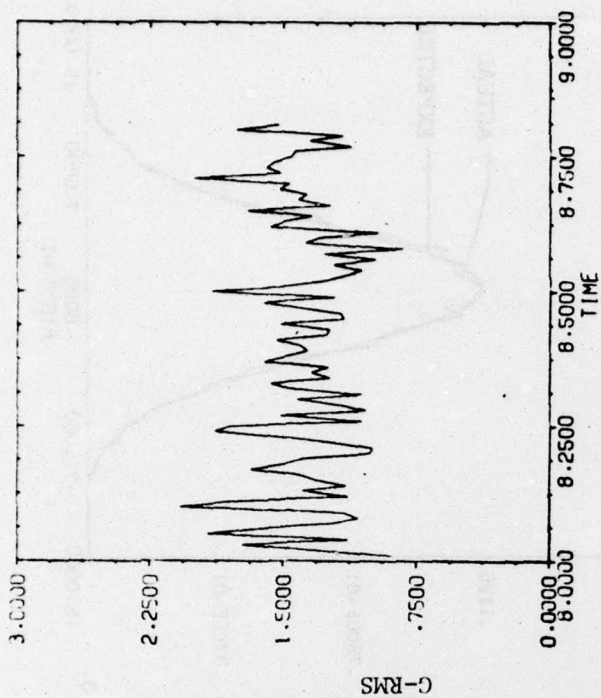


FIGURE B7 - LONGITUDINAL ACCELERATIONS, RUN NR 56X-G7  
TIME: 8.0 ... 8.8 SEC; VELOCITY 885 ... 1020 FT/SEC

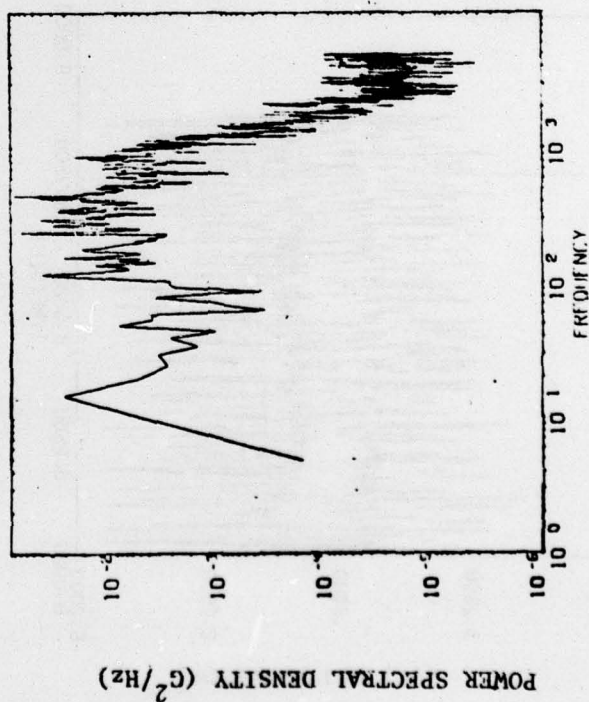
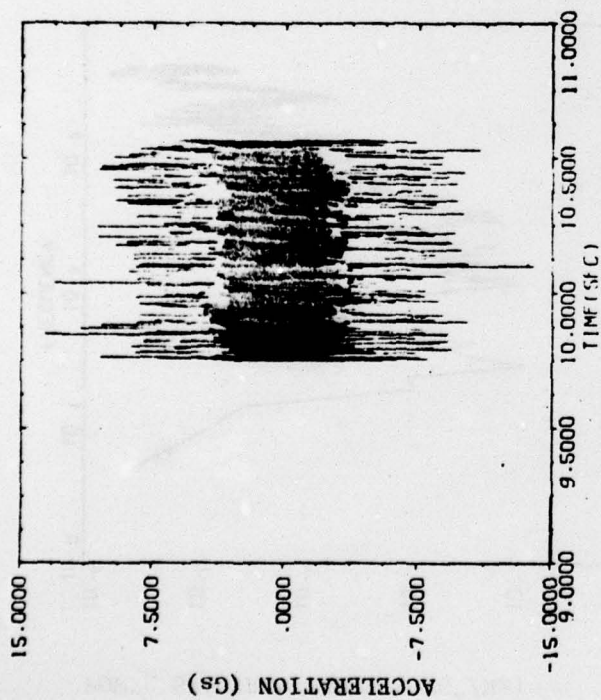
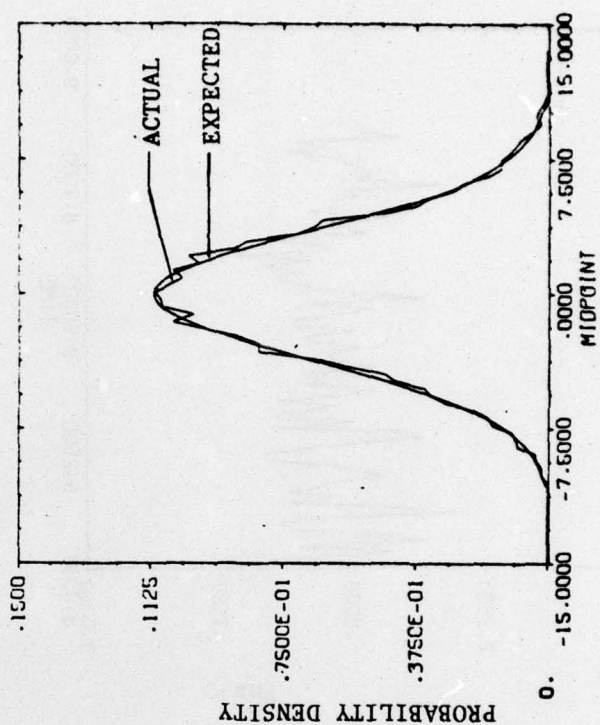
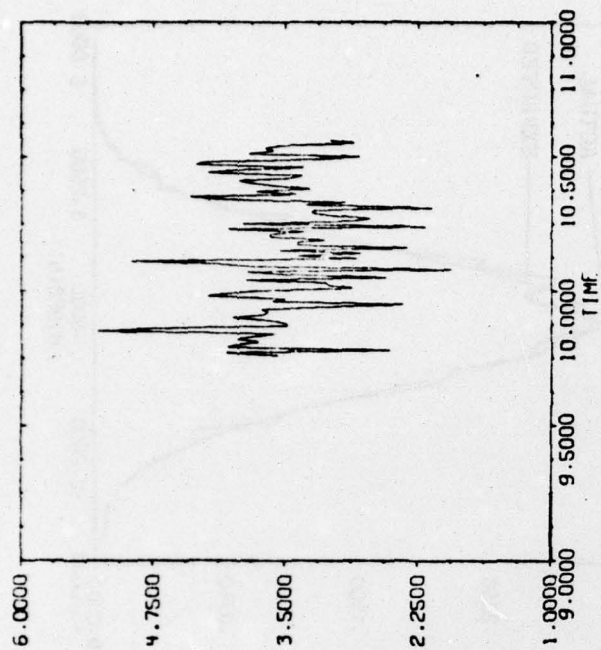


FIGURE B8 - VERTICAL ACCELERATION DATA, RUN NR 56X-G7  
TIME: 10.0 ... 10.8 SEC; VELOCITY: 1040 ... 990 FT/SEC



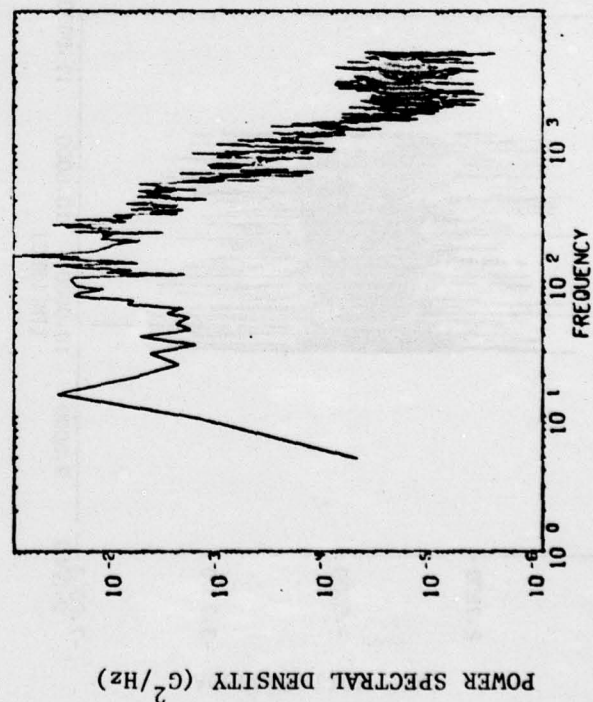
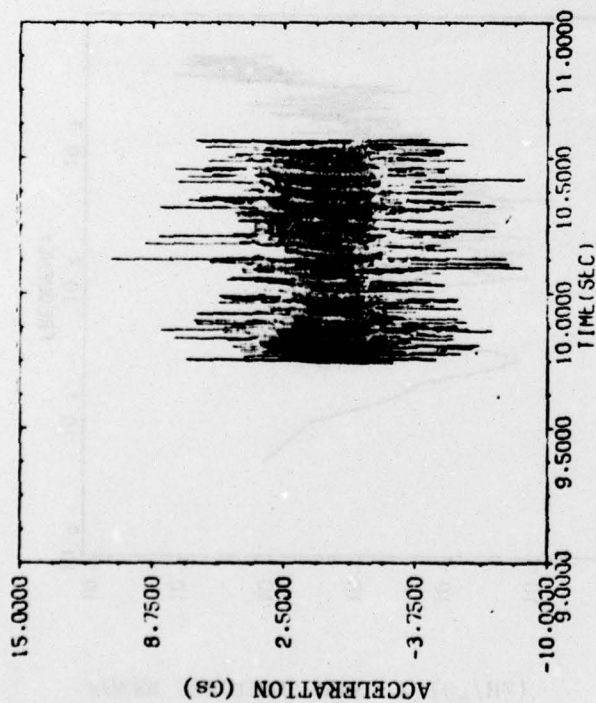
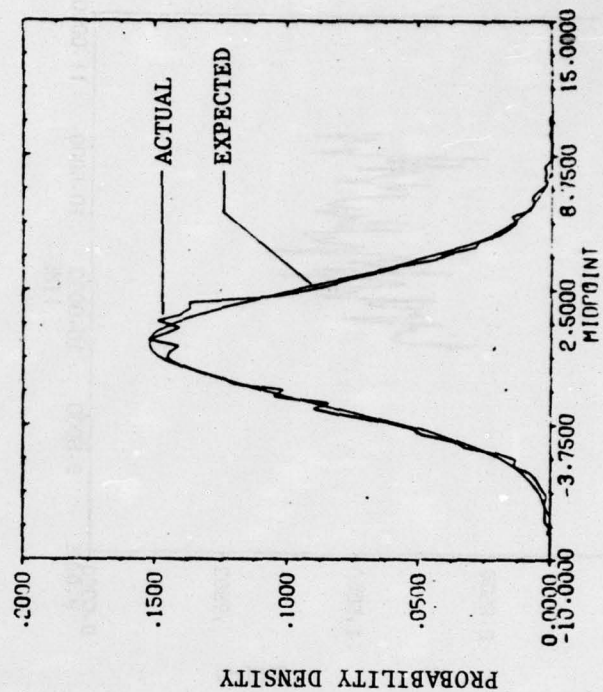
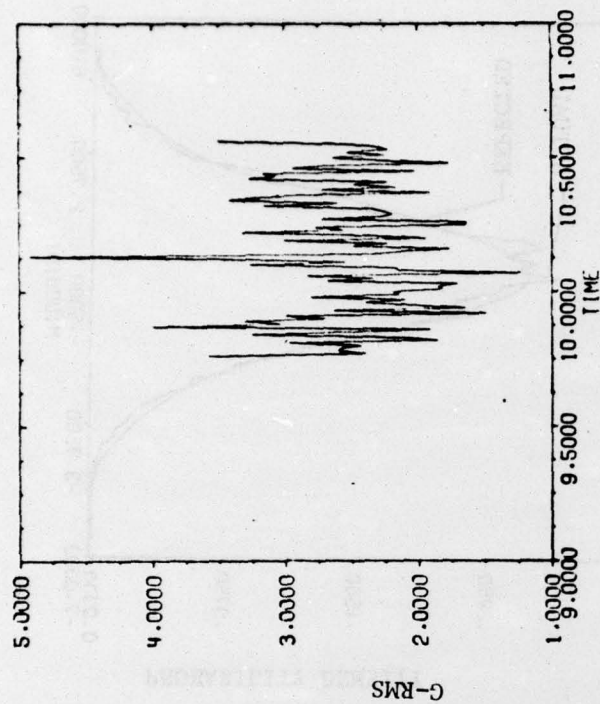


FIGURE B9 - LATERAL ACCELERATIONS, RUN NR 56X-G7  
TIME: 10.0 ... 10.8 SEC; VELOCITY: 1040 ... 990 FT/SEC

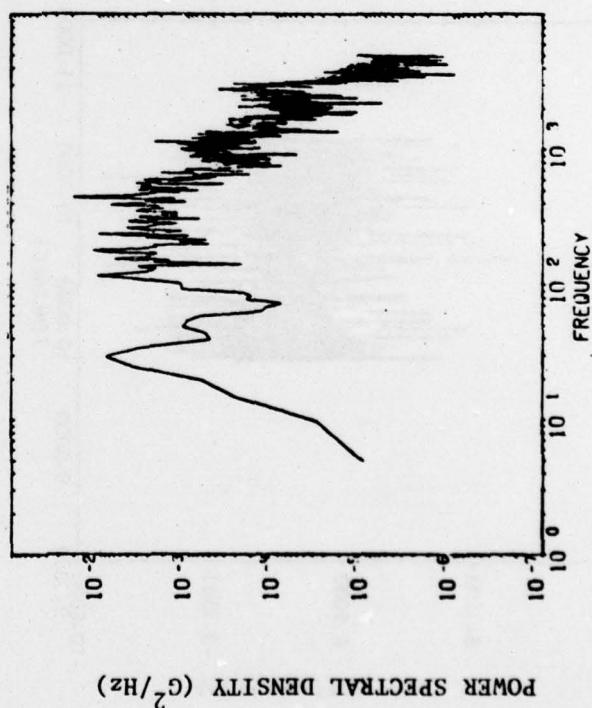
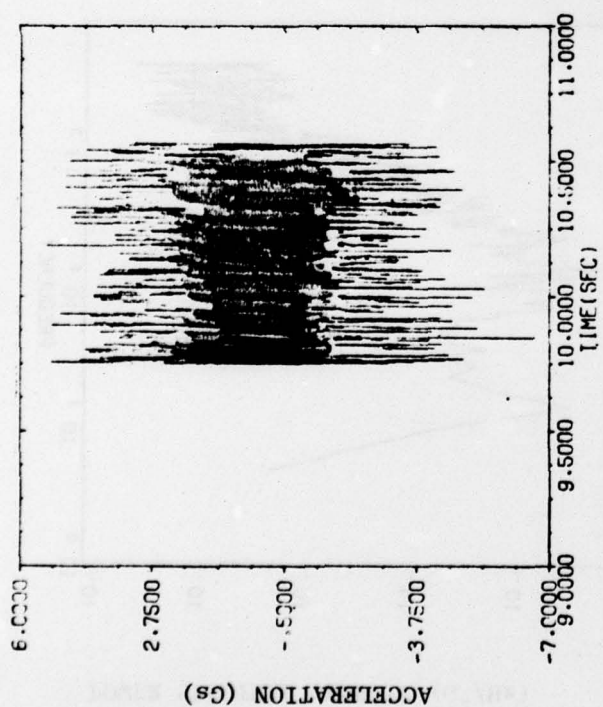
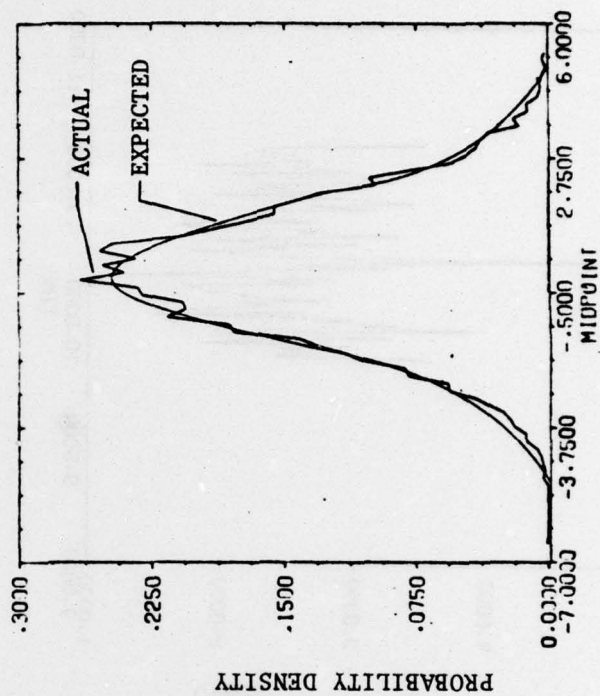
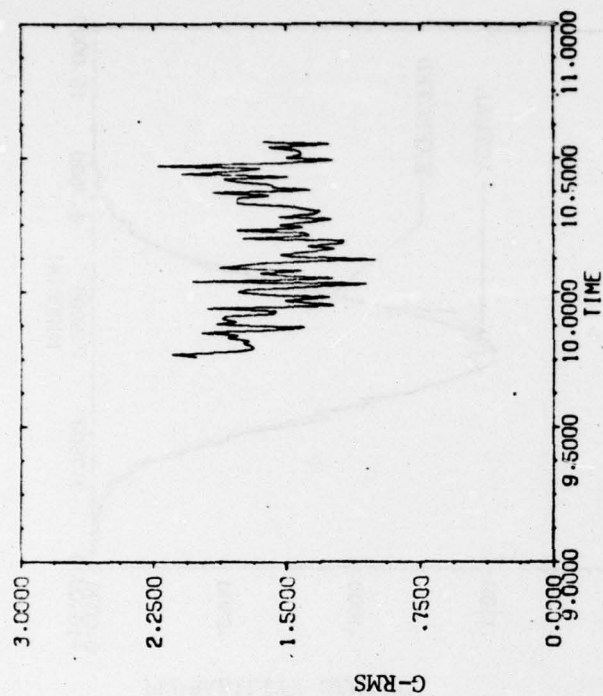


FIGURE B10 - LONGITUDINAL ACCELERATIONS, RUN NR 56X-G7  
TIME: 10.0 ... 10.8 SEC; VELOCITY: 1040 ... 990 FT/SEC

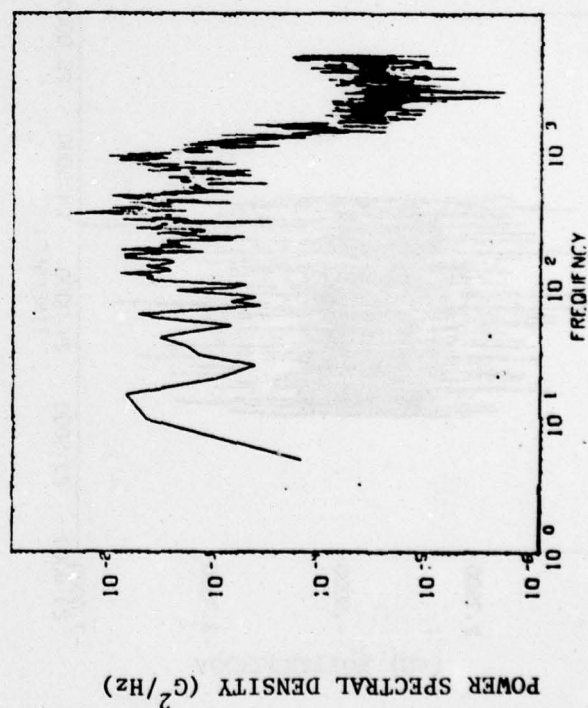
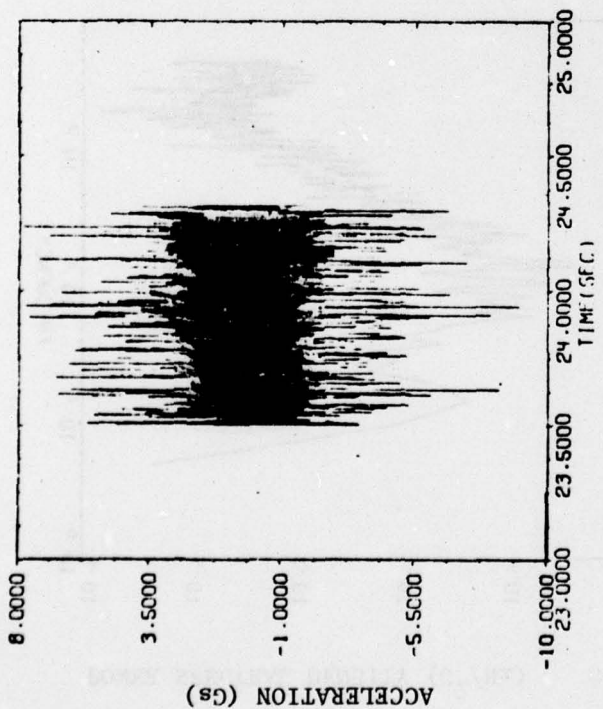
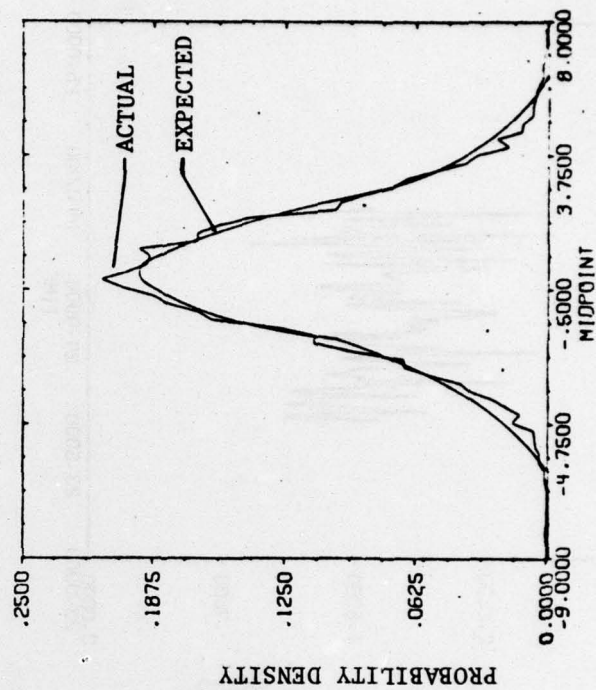
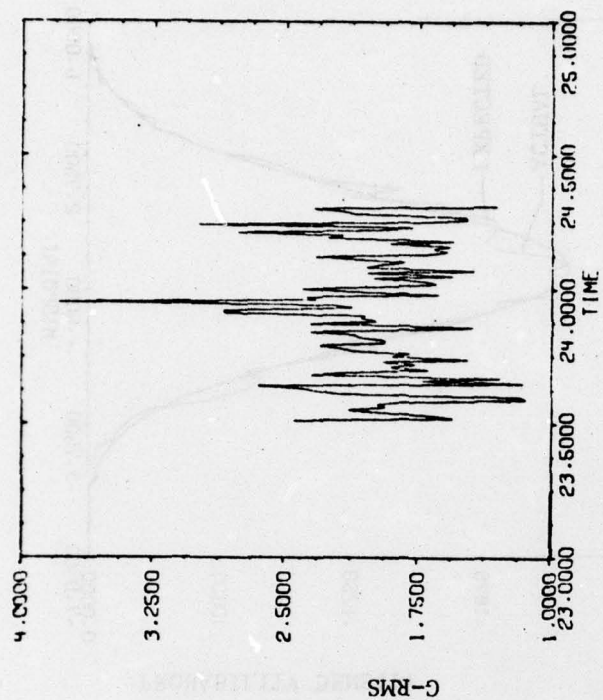


FIGURE B11 - VERTICAL ACCELERATION, RUN NR 56X-G7  
TIME: 23.6 ... 24.5 SEC; VELOCITY: 710 ... 675 FT/SEC



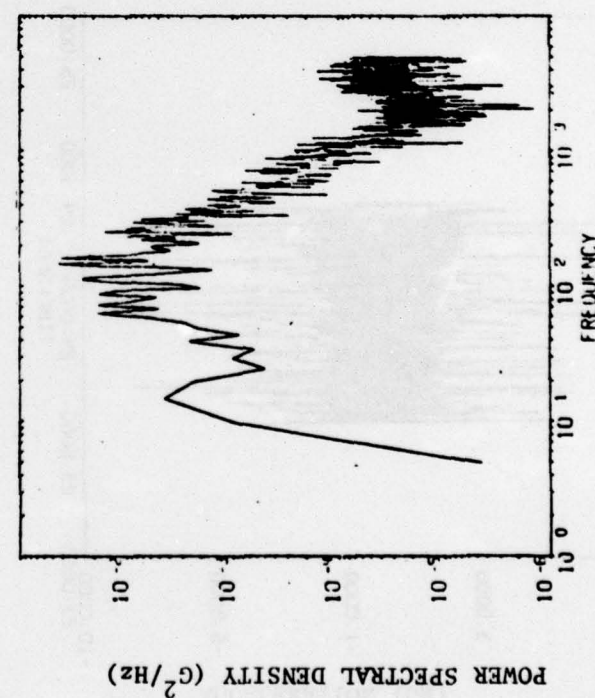
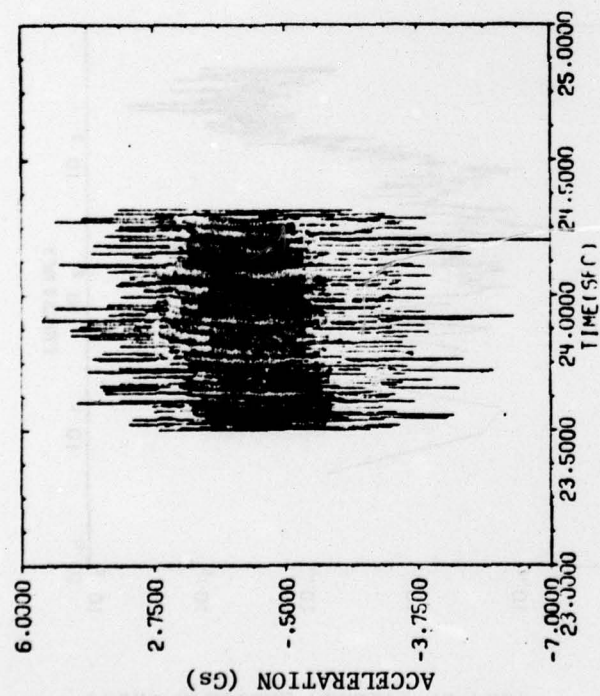
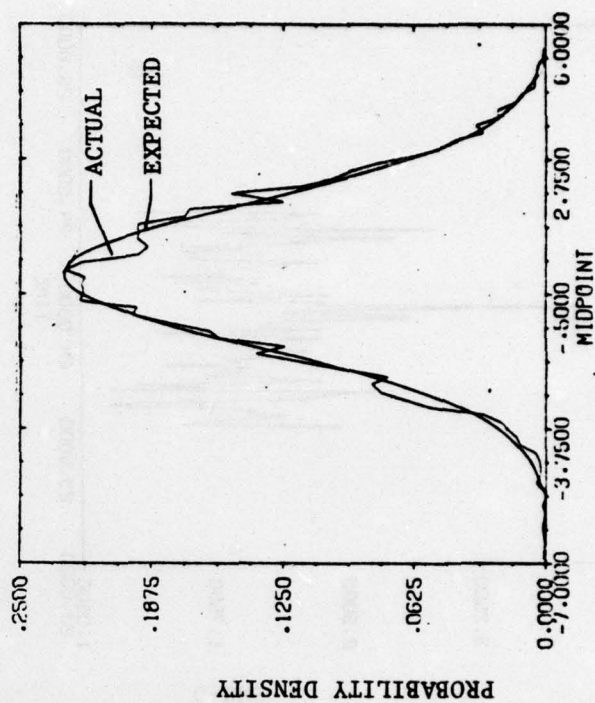
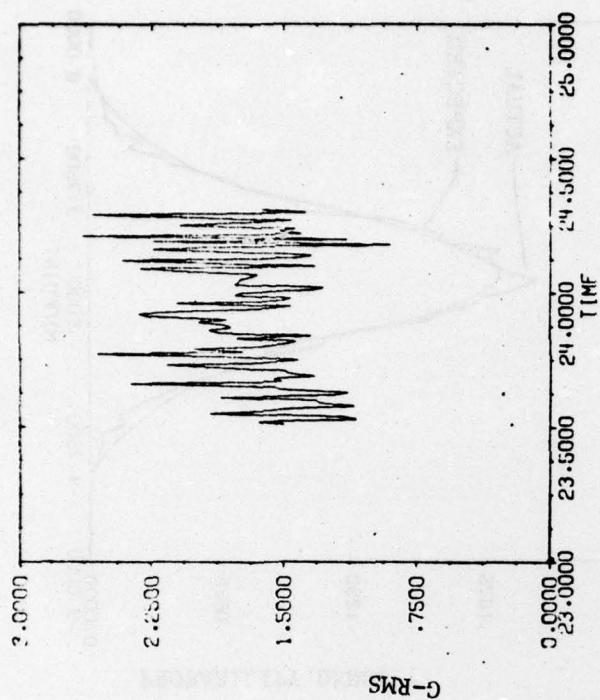


FIGURE B12 - LATERAL ACCELERATIONS, RUN NR 56X-G7  
TIME: 23.6 ... 24.5 SEC; VELOCITY 710 ... 675 FT/SEC

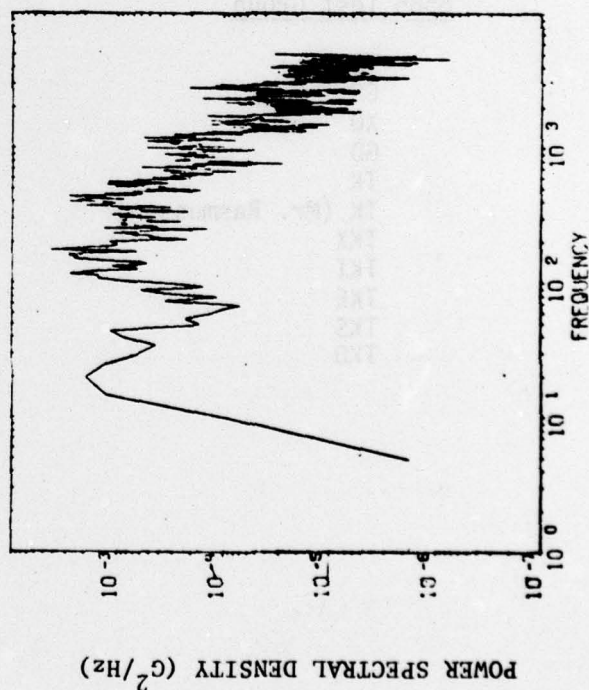
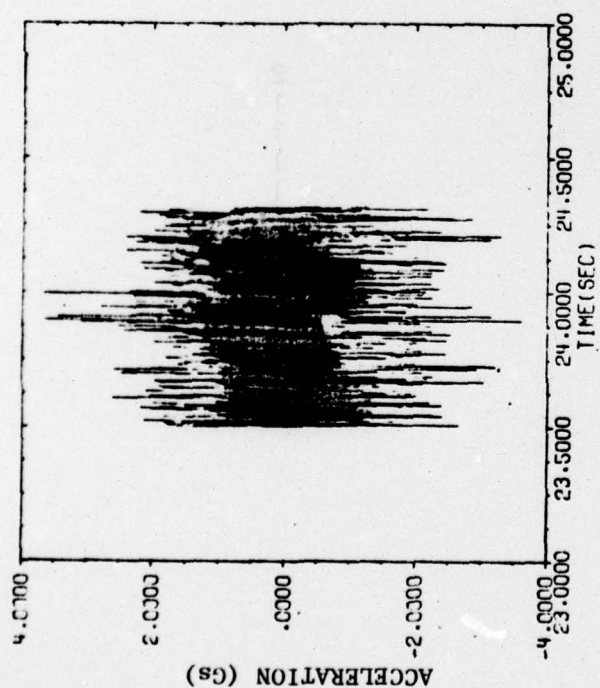
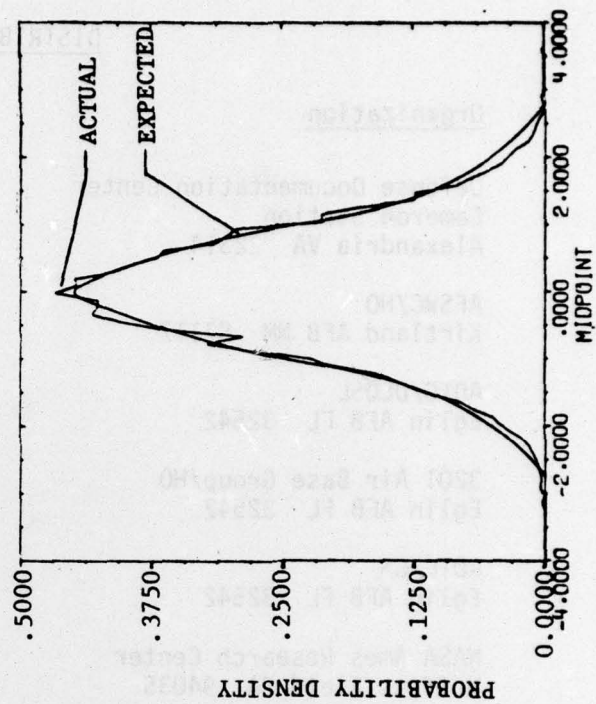
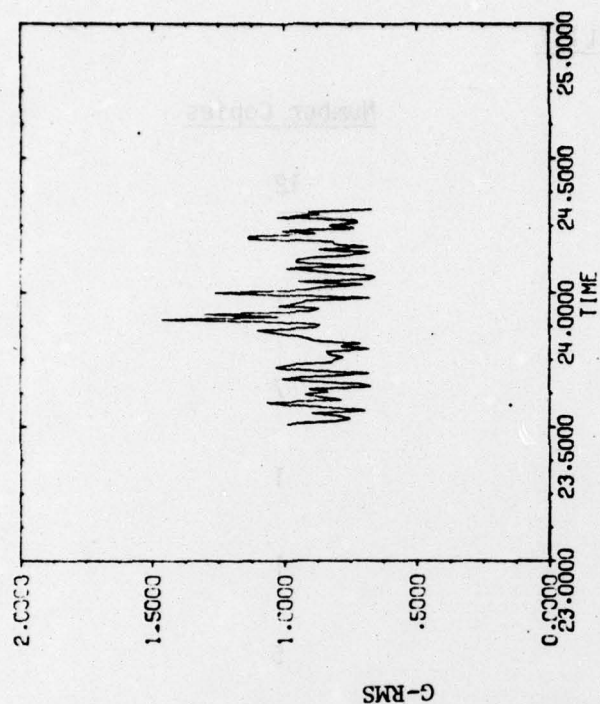


FIGURE B13 - LONGITUDINAL ACCELERATIONS, SLED RUN NR 56X-G7  
TIME: 23.6 ... 24.5 SEC; VELOCITY 710 ... 675 FT/SEC

# DISTRIBUTION LIST

<u>Organization</u>	<u>Number Copies</u>
Defense Documentation Center Cameron Station Alexandria VA 22314	12
AFSWC/HO Kirtland AFB NM 87117	1
ADTC/DLOSL Eglin AFB FL 32542	7
3201 Air Base Group/HO Eglin AFB FL 32542	1
ADTC/CS Eglin AFB FL 32542	1
NASA Ames Research Center Moffett Field CA 94035	5
<u>6585 Test Group</u>	
TSL	2
CC	1
XO	1
GD	1
TK	1
TK (Mr. Rasmussen)	1
TKX	10
TKI	4
TKE	1
TKS	1
TKO	10